論文 / 著書情報
Article / Book Information

題目(和文)	
Title(English)	Evaluation of integrated passive cooling methods to improve the outdoor and indoor microclimates of a residential house in Japan
著者(和文)	デル リオ デニス マリア アレハンドラ
Author(English)	Maria Alejandra Del Rio Denis
出典(和文)	学位:博士(工学), 学位授与機関:東京工業大学, 報告番号:甲第11651号, 授与年月日:2020年9月25日, 学位の種別:課程博士, 審査員:淺輪 貴史,中村 芳樹,大風 翼,鍵 直樹,村田 涼
Citation(English)	Degree:Doctor (Engineering), Conferring organization: Tokyo Institute of Technology, Report number:甲第11651号, Conferred date:2020/9/25, Degree Type:Course doctor, Examiner:,,,,
学位種別(和文)	博士論文
Type(English)	Doctoral Thesis

2020 PhD Thesis

Evaluation of integrated passive cooling methods to improve the outdoor and indoor microclimates of a residential house in Japan

Maria Alejandra Del Rio Denis

Supervisor: Associate Prof. Takashi Asawa

School of Environment and Society
Department of Architecture and Building Engineering
Graduate major in Urban Design and Built Environment
Tokyo Institute of Technology

Acknowledgments

I would like to thank Prof. Takashi Asawa for his precious guidance and support during these four years. At first, I want to sincerely thank him for giving me the opportunity to pursue doctoral course in his laboratory. His patience, advice, perseverance and optimism encouraged me to never give up during difficult times, and his guidance helped me to improve as a researcher and successfully complete this doctoral course. I also want to thank Ms. Yukari Hirayama and Misawa Homes Institute of Research and Development for their collaboration in the project. Without their support, case study and technology, this research would not have been possible. I also want to gratefully thank my labmates who always showed support and consideration towards one another, and made the laboratory a pleasant place to work.

I also cannot forget to mention the Embassy of Japan in Panama and Monbukagakusho (MEXT) scholarship for placing trust in me and giving me the opportunity to study in Japan. Tokyo Institute of Technology is one of the most prestigious universities in the world and I am happy to be a part of it.

Finally, I want to acknowledge my family and friends for their love, patience and support which served as encouragement for me to give my best in this doctoral course.

This thesis is dedicated to all the people who believed in me Thank you!

Abstract

In urban and suburban areas, hot outdoor thermal environment in summer months make it difficult to maintain a comfortable indoor thermal environment using only natural ventilation. A two-step research, comprising a field measurement and CFD simulation, was conducted to study and improve the outdoor and indoor microclimates of a house using passive cooling methods (PCMs), including evaporative cooling louver, vegetation, and sunscreen, installed in the semi-outdoor space and different ventilation settings at the indoor space, respectively. First, a field measurement was conducted to evaluate the microclimate in a semi-outdoor space under different amounts of solar radiation, surrounding vegetation, and distances from louver to window to find the best way that accumulates at most the cool air generated by the louver. Best results were found when the semi-outdoor space was exposed to low solar radiation, was fully surrounded by vegetation, and when the louver was closer to the window. Second, the modeling method of PCMs for CFD simulation were demonstrated using literature-based values and the field measurements. It also demonstrated model validity by comparing the obtained results with field measurements. The results show that CFD simulation with detailed modeling of these elements can replicate vertical temperature distributions at four different positions across the semi-outdoor space and indoor space. The maximum difference in air temperature between the measurements and simulation results was 0.7–1 °C. The sensitivities of each passive cooling element on the microclimates formed in both semi-outdoor and indoor spaces were confirmed. Finally, CFD simulations were conducted to find the best combination of PCMs and indoor conditions to improve the natural ventilation of the house in hot days of summer.

TABLE OF CONTENTS

LIST OF TABLES

LIST OF FIGURES

Nomenclatures

T_{amb}: Ambient temperature [°C]

WS_{out}: Outdoor wind speed [m/s]

WD_{out}: Outdoor wind direction [°]

T_{lo}: Air temperature at the back of the louver [°C]

T_{sop}: Air temperature at the center of the semi-outdoor space [°C]

WS_{sop}: Wind speed at the semi-outdoor space [m/s]

WD_{sop}: Wind direction at the semi-outdoor space [m/s]

T_{win}: Air temperature inside the window [°C]

T_{cin}: Air temperature at the center of the indoor space [°C]

WS_{win}: Wind speed inside the window [m/s]

WD_{win}: Wind speed inside the window [m/s]

T_{wb}: Wet bulb temperature [°C]

T_s: Surface temperature [°C]

T_{sout}: Surface temperature of the louver [°C]

T_{adiff}: Vertical air temperature difference $T_{lo} - T_{amb}$ or $T_{sop} - T_{amb}$ [°C]

T_{diff}: Air temperature difference $T_{sop} - T_{lo}$ [°C]

v: Inflow fixed velocity [m/s]

$\boldsymbol{F_i}$: Extra term added in the momentum equation

$\boldsymbol{F_k}$: Extra term added in the transport equation of k

$\boldsymbol{F_\varepsilon}$: Extra term added in the transport equation of ε

η: Fraction of the area covered with plants

a: Leaf area density (LAD)

C_d: Drag coefficient

k: Turbulence energy

ε: Energy dissipation rate

C_{p1}: Model constant

u_i: Mean velocity for *i* direction [m/s]

u_j: Mean velocity for *j* direction [m/s]

σ_{ij}: Stress tensor [Pa]

g_i: Gravitational acceleration for *i* direction [m/s^2]

ς_i: Pressure loss for *i* direction per unit length [Pa/m]

α_F: Porosity of porous media [-]

ρ_F: Fluid density [kg/m^3]

ρ_S: Solid density [kg/m^3]

C_{PF}: Specific heat of fluid at constant pressure [J/(kg K)]

C_S: Specific heat of solid [J/(kg K)]

K_F: Heat conductivity of fluid [W/m]

K_S: Heat conductivity of solid [W/m]

T_F: Fluid temperature [K]

T_S: Solid temperature [K]

q_F: Heat generation in fluid per unit volume [W/m^3]

q_S: Heat generation in solid per unit volume [W/m^3]

α_{ij}: Tensor of area ratio [-]

χ: Surface area ratio (contact ratio between fluid and solid per unit volume) [m^2/m^3]

h: Convective heat transfer coefficient [W/(m^2 K)]

CHAPTER 1. INTRODUCTION

1.1. Background

1.1.1. Microclimate: the relationship between climate, site and building.

The way cities are shaped has an important impact on the urban microclimate; and local climate varies significantly within a small area due to changes in altitude and rainfall. Therefore, urbanization or the replacement of natural vegetation with constructed buildings and infrastructure generates a unique local environment or microclimate around buildings [1]. Urban microclimate directly influences building energy consumption and indoor thermal comfort [2]. Ideally, the microclimate that is created around the building must do to make for a comfortable interior and exterior environment around the building [3].

In Japan, traditional houses were adapted to the very hot and humid summers to maximize the natural ventilation using post-and-bean construction which allowed the lightweight paper wall panels to be moved out of the way in the summer. The engawa (Figure 1.1) provided a semi-outdoor space with the large overhanging roofs which shaded the house. Moreover, traditional houses also counted with a large outdoor space with garden and ponds which allowed for a comfortable outdoor and indoor microclimate [4].

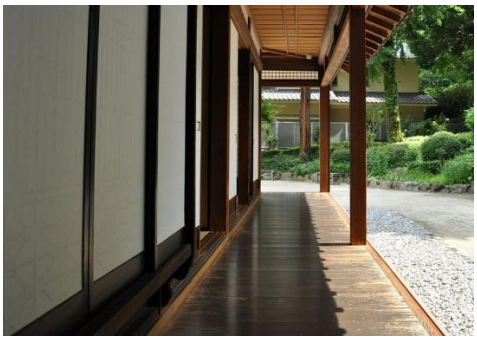

Figure 1.1 The engawa in a japanese traditional house

However, with the expansion of urban and suburban areas, the combination of factors such as reduced vegetation (reduced evapo-transpiration processes), excess of heat stored by construction materials, decreased long-wave radiation from urban areas, reduction of wind speed due to wind sheltering by buildings [cited by [3] and consequent reduced convective removal form urban surfaces to the atmosphere [5], causes much higher temperatures than rural areas – namely the urban heat island (UHI) effect.

The UHI effect in combination with compact design of houses with reduced green spaces makes for an uncomfortable outdoor and indoor microclimate thus reducing the potential use of natural ventilation during summers.

1.1.2. The heat island effect, human health and energy usage in buildings.

With expansion of the urban scale, the mitigation of the UHI effect has become increasingly important [2]. Residents spend 85-90% of their time indoors, thus the indoor air quality is closely related to human health [6]. Air temperature is one of the most important parameters that gives us sense of comfort. Thus, the UHI effect in combination with compact design of houses with reduced green spaces has made it difficult to live comfortably in the hot-humid summer heat of Tokyo only using passive cooling methods such as natural ventilation and solar shading. In these circumstances residents opt to use air conditioners instead of natural ventilation to maintain a comfortable indoor thermal environment. エラー! 参照元が見つかりません。 (TMG, 2017) shows that the ownership of room air conditioners have increased over the years and is expected to increase due to global warming.

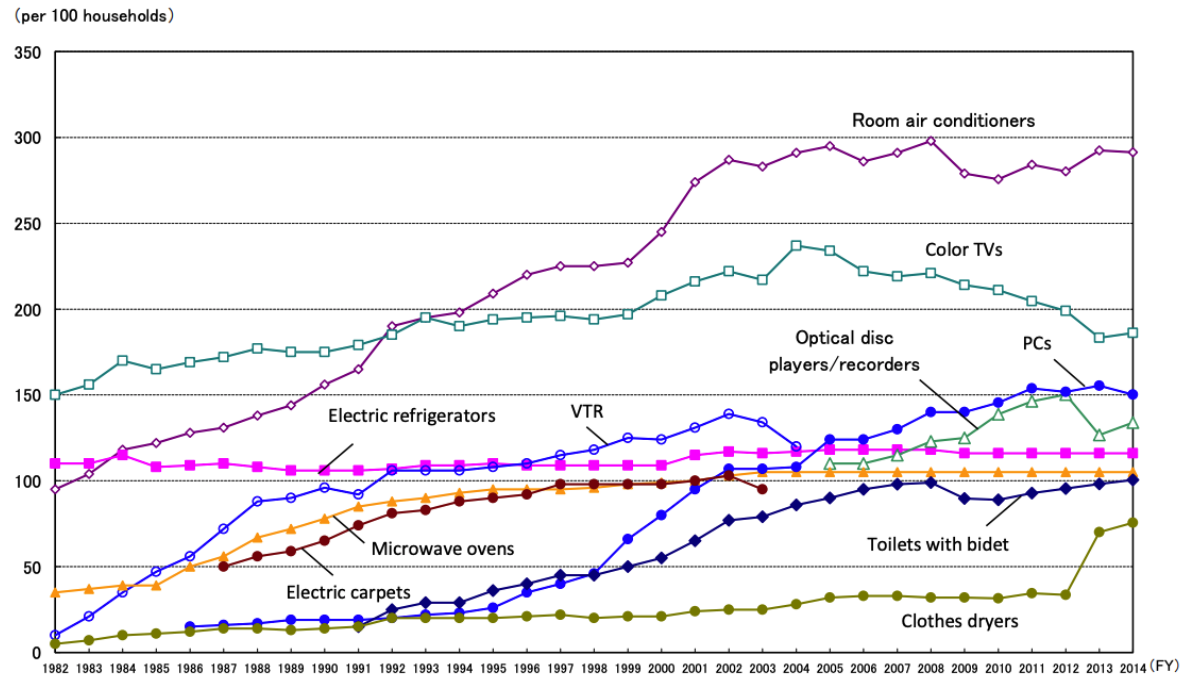

Figure 1.2 Trends in the ownership rates of home appliances in Tokyo (1992-2014)

Although air conditioners offer a fast solution to improve the indoor microclimate, its constant use can worsen the indoor air quality of a building due to lack of fresh air which can affect the health of occupants

and productivity, namely the sick building syndrome. In addition, it increases the anthropogenic heat which worsen the UHI effect. Therefore, it is important to provide a comfortable indoor thermal environment during summer by improving the outdoor microclimate. In return, users can opt for either using natural ventilation or air conditioners (mixed mode ventilation) to maintain a comfortable indoor microclimate.

Moreover, in the summer of 2018, eastern and western Japan experienced unprecedentedly hot summer conditions. Figure 1.3 shows mean temperature anomalies (deviations from the baseline) with the highest record since 1946 –of 2.8 ºC and 1.7 ºC above normal; where Kumagaya in Saitama Prefecture recorded a maximum temperature of 41.1 ºC (JMA, 2018). Hence, due to urbanization, the UHI effect and global warming, it is important to optimize buildings in terms of energy demand considering local urban microclimates [3].

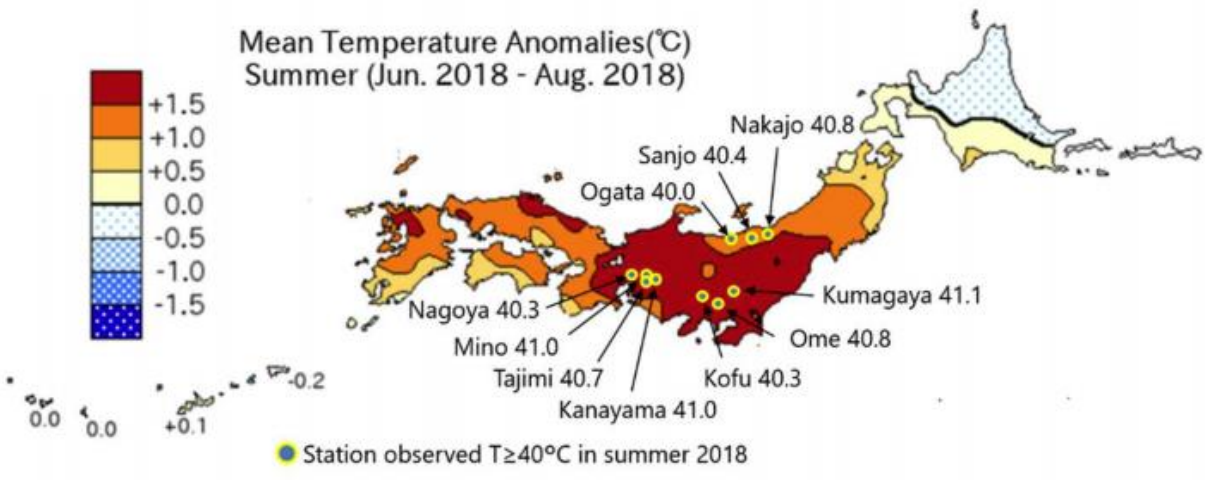

Figure 1.3 Seasonal mean temperature anomaly (ºC) for Japan in summer 2018.

1.1.3. Passive cooling methods.

To mitigate severe thermal environment caused by UHI, the microclimate surrounding existing buildings can be altered to promote a comfortable indoor environment. The usage of passive cooling methods [7,8] in cities and residential areas is an adaptive measure employed to deal with such severe thermal environments. Figure 1.4 shows the three tier approach to sustainable design of buildings. Passive cooling design focuses on heat gain control and heat dissipation in a building in order to improve the indoor thermal comfort with low or no energy consumption (first and second tier). These techniques include:

- Heat avoidance techniques: Considering that east and west walls receive most of the high solar radiation during the day; basic building design need to be taken into consideration to minimize the heat gain in the building. Thus, ideally, heat avoidance techniques (passive building design) must start in the early design stage of a building – before construction. Strategies include floor plan and building form, windows (location, type, etc.) and shading (outdoor vegetation, shading devices, etc.), high albedo colors (reflect solar radiation), thermal insulation, and control of internal heat sources [4].
- Heat dissipation techniques: Natural ventilation is the most known passive cooling technique to dissipate heat inside the house. This technique is better applied in combination with heat avoidance techniques. There are different ventilation and heat dissipation techniques for cooling the building with low to no energy including: cooling with ventilation (comfort ventilation or night flush cooling), radiant cooling (night), evaporative cooling, and earth coupling.

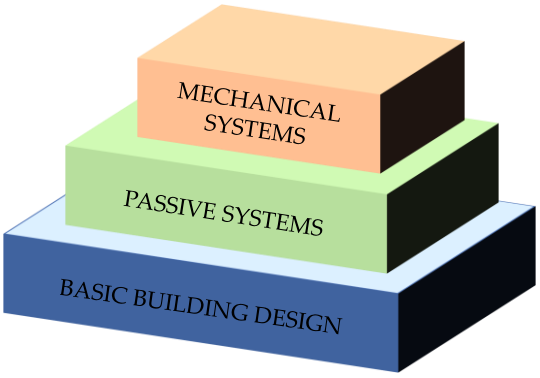

Figure 1.4 Three tier approach to sustainable design of buildings [4]

1.1.3.1. Vegetation

In respect of improving the outdoor thermal environment in existing buildings, it is evident that the usage of trees and green covers is one of the most effective ways [7,8]. Considering that, the thermal environment in rural areas is significantly cooler than urban areas due to the predominance of vegetation. Several studies have shown that urban greening is beneficial to the outdoor microclimate because it reduces the air and surface temperatures compared with those in non-vegetated areas due to characteristics of urban greening such as evapotranspiration (if regularly irrigated), small heat capacity, shading, and radiation attenuation due to the presence of foliage [9–12]. Trees also help to mitigate the greenhouse effect, filter pollutants, mask noise, prevent erosion, and calm human observers [13]. Srivanit and Hokao [11] showed

that the green space was 0.7–1.4 °C cooler than non-green spaces with a maximum reduction of 2.3 °C. Yoshida et al. [14] showed that the air temperature under a tree canopy during daytime was ~1 °C lower on average throughout the measurement period compared with that in open space. Berry et al. (2013) [cited by [12]] demonstrated that tree shade could reduce wall surface temperatures by up to 9 °C and external air temperatures by up to 1 °C. Lee et al. [15] studied the effects of a small planted area with watering outside a window, and the results showed that the ambient temperature was reduced by 2 °C. In addition, the use of plants for passive cooling of buildings can also reduce air infiltration by modifying wind speed and direction and they can limit nocturnal thermal losses, blocking outgoing long-wave radiation fluxed with large canopies [cited by [16].

Urban trees, alone or in combination with shading, can create a cooler environment in summer so buildings will consume less energy for air conditioning [12,17]. However, with urbanization, there is limited amount of green spaces to grow trees and shrubs to achieve a higher cooling performance. Thus, alternative solutions that combine multiple passive cooling methods are required to improve the microclimate of compact urban areas.

1.1.3.2. Evaporative cooling

Direct evaporative cooling is the simplest and oldest form of air conditioning [8], and one of the most effective ways of passive cooling for buildings and urban spaces in hot regions [cited by [18]. Evaporative cooling cools the air by direct contact with water; cooling from its dry bulb-temperature to its wet bulb temperature if the water is fully vaporized. When the ambient humidity is increased, the cooling efficiency becomes lower because of the limitations in the amount of vapor that could be added to the air [19]. The limit of the evaporative cooling potential is given by the wet bulb temperature of the air to be cooled [cited by [8]. Evaporative cooling systems are dependent on climatic conditions and although is expected to be more effective in a hot and dry climate, studies [20,21] have shown that they can function even under hot and humid climates. The summer season in Japan is characterized by hot and humid weather with abundant rainfall but the relative humidity decreases to approximately 50% during daytime in sunny days. The use of evaporative cooling is a widely used passive cooling method in Japanese traditional vernacular houses as well [22]. Therefore, evaporative cooling has a cooling potential to improve microclimate in hot hours in Japan. The development of practical passive cooling methods to improve the microclimate of outdoor spaces in Japan during summer has been studied extensively [15,23–25]. He and Hoyano (2010) developed a passive

evaporative cooling wall (Figure 1.5a) constructed of porous ceramics with high water hold and soak up ability that can reduce the air temperature passing by around 2.0°C during summer daytime. Hirayama et al. (2014) [24] developed an evaporative cooling louver (Figure 1.5b, Figure 1.6), which can lower the air temperature by approximately 3.0 °C at maximum within the vicinity of the louver. The evaporative cooling louver is a stand-alone aluminum louver system coated with hydrophilic resin, porous particles, and photocatalyst (TiO_2) to disperse water over the entire surface with a small amount of water supply. Approximately 3.6 L/(m^2h) of water is dripped continuously from the top of the louver. The airflow can easily pass through the slats to cool the air. The louver provides (1) shade against direct solar radiation, (2) radiation cooling, and (3) ventilation cooling with cooled airflow, and (4) provide privacy near the window. Moreover, the louver stands-alone with independent foundation (350x350 mm); offering practical applications for its installation in limited outdoor spaces. Even though the louver improves the microclimate within its vicinity, its actual performance inside buildings has not yet been evaluated. Therefore, more information on the cooling effect of the louver, either alone or in combination with other passive cooling methods, is required to provide design recommendations for generating cool microclimates inside buildings. Other technologies include evaporative cooling pavement system or retentive water cooling pavement [26].

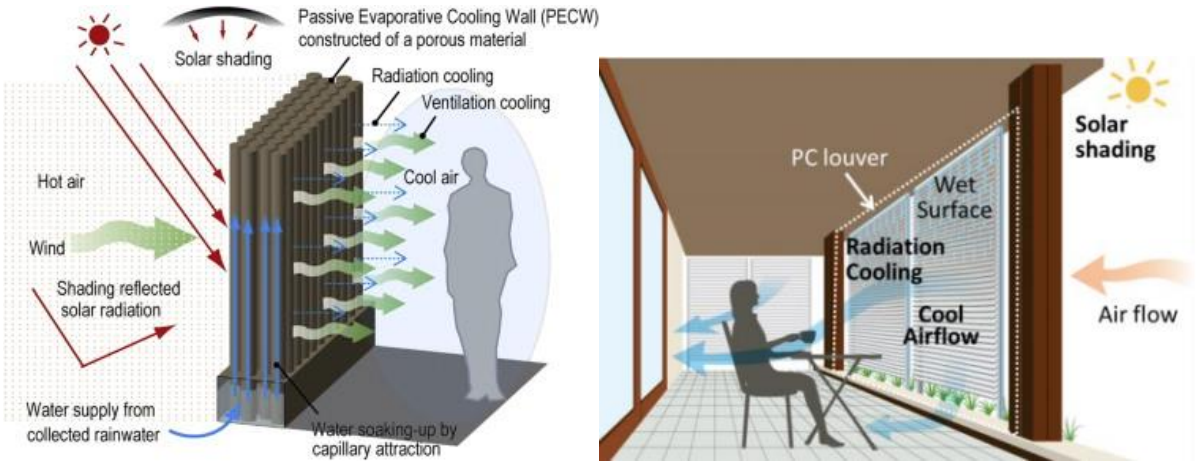

(a) (b)

Figure 1.5. Overview of stand-alone evaporative cooling technologies. (a) Passive evaporative cooling wall (b) Evaporative cooling louver.

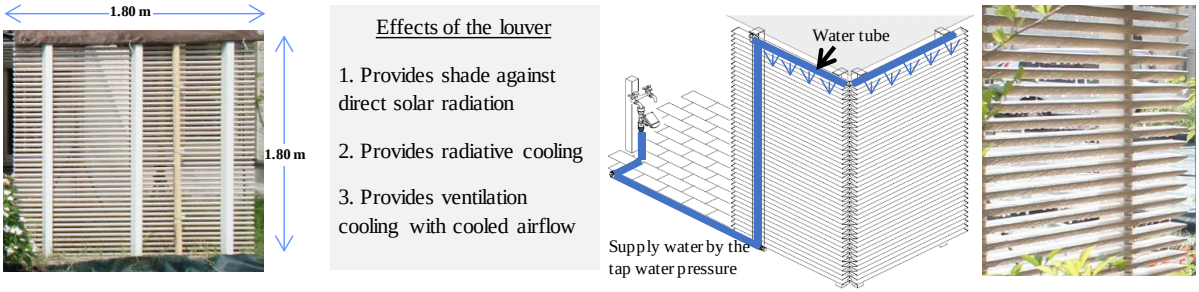

Figure 1.6. Details of the evaporative cooling louver. Left to right: dimensions, passive cooling effects, watering method, image of louver watering.

1.1.3.3. Natural ventilation

Natural ventilation (NV) - based on pressure differences created by wind and buoyancy driven ventilation - is one of the main techniques to moderate temperature in buildings [27]. The usage of NV in buildings have demonstrated significant potential of energy savings [6] and improvement on occupant satisfaction and indoor air quality in favorable climatic conditions [28]. The usage of NV is dependent on the window opening behavior of occupants, determined by the outdoor microclimate [29,30]. Therefore, in order to use natural ventilation to moderate temperature in buildings there is need to mitigate the hot outdoor thermal environment. Moreover, although NV by opening a window seems simple, the combination of wind and buoyancy driven ventilation can oppose or complement each other depending on the position of the opening and the wind direction. In addition, other parameters such as wing walls, horizontal overhangs, window types, inlet and outlet sizes and location, insect screens, roof vents, fans, building layout, indoor partitions and placement of furniture can affect natural ventilation. Hence, predicting and controlling the indoor environment in window-based ventilation systems remains essentially an open issue [30].

- Driving forces of natural ventilation: The pressure difference driving the airflow is a function of two driving forces: wind and buoyancy. Air flows either because of natural convection currents, caused by differences in temperature, or because of differences in pressure. Wind pressures are generally positive on the windward side of a building and negative on the leeward side. The occurrence and change of wind pressures on building surfaces depend upon wind speed and wind direction relative to the building shape, location, surroundings. Moreover, the stack effect due to air temperature difference causes density differentials and pressure differences that drive the air to move. Thus, even the lowest wind speeds will induce pressure distribution on the building envelope that will also act to drive airflow [31].

- Ventilation strategies: Figure 1.7 shows the airflow path defined by different ventilation modes: single-sided ventilation, cross ventilation and stack ventilation [31]. Single-sided ventilation is the least attractive natural ventilation solution because it causes lower ventilation rates. Cross ventilation is usually driven by wind-generated pressure differences inducing positive pressures on windward faces and negative pressures on leeward surfaces. Stack effect is created by air temperature differences when the indoor air temperature is higher than outdoors which causes indoor warm air (less dense air) to rise and exit through a high level opening such as roof window or a roof vent. Thus, the stack effect causes air movement by air temperature differences inducing cool air from a low level window (opening) and exiting warm air through a high level window.

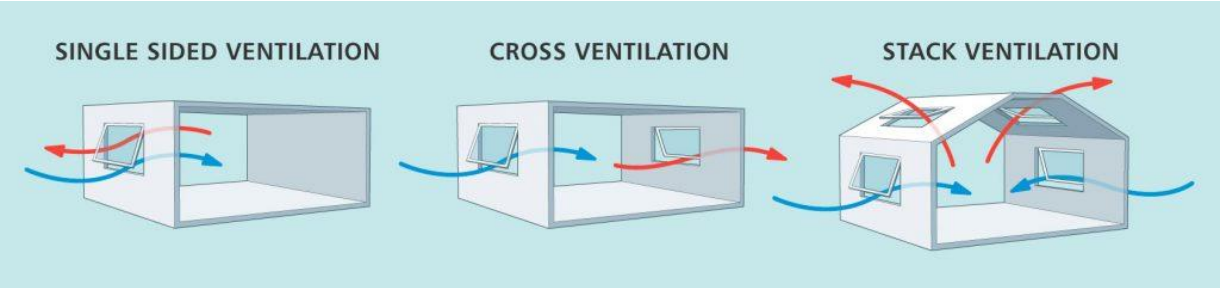

Figure 1.7. Example of natural ventilation techniques. Left to right: single sided ventilation, cross ventilation and stack ventilation.

1.1.4. Previous studies on outdoor and indoor microclimates

The design of sustainable and comfortable urban spaces and buildings has become increasingly important [cited by [32]. Specifically, studies on urban microclimate are gaining popularity [33]; and several researchers have studied methods to improve the urban microclimate [32–35]; however, only a few of them have studied its effect on the indoor thermal environment [36]. Moreover, extensive studies have been conducted on natural ventilation [27,29,30,37–41] related to building design and ventilation techniques (e.g. the size and location of ventilation openings, building orientation and layout, balconies in building facades and other protrusions) [cited by [36]. However, only a few of them have focused on studying the relationship between outdoor and indoor microclimate to improve natural ventilation [15,36,42]. Yuan et al [36] studied the effect of vertical farming on natural ventilation of a residence using CFD simulation and found that is possible to improve the natural ventilation by appropriately modifying vegetable arrangement and vegetable species. Toe and Kubota [42] studied and proposed passive cooling techniques to improve the relationship

between the indoor-outdoor temperature of houses. Lee at al., [15] studied the cooling effect of plants in the indoor space – wind speed was reduced but cool air flowed inside.

Moreover, Table 1.1 shows a list of previous research that investigate outdoor microclimate and indoor microclimate. Most of the research that have carried out field measurements on outdoor, indoor or combination of both microclimates records its data with one measurement point height at around 1 to 2 meters above the ground. However, few researches have considered studying outdoor and indoor microclimate by collecting data using multiple point heights.

Table 1.1. Previous research on outdoor and indoor microclimates

Author	Research	Outdoor	Indoor	Measurement point height	Height [m]	Methodology
[11]	Cooling effect of greening	o		Single	1.5 m	Field measurement
[14]	Cooling effect of greening	o		Single	1.0 m	Field measurement
[43]	Summer microclimate of a residence	o		Single	1.2 m	Field measurement and CFD
[44]	Summer microclimate of a semi-enclosed space	o		Single	1.2 m	Field measurement and CFD
[10]	Effect of urban vegetation on outdoor thermal environment	o		Single	10 cm (scale model)	Field measurement
[45]	Evaluation of natural ventilation potential	o	o	Single	1.0 m	Field measurement
[46]	Windows parameters on indoor natural ventilation		o	Single	1.0 m	Field measurement and CFD
[47]	Evaluation of natural ventilation potential	o	o	Single	1.0 m	Field measurement
[42]	Passive cooling techniques for improving indoor thermal comfort	o	o	Multiple	0.5 m, 1.0 m, 1.5 m, 2.0 m, 2.5m, etc.	Field measurement
[15]	Cooling effects of plants on natural ventilation	o	o	Multiple	0.1 m, 0.4 m, 0.6 m, 1.0 m, 1.2 m, etc.	Field measurement

1.2. Purpose of research

Considering the above mentioned backgrounds and viewpoints, there is need for studying the application of passive cooling methods simultaneously to improve the outdoor and indoor microclimate during summer months in urban / suburban houses with limited outdoor spaces. To fill this research gap, this study adopts field measurement and microclimate modelling using computer fluid dynamics (CFD) to investigate the effects of passive cooling methods (PCMs) and ventilation strategies for improving the outdoor and indoor microclimate of a house during summer. Both conducting field experiments and CFD simulation are important because the measured microclimate data can be used to verify the CFD model, which can be used to conduct multiple parametric studies. The PCMs used in this study comprises evaporative cooling louvers [24], vegetations and sunscreen.

This study was carried out to find the most effective: (1) PCMs configuration for optimal cool microclimate formation in a semi-outdoor space; (2) ventilation strategies for optimal induction of cool air formed in a semi-outdoor space for natural ventilation; in order to provide design recommendations for generating cool microclimates inside buildings.

1.2.1. Novelty

- This study adopts field measurements and microclimate modeling using CFD simulation.
- Conducts studies in both the outdoor and indoor microclimates of a house.
- Studies the application of passive cooling methods simultaneously for improving the outdoor and indoor microclimates.
- Uses multiple measurement points horizontally and vertically to evaluate the vertical temperature distribution in outdoor, semi-outdoor and indoor spaces.

1.3. Thesis structure

The thesis structure shown in Figure 1.8 is comprised of the following parts:

- Chapter 1: Motivation (research background) and purpose of research.

- Chapter 2: Field experiment of outdoor microclimate and indoor microclimate for a house with multiple PCMs in a semi-outdoor space. This study examines the characteristics of the distribution of cool air formed in a semi-outdoor space by PCMs in front of a window. The capability of the PCMs is evaluated in terms of inducing the cool air from the outdoor environment to the indoor environment for natural ventilation.
- Chapter 3: Modeling and validation of CFD simulation using the field experiment results.
- Chapter 4: Sensitivity analysis of different settings and combinations of PCMs is performed using the validated CFD simulation.
- Chapter 5: Optimization of the outdoor and indoor microclimates using the validated CFD model to find the best PCMs configuration and best ventilation strategies for optimal cool microclimate formation and induction of cool air. Evaluation of the effect of different wind directions in the optimized case.
- Chapter 6: Conclusions and future work

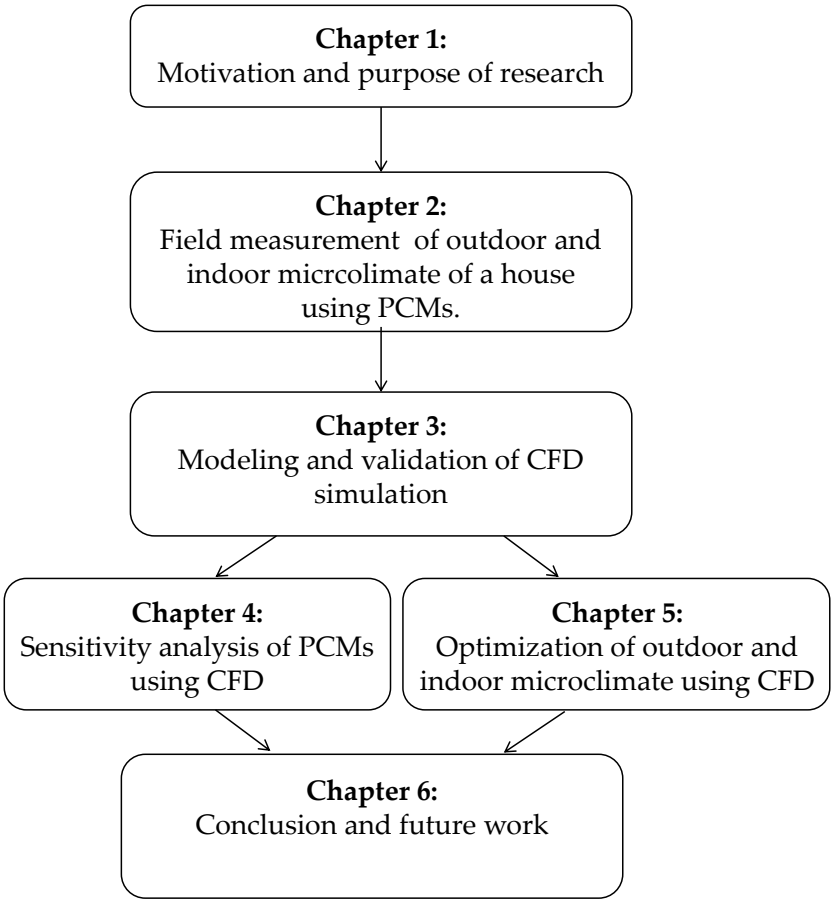

Figure 1.8 Thesis structure

CHAPTER 2. FIELD MEASUREMENT

2.1. Case study

2.1.1. Background: Brief history of Japan's path to energy-saving architecture

Japan, as the second largest economy in the word, has been long troubled with energy supply due to the low self-sufficient rate of energy. In 1980s, with the continuously rising yen, Japan, as an export and trading giant, placed great importance on reduction of energy cost with the view of improving the market competitiveness of its products. By the late 1980s, with the continuous improvement of Japanese living standard, energy saving and global warming prevention became a concern, and in 1997 Japan signed the Kyoto Protocol. Since then, Japanese government have taken several control measures to improve the effect of energy saving and greenhouse gases emission reduction of the architecture. Thus, due to the force of law and the attraction of policy support, Japan's green architecture has grown hugely - achieving remarkable results through decades of unremitting efforts. Accordingly, architecture enterprises in Japan have carried out lots of studies and development on energy-saving architecture, and we can take a cue from Misawa Homes [48].

2.1.2. Target residential area

Misawa Homes Co., Ltd. is one of the largest developers of residential homes in Japan. Its own research facility – Misawa Homes Institute of Research and Development Co., Ltd. (MHIRD) – carries out lots of studies and development on energy-saving architecture. In 2014, Japanese Government decreed that more than half of the newly built homes in the country by 2020 should be Zero Energy Homes (ZEH) [49]. In recent years, Misawa homes have focused on microclimate design, which strives to produce a comfortable indoor environment throughout the year by taking advantage of the natural environment, climate and geographic features of the site. The concept of microclimate design has been implemented in large scale for the development of M-Smart City Kumagaya (Saitama, Japan) – a suburban city at 60 km north of Tokyo Kumagaya City in Saitama prefecture known for severely hot weather during summer caused by very hot winds from Tokyo and Chichibu basin in the west of the prefecture. In addition, the city has no issues of noise or air pollution. Consequently, it is important to transform the city into a "refreshing town" in order to

make the residential houses with high natural ventilation efficiency – thus more energy efficient - in comparison to houses built in Tokyo area [49].

2.1.3. Climate of Kumagaya City

Kumagaya City has a humid subtropical climate and one of the hottest summers in Japan. Historically, the air temperature in this city has reached 39.8 and 39.7 °C in June 2011 and September 2000, respectively [50]. In addition, in the summer of 2018, the city recorded a maximum temperature of 41.1ºC [JMA, 2018]. Recent weather data (2007-2017) (Table 2.1) for the city indicate that evaporative cooling has a cooling potential of 4.6−8.9 °C due to the water pressure deficit of air and wet surface during summer. Prevailing wind direction during winter is NNW and summer SSE. Natural ventilation may be used especially in the transition seasons (after the hottest season). The time of using air conditioning during summer in Tokyo could be shortened up to 300 hours.

Table 2.1. Dry-wet bulb temperature difference (2007-2017)

	Dry bulb temp.	Relative Humidity	Wet bulb temp.	Dry-Wet bulb temp.	Time
	℃	%	℃	℃	h/yr
over 32℃	33.9	48.7	25.0	8.9	229
30 - 32℃	30.9	55.5	23.8	7.1	197
28 - 30℃	28.9	60.7	23.0	5.9	319
26 - 28℃	26.9	67.0	22.2	4.6	503

2.1.4. Characteristics of the passive house

The houses are highly insulated and airtight. The walls and floors are wooden panels that consist of 75-mm-thick 24 kg/m^3 high-grade glass wool, and the ceiling is insulated with 200-mm-thick glass wool. The windows are made of plastic sashes with double-glazed, low-emissivity glass containing argon gas between the glass panes. The heat loss coefficient per unit floor area of the house is 1.77 W/ (m^2K). The home is equipped with photovoltaic system as well as gas co-generation system and controlled by newly developed home energy management system [HEMS] [49].

2.1.4.1. Passive cooling technologies

- Natural ventilation: In conventional houses, occupants manually control natural ventilation. In contrast, these houses have a unique system that senses outdoor and indoor temperature to automatically control

the opening or closing the air intake opening and heat exhaust sky window. The system also controls the room air conditioner to minimize the cooling energy. Air conditionings turn off as the outdoor temperature becomes 3°C lower than indoor temperature and simultaneously air-intake opening and heat exhaust sky window are opened.

- Evaporative cooling: MHIRD also introduced passive cooling technologies which uses evaporative cooling such as: vegetation, sprinklers, water retentive interlocking blocks at the walkway and parking (cools the temperature around feet), and the evaporative cooling louver (Figure 1.6) – (located at face level). Even though it is known that the louver improves the microclimate within its vicinity, its actual performance inside buildings has not yet been evaluated. Therefore, this field measurement uses the evaporative cooling louver in combination with other passive cooling methods to evaluate the generation of cool microclimate inside buildings.

2.2.Methodology

2.2.1. House selected for the field measurement

A detached two-story passive house located in the suburban residential complex – M-Smart City (N36°8′50.6″, E139°23′19.1″) – was selected for this study. As mentioned in the previous section this passive house has already a high energy performance due to its features. However, there is still need to investigate the effects of passive cooling methods (PCMs) on outdoor and indoor microclimates. Figure 2.1 shows the floor plan of the house. The surroundings of the house include a road facing northeast, two detached two-story houses one facing the southeast façade and the other facing the northwest façade, and an empty lot facing the southwest façade. The southwest courtyard was selected as the outdoor area for the experiment, whereas the common space that shares the kitchen, living room, and dining room was chosen as the indoor area, with a total area and volume of 29.8 m^2 and 71.55 m^3, respectively.

(a)

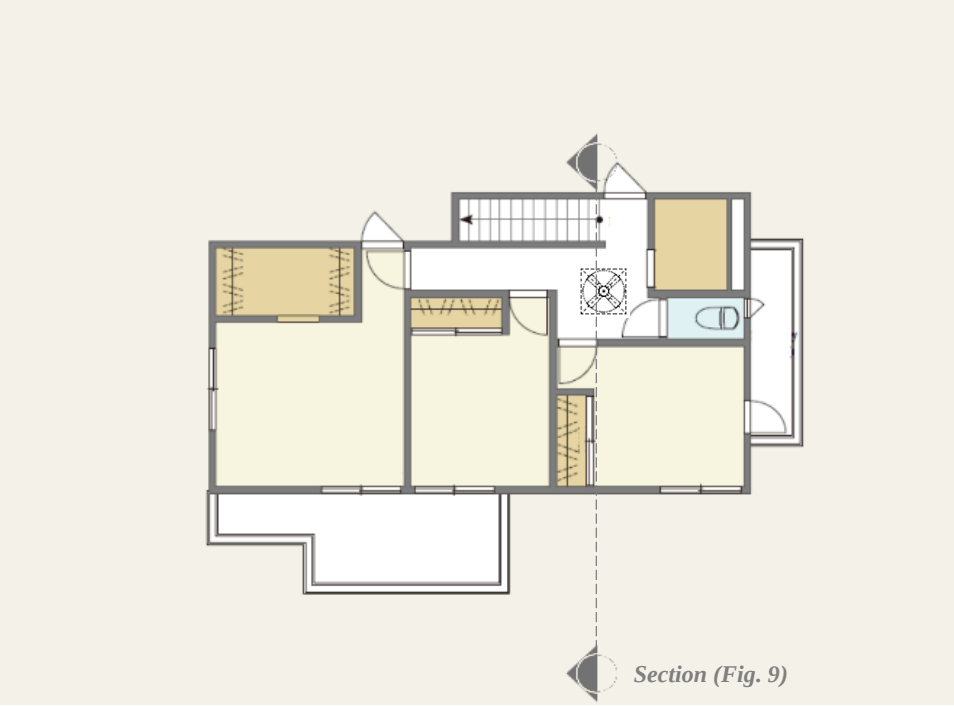

(b)

Figure 2.1 Floor plan of the house. (a) first floor (b) second floor

2.2.2. Experimental design

Figure 2.2 shows the target area of the house selected for the study: the southwest courtyard and the indoor area, which represents the outdoor and indoor microclimate, respectively. PCMs comprising an evaporative cooling louver (Figure 1.6, Figure 2.3); surrounding vegetation (potted plants and planted trees) (Figure 2.2, Table 2.2, Figure 2.5); and a sun screen (solar transmittance: 4.9 %) were installed in front of two windows facing the courtyard, creating two semi-outdoor spaces: Space A and Space B. The distance between the louver and window (L-W) for Space A is 1 m and for Space B is 2.8 m. The water supply amount during the experiment was 1.8 L/ (m^2h) per evaporative cooling louver's vertical plane (Figure 2.3). The temperature of the water was 25.0 ºC. Furthermore, the ground was covered with grass and the number of potted plants surrounding each semi-outdoor space was varied, as shown in Table 2.2.

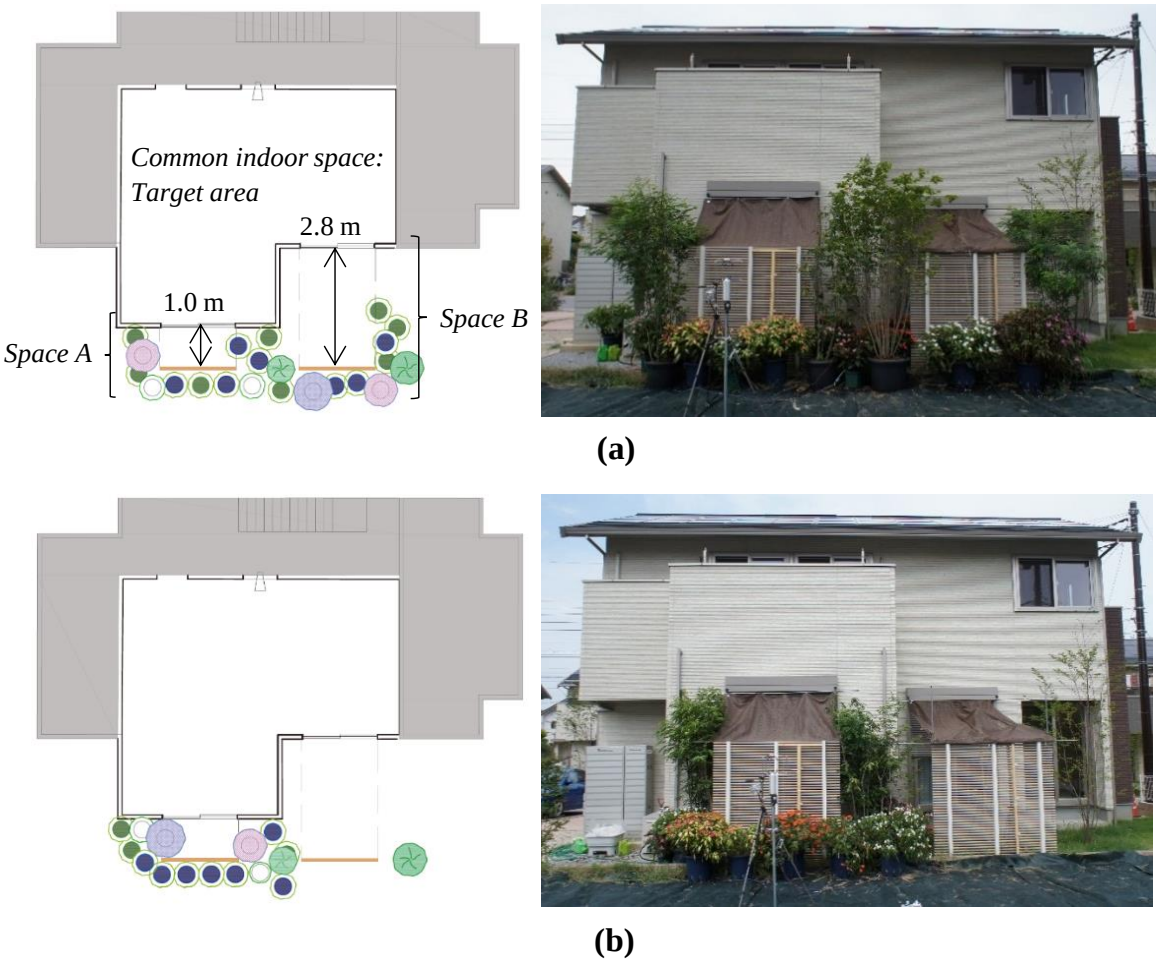

Figure 2.2. PCMs settings for (a) Day 1 and (b) Day 2. Left to right: Floor plan and view of southwest facade.

Table 2.2. Amount of vegetation surrounding the semi-outdoor space for each case.

Photograph of vegetation		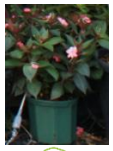	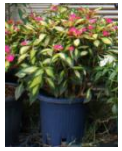						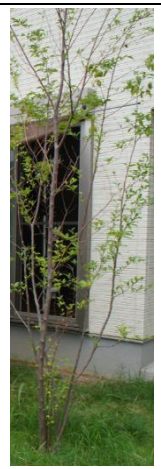		
Drawing representation											
Type of vegetation		Flower	Flower	Quercus glauca	Fraxinus griffithii	Quercus glauca	Fraxinus griffithii	Amelanchier canadensis	Styrax japonicus		Amount that surrounds the semi-outdoor space
Size (m)	Height (pot)	0.20	0.35	0.35	0.35	0.35	0.35	Planted	Planted		
	Height (plant)	0.50	0.55	2.50	2.40	2.30	2.00	2.00	3.50		
	ø (plant)	0.60	0.70	0.50	0.90	0.40	0.80	0.60	0.80	Total	
Amount of vegetation per case	Case 1	5	4	2	0	0	0	1	0	12	Maximum
	CASE 2	3	3	0	1	0	1	0	1	9	Half
	CASE 3	3	7	1	1	1	1	1	0	15	Maximum
	CASE 4	0	0	0	0	0	0	0	1	1	None

Figure 2.3. Close-up views of the louver watering.

2.2.3. Ventilation settings

Apart from installing PCMs in the semi-outdoor space for improving the outdoor microclimate, the indoor conditions were fixed to determine the best ventilation settings that will induce outdoor cool air into the indoor space. Table 2.3 and Figure 2.4 show the ventilation settings used in the experiments. The ventilation settings included:

- Inflow (windward ventilation): Leaving the sliding window "fully open" or "half-open" with exterior shutter.

Flow between rooms or cross ventilation: Opening the kitchen door or using a blower door installed in the living room door (Figure 2.4c. In general, a blower door is used between outdoor and indoor spaces to measure the airtightness of a building. For this study, blower door was installed to experimentally check the relationship between ventilation amount and cool air induction. Because experimental periods with appropriate weather conditions were limited, so we applied such an experimental setting. Thus, the blower door was used between indoor spaces to force air movement by air aspiration in order to determine the rate of indoor ventilation needed to improve the intake of cool air through the window.

- Outflow (leeward ventilation): Stack ventilation for heat exhaust using a sky window.

For reference, all the other doors and windows were closed. Moreover, the airtightness of the common space was 5.6 cm^2/m^2 because the air vents, windows, and indoor doors were not sealed. The amount of aspirated air was set at 710–730 m^3/h, which is equivalent to 10 times the volume of the common space, by assuming the air change rate at natural ventilation.

Table 2.3. Louver watering conditions and ventilation settings for each case

Case	Subcase	Duration of experiment	Time (min)	Louver watering	Vegetation watered	Ventilation setting (Cross ventilation + Stack ventilation)				
						Window opening	Window area (m)	Room ventilation	Air aspiration (m^3/h)	Sky window
CASE 1 CASE 2	C1	Day 1 14:30–16:25	25	No	No	Fully open	0.7 × 2.0	Open kitchen door	—	Open
	C2		25	Yes	Yes	Half open	0.7 × 1.0	Open kitchen door	—	Open
	C3		25	Yes	No	Half open	0.7 × 1.0	Blower door	710–730	Open
	C4		25	Yes	No	Fully open	0.7 × 2.0	Open kitchen door	—	Open
CASE 3 CASE 4	C5	Day 2 12:20–13:35	15	No	No	Fully open	0.7 × 2.0	Blower door	710–730	Open
	C6		15	Yes	Yes	Half open	0.7 × 1.0	Blower door	710–730	Open
	C7		15	Yes	No	Fully open	0.7 × 2.0	Blower door	710–730	Open
	C8		15	Yes	No	Half open	0.7 × 1.0	Blower door	710–730	Open

Note: There was a 5-min break between each subcase in order to change the ventilation settings.

Figure 2.4. Location and photos of ventilation settings.

2.3.Experimental cases

The experiment was conducted during September (transition seasons) when conditions were favorable for PCMs use; i.e., after an intensive cooling season, extending the time and period during which natural ventilation could be used. The field measurements were carried out over the course of six days and two days were specifically chosen (September 12, 2016 (Day 1) and September 17, 2016 (Day 2)) to evaluate the formation of cool microclimate under cloudy and sunny conditions, respectively. Figure 2.5 shows the close-up PCMs settings for each case as follows:

- CASE 1: Space A fully surrounded by vegetation under cloudy conditions (Day 1).
- CASE 2: Space B partially surrounded by vegetation under cloudy conditions.
- CASE 3: Space A fully surrounded by vegetation under sunny conditions (Day 2).
- CASE 4: Space B without surrounding vegetation under sunny conditions. CASE 4 subcase C5 is the default condition because there was no vegetation, the louver was not watered, and the L-W distance was longer.

(a)

(b)

Figure 2.5. Close-up views for each case in (a) Day 1 (b) Day 2. Left to right. CASE 1, CASE 2, CASE 3 and CASE 4.

2.4.Data collection

Field measurements were conducted to evaluate the microclimate created by the PCMs and induction of cool air based on the ventilation settings. The data recorded include the general weather conditions outside the semi-outdoor space as well as the vertical air temperature distribution and wind conditions inside the semi-outdoor space and indoor space. The details of the equipment used for the experiments and measuring points are presented in Table 2.4. Figure 2.6 and Figure 2.7 shows the photos and locations of the measuring points. Table 2.5 shows the detail location of points for wind speed and wind direction at the outdoor, semi-outdoor and indoor space. The weather conditions, namely, horizontal solar radiation, ambient temperature (T_{amb}), relative humidity, wet bulb temperature (T_{wb}), outdoor wind speed (WS_{out}), and outdoor wind direction (WD_{out}) were recorded outside the semi-outdoor space at 1.5 m above the ground level (GL + 1.5 m). The vertical air temperature distribution inside the semi-outdoor space was recorded at the back of the louver (T_{lo}) from GL + 0.1 m to GL + 1.5 m; and center of the semi-outdoor space (T_{sop}) from GL + 0.1 m to GL + 2.0 m. In addition, the wind speed (WS_{sop}) and wind direction (WD_{sop}) were recorded at GL + 1.0 m. Furthermore, the air temperature inside the window (T_{win}) and center of the indoor space (T_{cin}) were recorded from GL + 0.5 m to GL + 2.5 m (or 0.1 m above the floor level (FL + 0.1 m) to FL + 2.0 m). The wind speed inside the window (WS_{win}) and wind direction (WD_{win}) were recorded from FL + 0.3 m to FL + 1.7 m (refer to Table 2.5).

Table 2.4. Measurement equipment

Measured parameter	Equipment	Accuracy
Horizontal solar radiation	Thermopile pyranometer	±5%
Representative ambient temperature	T-type 0.1-mm thermocouple inside ventilated tube	0.1°C
Air temperature	T-type 0.1-mm thermocouple (with shield)	0.1°C
Representative relative humidity	Resistance change-type humidity sensor (Model: CHS-MSS, TDK Corporation, Japan)	±3% (<90%RH) ±5% (>90%RH)
Wind velocity and direction	3-axis ultrasonic anemometer (Model: CYG-81000, R.M. Young Company, USA)	±2° ±0.1m/s
Wind velocity and direction	Ultrasonic wind sensor (Model: WMT52, Vaisala Corporation, Finland)	±5° ±0.3m/s
Thermograph	Infrared camera (Model: Thermo GEAR G100, Nippon Avionics Co.,Ltd., Japan)	±2°C
Blower door	Airtightness performance instrument	
Data	Data logger (Model: LR5400, Hioki E.E. Corporation, Japan)	

(a) Thermocouple with shield

(b) T_{amb}, Solar radiation, RH, WS_{out}, WD_{ou}

(c) T_{sop}, WS_{sop}, WD_{sop}

(d) T_{win}, T_{cin}, WS_{win}, WD_{win}

Figure 2.6. Photo of the measurement equipment.

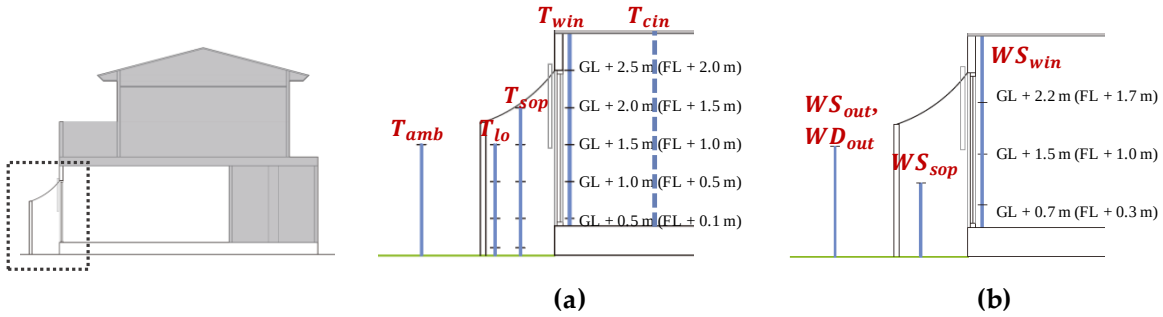

Figure 2.7. Location of measurement points. E.g. for Space A. (a) Air temperature (b) Wind speed and direction

Table 2.5. Detail location of measurement points for wind speed and wind direction.

Outdoor space		
WS_{out} , WD_{out} **(GL + 1.5 m)**		
Semi-outdoor space	Space A	Space B
WS_{sop} , WD_{sop} **(GL + 1.0 m)**	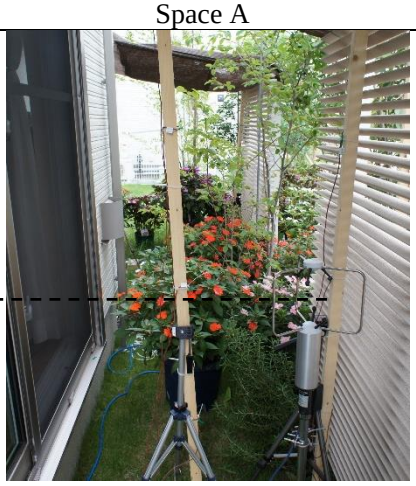	No point installed
Inside window	Space A	Space B
WS_{win} , WD_{win} **(GL + 2.2 m)** **(GL + 1.4 m)** **(GL + 0.7 m)**		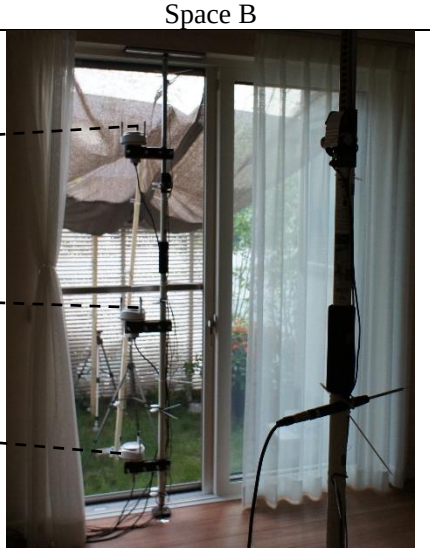

All of the data were recorded within 1-s intervals. The house used for conducting the field measurement was neither furnished nor occupied. Hence, the measuring equipment were the only sources of heat. In addition, the indoor space was revised with thermographs and the surface temperature was almost equivalent to the air temperature. This implies that the MRT (Mean Radiant Temperature) hardly affects the experimental results.

2.5. Results

2.5.1. Weather conditions

Figure 2.8 shows the weather conditions before and during the field measurements for Day 1 and Day 2. On Day 1, the solar radiation is more than 500 W/m^2 before 13:30 and the solar radiation is low with an average of 85 W/m^2 during the experiment (from 14:20 to 16:25). In contrast, on Day 2, the solar radiation is less than 300 W/m^2 before 11:30 whereas the solar radiation is high with an average value of 567 W/m^2 during the experiment. This shows that when measurements were conducted; Day 1 had cloudy conditions whereas Day 2 had sunny conditions. In addition, the average WD_{out} is 0.6 and 0.7 m/s for Day 1 and Day 2, respectively, while the average WD_{out} falls within a range of 163–169°, indicating that the wind direction is approximately perpendicular to the windows. The average relative humidity values are 52% and 50% for Day 1 and Day 2, respectively, indicating that the conditions are favorable to reduce the ambient temperature using direct evaporative cooling. Based on the difference between the ambient temperature and wet bulb temperature ($T_{amb} - T_{wb}$), the PCMs have the potential to reduce the T_{amb} by an average of 7.1 and 7.8 °C for Day 1 and Day 2, respectively. These values correspond to the theoretical maximum potential of the evaporative cooling louver at a relative humidity of 100%.

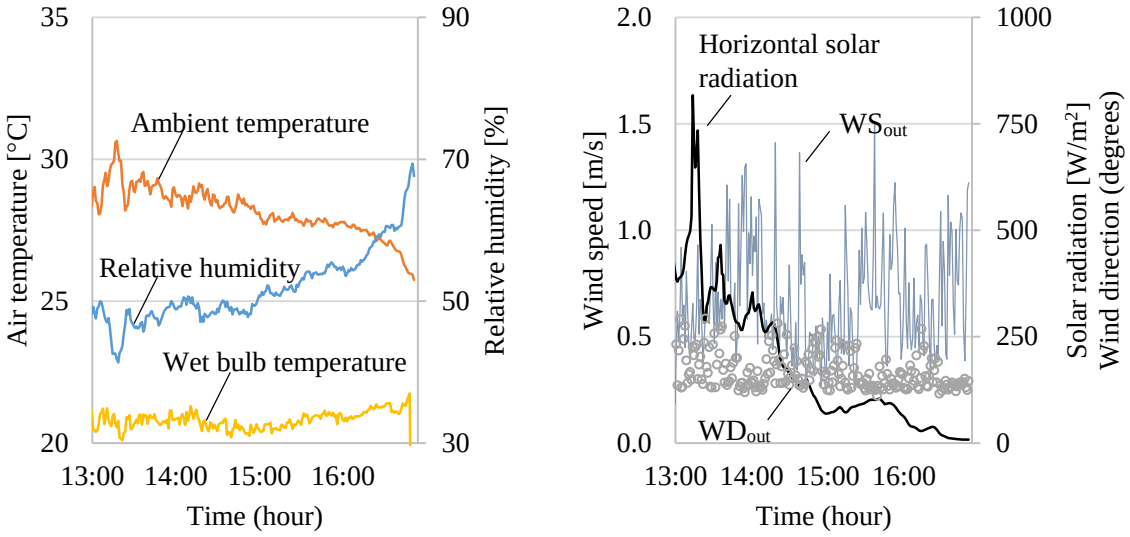

(a)

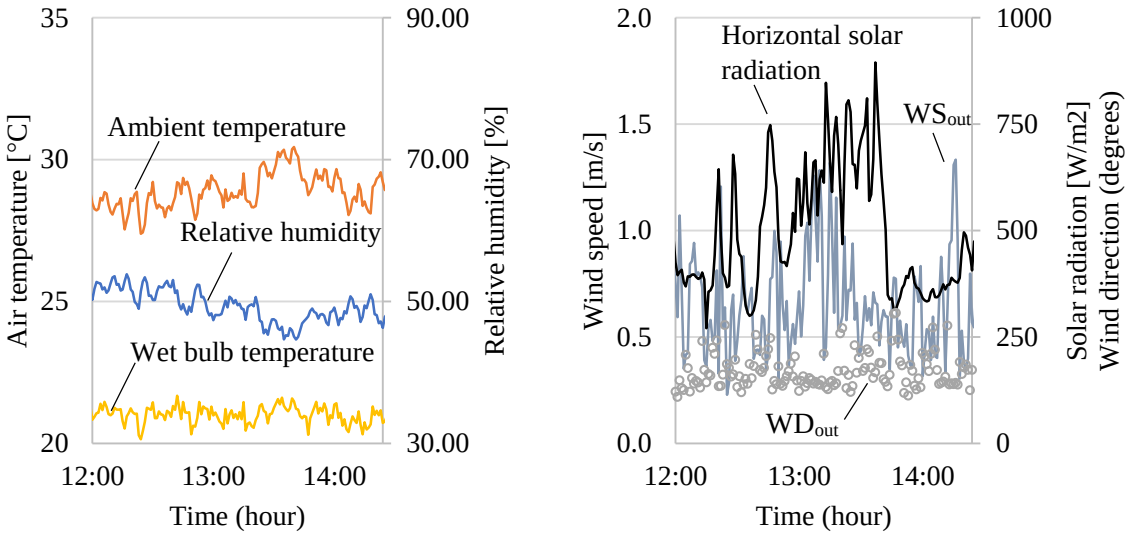

(b)

Figure 2.8. Weather conditions before and during the experiment. (a) Day 1 (b) Day 2.

2.5.2. **Surface temperature of the louver**

Figure 2.9 shows the surface temperatures of the louver for Day 1 and Day 2 when it is dry, wet (previously watered), and while it is being watered. T_{sout} is the surface temperature of the louver collected by thermographs (Figure 2.9); and T_s is the surface temperature recorded using a thermocouple located at the upper side of a slat. Figure 2.9a shows that when the louver is dry, the T_{sout} is higher than the T_{amb} by 3.6 °C and the T_s is higher than the T_{amb} and the T_{wb} by 1.3 and 9.6 °C, respectively. In contrast, further

reductions are observed when the louver is continuously watered and the values vary in accordance with the amount of solar radiation for each day. On Day 1 (Figure 2.9b), it can be seen that the T_{sout} is lower than the T_{amb} with a difference of 2.3 °C. T_s is lower than the T_{amb} by 4 °C whereas it is higher than the T_{wb} by 3.1 °C. On Day 2 (Figure 2.9d), it can be seen that the T_{sout} is less than the T_{amb} by 1 °C. The T_s is lower than the T_{amb} by 2.9 °C whereas it is higher than the T_{wb} by 4.3 °C. This indicates that the T_{sout} is typically 2 °C higher than the T_s when the louver is both dry and watered, regardless of the amount of solar radiation. Moreover, the most significant reduction of the T_s is observed on Day 1, where the T_s decreases by 6.2°C when the louver is watered.

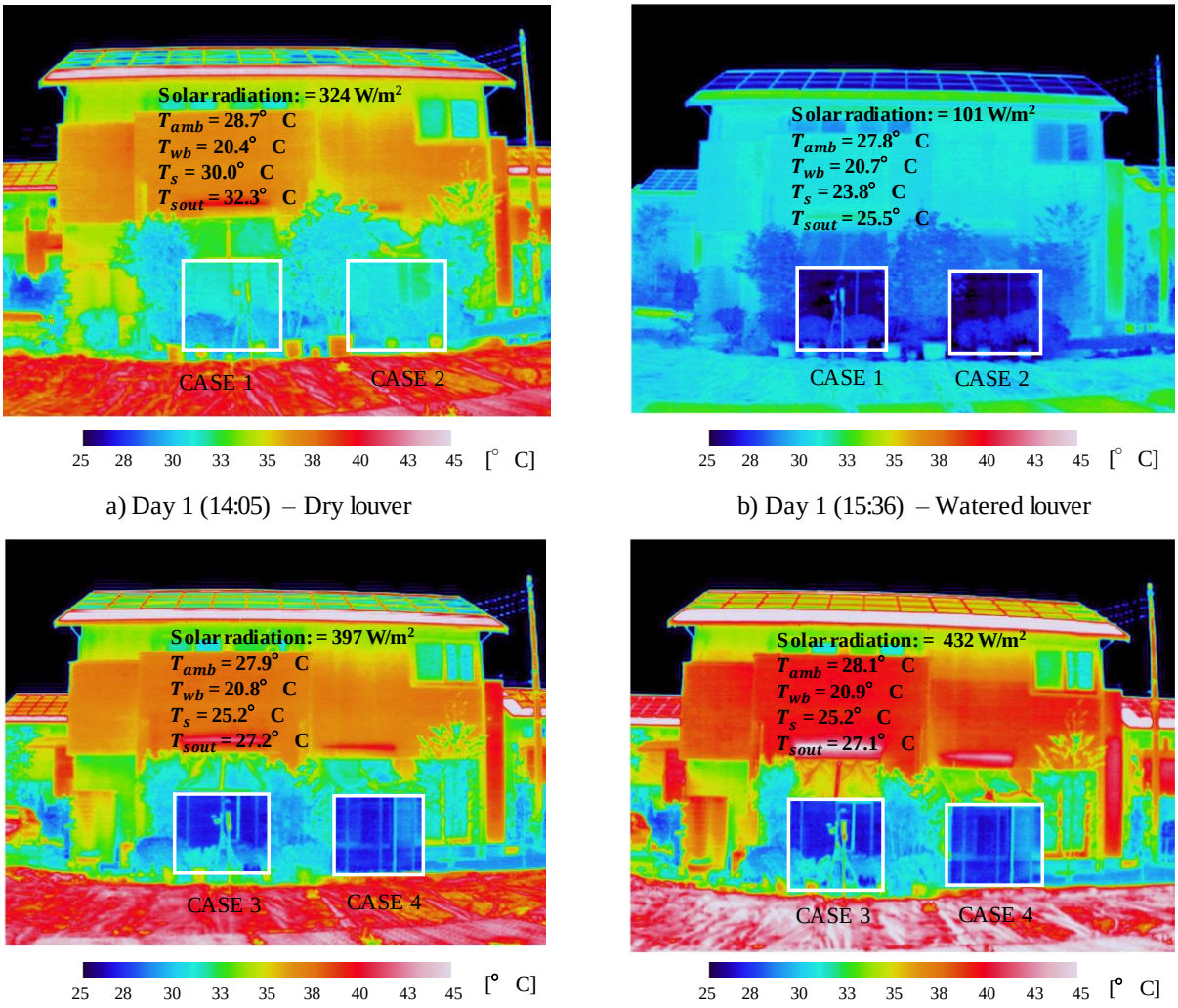

a) Day 1 (14:05) – Dry louver

b) Day 1 (15:36) – Watered louver

c) Day 2 (12:10) – Wet louver (previously watered)

d) Day 2 (12:51) – Watered louver

Figure 2.9. Thermal images for the louver under different watering conditions and solar radiation.

2.5.3. **Air temperature and wind conditions inside the semi-outdoor space**

2.5.3.1. Air temperature at the back of the louver before and after the louver is watered

Figure 2.10 shows the comparison of the air temperature at the back of the louver (T_{lo}) before and after the louver is watered for each case. It can be observed from Figure 2.10a,c that after the louver begins to be watered at 14:55 and 12:35 on Day 1 and Day 2 (Table 2.3), it takes ~5–8 min for the T_{lo} to reach to maximum reduction before it eventually stabilizes at GL + 0.1 m. After the louver is watered, the T_{lo} is reduced by 3.1, 2.6, and 3.2 °C at GL + 0.1 m for CASE 1, CASE 2 and CASE 3, respectively. In contrast, for CASE 4 (Figure 2.10d), there is no significant reduction in the T_{lo} even after the louver is watered.

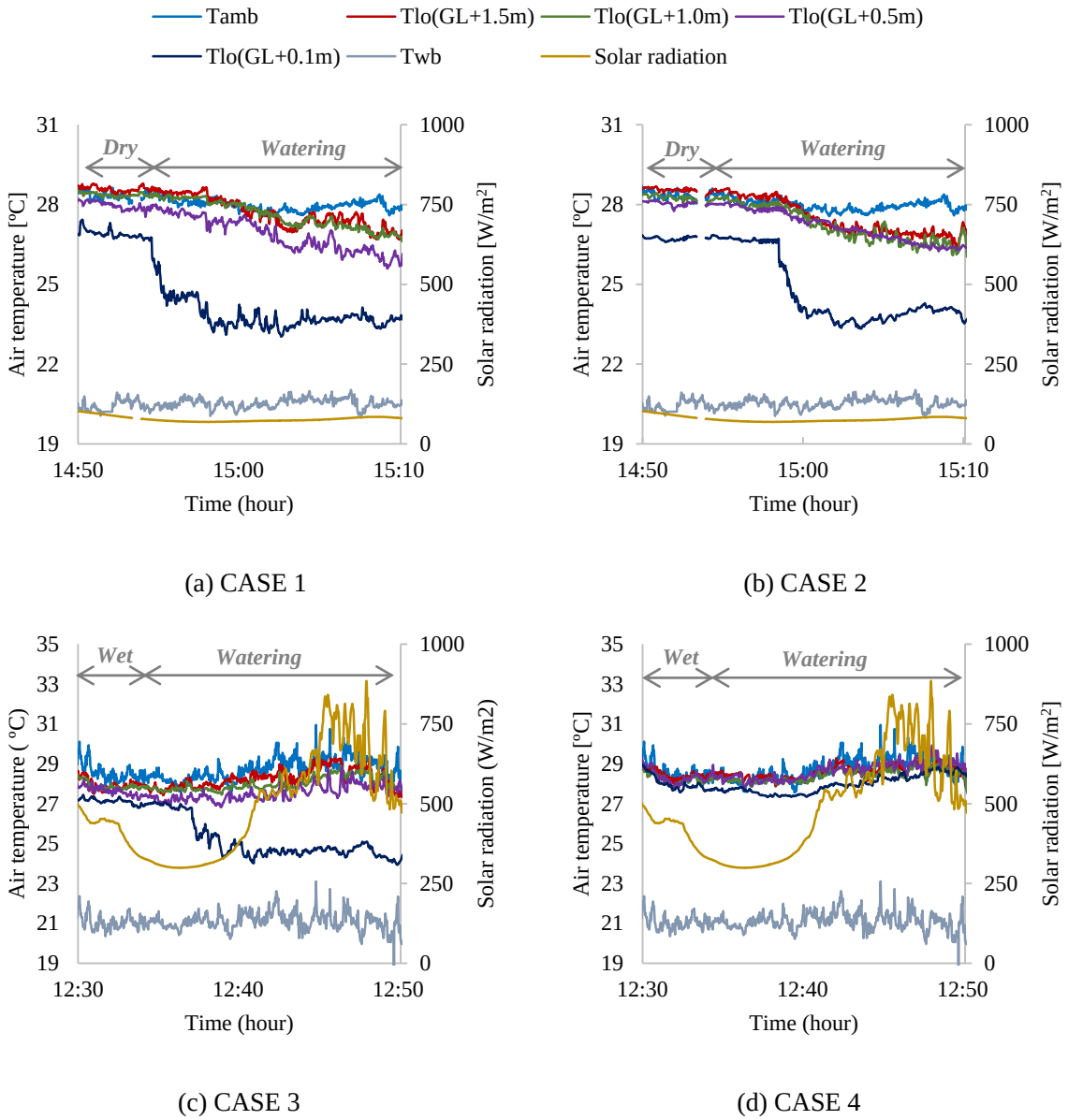

Figure 2.10. Air temperature at the back of the louver before and after the louver is watered for (a) CASE 1, (b) CASE 2, (c) CASE 3 and (d) CASE 4.

Furthermore, Figure 2.11 shows the average vertical air temperature distribution difference (T_{adiff}) between the air temperature at the back of the louver (T_{lo}) and the ambient temperature (T_{amb}) before and after the louver is watered for each case. On Day 1 for CASE 1 (Space A) Figure 2.11a shows that when the louver is dry (subcase C1) the T_{lo} is lower than the T_{amb} by 0.4–1.2 °C below GL + 0.5 m whereas the T_{lo} is higher than the T_{amb} by 0.2–0.4 °C above GL + 1.0 m. In contrast, when the louver is watered (subcases C2, C3, and C4), the T_{lo} is lower than the T_{amb} by 0.8–4.1°C at all points; i.e., from GL + 1.5 m to GL + 0.1 m. This indicates that when the louver is dry the T_{lo} is reduced due to shading effect of the PCMs whereas after the louver is watered the T_{lo} is reduced due to the evaporative cooling effect; i.e., the T_{lo} is further reduced by 1.2–2.8 °C from GL + 1.5 m to GL + 0.1 m. The result for CASE 2 (Space B) (Figure 2.11b) is similar to CASE 1, where the shading effect reduces the T_{lo} below GL + 0.5 m while the watered louver and vegetation reduces the T_{lo} at all measuring points. For CASE 3 (Space A) Figure 2.11c shows that the T_{lo} is reduced at all measuring points when the louver is wet (previously watered) (subcase C5) by 0.5–1.4°C from GL + 1.5 m to GL + 0.1 m. After the louver is watered (subcases C6, C7, and C8), the average T_{lo} is reduced by 0.2–4.1°C at all measuring points. This indicates that when the louver is watered the reduction of the T_{lo} is only 2.7 °C at GL + 0.1 m. This clearly shows the effect of solar radiation on the generation of cool air at the back of the louver because the cooling effect of PCMs is more difficult to achieve with sunny conditions (Day 2). Therefore, the evaporative cooling effect is stronger for CASE 1 (cloudy conditions) compared with that for CASE 3, which is indicated by the higher reduction of the T_{lo} from GL + 1.5 m to GL + 0.1 m. Moreover, for CASE 4 as shown in Figure 2.11d there is no significant difference in the vertical temperature distribution between wet and watered louver. When the louver is wet (subcase C5), the T_{lo} is less than T_{amb} by 0.1–0.5 °C below GL + 1.5 m and after the louver is watered (subcases C6, C7, and C8), the average T_{lo} is less than T_{amb} by 0.1–0.6 °C at all measuring points. Based on the results for CASE 1, CASE 2, and CASE 3 in Figure 2.11, the maximum reduction of T_{lo} (4.1 °C) is achieved at GL + 0.1 m - the point nearest to the ground. In contrast, the maximum reduction of 0.6 °C for T_{lo} is achieved at GL + 0.1 m for CASE 4. This demonstrates that surrounding the semi-outdoor space with vegetation improves the evaporative cooling effect at the back of the louver.

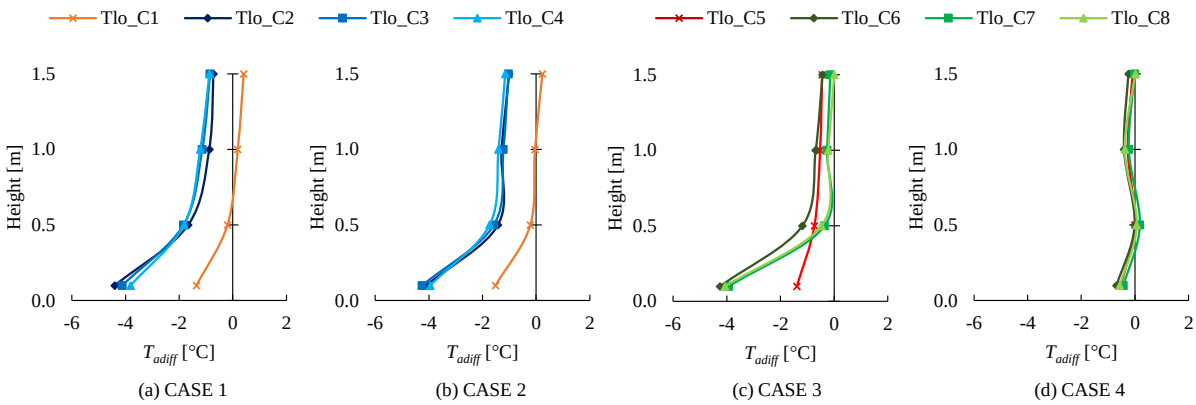

Figure 2.11. Vertical air temperature difference (T_{lo} - T_{amb}) at the back of the louver before and after the louver is watered for each case.

2.5.4. Air temperature at the center of the semi-outdoor space after the louver is watered

Figure 2.12 shows the vertical air temperature distribution difference (T_{adiff}) between the air temperature at the center of the semi-outdoor space (T_{sop}) and the ambient temperature (T_{amb}). Results in this section show the capability of each case to accumulate cool air generated by the louver in the semi-outdoor space. For CASE 1 (Figure 2.12a), the average T_{sop} is higher than the T_{amb} by 0.1°C at GL + 2.0 m when the louver is watered (subcases C2, C3, and C4) while T_{sop} is lower than T_{amb} by 0.5–2.8 °C below GL + 1.5 m. For CASE 2 (Figure 2.12b), the average T_{sop} is equal to T_{amb} at GL + 2.0 m whereas the average T_{sop} is lower than T_{amb} by 0.4–2.1°C from GL + 1.5 m to GL + 0.1 m. In contrast to Figure 2.11a-b, the cool air generated at the back of the louver tends to accumulate in the semi-outdoor space at points below GL + 1.5 m while the T_{sop} is 0.1 °C higher than the T_{amb} at GL + 2.0 m. For CASE 3 (Figure 2.12c) the average T_{sop} is higher than the T_{amb} by 0.1–1.7 °C at points above GL + 1.0 m whereas the average T_{sop} is lower than the T_{amb} by 1.0–3.3 °C at points below GL + 0.5 m for subcases C6, C7, and C8. The result difference between CASE 1 (Day 1) and CASE 3 (Day 2) demonstrates the effect of the solar radiation has on the accumulation of cool air at the semi-outdoor space. For CASE 3 heated air is accumulated in the semi-outdoor space, thus the accumulation of cool air can be seen up to point GL + 0.5 m. These results indicate in order to accumulate cool air at higher levels above the ground it is essential to protect the semi-outdoor space from high solar radiation. Moreover, for CASE 4 (Figure 2.12d),the T_{sop} is higher than the T_{amb} at all measuring points. These results demonstrate that surrounding the semi-outdoor space with vegetation

does not only improve the cooling efficiency of the louver but also keeps the cool air accumulated in the semi-outdoor space.

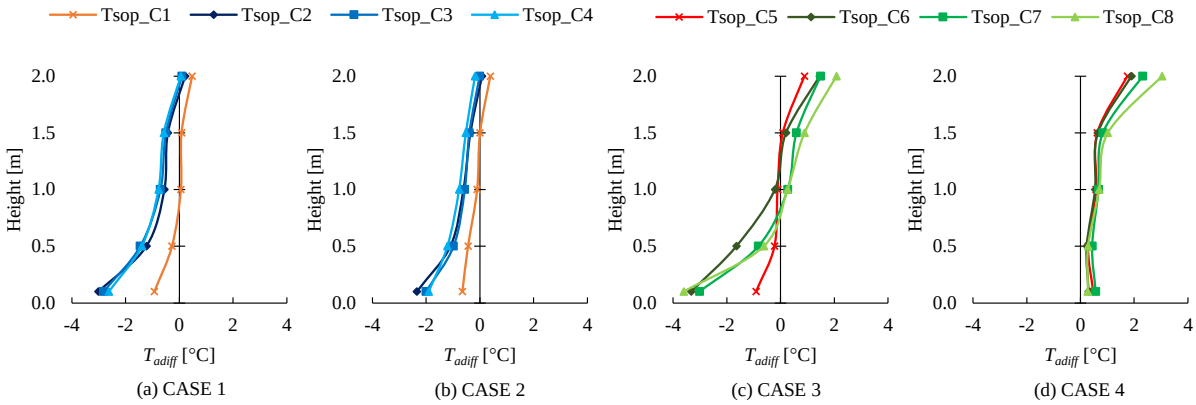

Figure 2.12. Vertical air temperature difference (T_{sop} - T_{amb}) at the center of the semi-outdoor space before and after the louver is watered for each case.

Furthermore, the effect of the distance between Space A and Space B on the accumulation of cool air generated by the louver is analyzed by comparing the difference between the air temperature at the center of the semi-outdoor space (T_{sop}) and air temperature at the back of the louver (T_{lo}) for CASE 1 and CASE 2. These cases are chosen because the T_{lo} values are similar and the primary difference between both cases is the distance between the points T_{sop} and T_{lo}. Table 2.6 shows the air temperature difference (T_{diff}) for each case, which is defined as the difference between the T_{sop} and the T_{lo}. It can be seen that the cooling effects are reduced by 0.3–1.3 °C and 0.6–2.0 °C in Space A and Space B, respectively. Thus, it can be deduced that the cool air generated by the louver is dissipated as the distance of the semi-outdoor space is increased.

Table 2.6. Relationship between the formation of cool microclimate and the distance between the center of the semi-outdoor space and back of the louver.

Distance between the measuring point T_{lo} and T_{sop}	Space A = 0.5 m			Space B = 1.4 m		
Case	CASE 1			CASE 2		
Height	T_{lo} [°C]	T_{sop} [°C]	[T_{diff}] [°C]	T_{lo} [°C]	T_{sop} [°C]	[T_{diff}] [°C]
GL + 1.5 m	26.9	27.2	0.3	26.7	27.3	0.6
GL + 1.0 m	26.7	27.1	0.4	26.4	27.1	0.7
GL + 0.5 m	26.0	26.4	0.4	26.2	26.6	0.5
GL + 0.1 m	23.6	24.9	1.3	23.6	25.6	2.0

2.5.5. Wind speed at the center of the semi-outdoor space

Figure 2.13 shows the wind conditions outside and inside Space A. As shown in Figure 2.2 and Figure 2.5, Space A (CASE 1) and Space B (CASE 3) even though both are fully surrounded by vegetation, the arrangement of the potted plants is different. Wind conditions for CASE 1 indicate that the average WS_{out} is 0.6 m/s and the average WD_{out} is SSE. In contrast, the wind conditions change inside the semi-outdoor space (Space A), where the average WS_{sop} is reduced to 0.3 m/s and the average WD_{sop} changes to WSW. For CASE 3, the average WS_{out} is 0.7 m/s and the average WD_{out} is south. In contrast, the value of WS_{sop} increased to 0.8 m/s and the average WD_{sop} remained as south. Therefore, there is reduction of wind speed in Space A for CASE 1 whereas there is no reduction of wind speed for CASE 3. This difference is likely because in CASE 1, a tall potted plant (Quercus glauca) blocks a portion of the louver whereas in CASE 3, the louver is completely exposed and therefore, the wind passes through the louver slats at a higher speed. These results show the importance of arrangement of vegetation when using the evaporative cooling louver to maximize the wind passing through the louver salts.

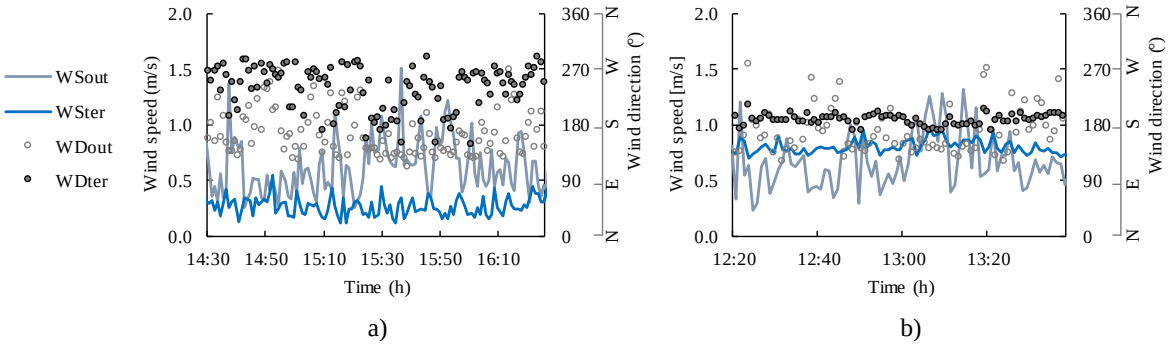

Figure 2.13. Wind speed and wind direction outside and inside Space A for (a) CASE 1 and (b) CASE 3.

2.5.6. Air temperature and wind speed inside the window based on ventilation settings

2.5.6.1. Induction of cool air

Figure 2.14 shows the variation in air temperature inside the window for different ventilation settings (Table 2.3). For CASE 1 and CASE 2 on Day 1 when the louver is dry (subcase C1) values of T_{win} are equal. After the louver is watered (subcases C2, C3, and C4), the average T_{win} in CASE 1 is reduced by 0.1–0.5 °C at all measuring points in contrast to CASE 2. Thus, even though T_{sop} for CASE 1 and CASE 2 is similar,

T_{win} was not reduced because T_{win} is higher than T_{amb} (Figure 2.14b). This suggested that the cool air accumulated in Space B was dissipated before it reached the window; due to the combination of the large louver window (L-W) distance and the amount of vegetation that partially surrounded the semi-outdoor space. Moreover, as shown in Figure 2.14c-d, when the louver is wet (subcase C5), the T_{win} values for CASE 3 are lower than those for CASE 4 by 0.5–0.6 °C at points below GL + 2.0 m on Day 2. However, the value of T_{win} is 0.4 °C higher at GL + 2.5 m. This result implies that the solar radiation had a larger effect on CASE 3 compared with that in CASE 4, where the perpendicular wall may have provided added shade to the window. Moreover, when the louver is watered (subcases C6, C7, and C8), the average T_{win} values for CASE 3 are lower than those for CASE 4 by 0.6–0.9 °C at points below GL + 2.0 m, while the average T_{win} is 0.9 °C higher at GL + 2.5 m. The results confirm the induction of cool air for CASE 1 and CASE 3. The lack of induction of cool air for CASE 2 and CASE 4 is likely because the large L-W distance in Space and amount of vegetation in CASE 2, whereas Space B in CASE 4 is not surrounded by vegetation at all. Thus, both configurations affected the accumulation of cool air generated by the watered louver, and the cool air did not reach the window.

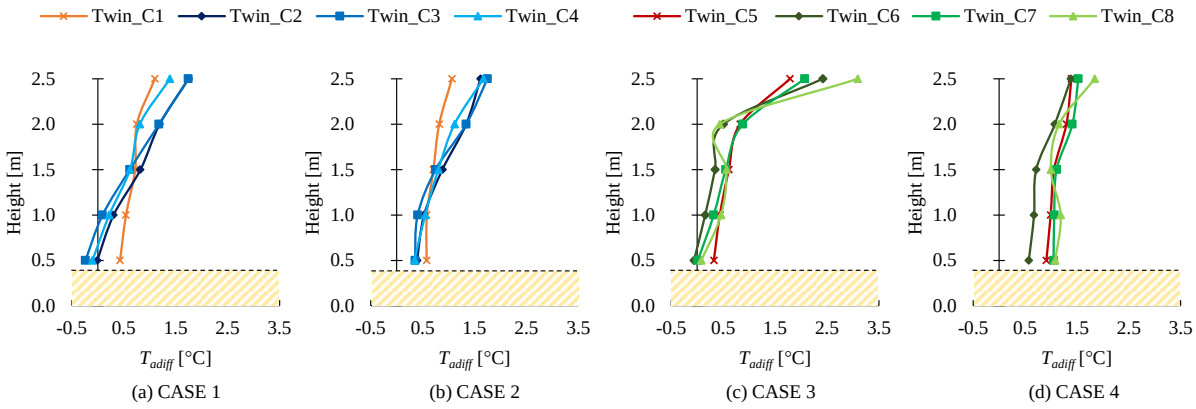

Figure 2.14. Vertical air temperature difference ($T_{win} - T_{amb}$) inside the window before and after the louver is watered for each case.

2.5.7. **Effect of ventilation settings on the wind speed**

Figure 2.15 shows the variation of wind speed inside the window (WS_{win}) for different ventilation settings. It can be observed from Figure 2.15a-b that the WS_{win} at GL + 0.7 m increases by 0.05 m/s with blower door (subcase C3) compared to that with open kitchen door (subcase C2). This indicates that when the rate of air change between rooms is increased, the wind speed of the cool air crossing the window increases, which confirms the importance of using indoor cross ventilation for improving natural ventilation. Furthermore, it is found that the wind speed is influenced by the window area. When the window is half open (subcases C2, C3, C6, and C8), the WS_{win} is ~0.10 m/s at GL + 2.2 m, indicating that there is almost no air crossing the window in that area due to the shutter. Under the shutter (GL + 1.4 m and GL + 0.7 m), the average WS_{win} values are 0.20 and 0.15 m/s for Space A and Space B, respectively. In contrast, when the window is fully open, there is a slight variation of the wind speed from GL + 2.2 m to GL + 0.7 m, where the average WS_{win} values are 0.20 and 0.15 m/s for the window in Space A and Space B, respectively. This indicates that the incoming wind speed is generally higher for the window in Space A compared to that for Space B.

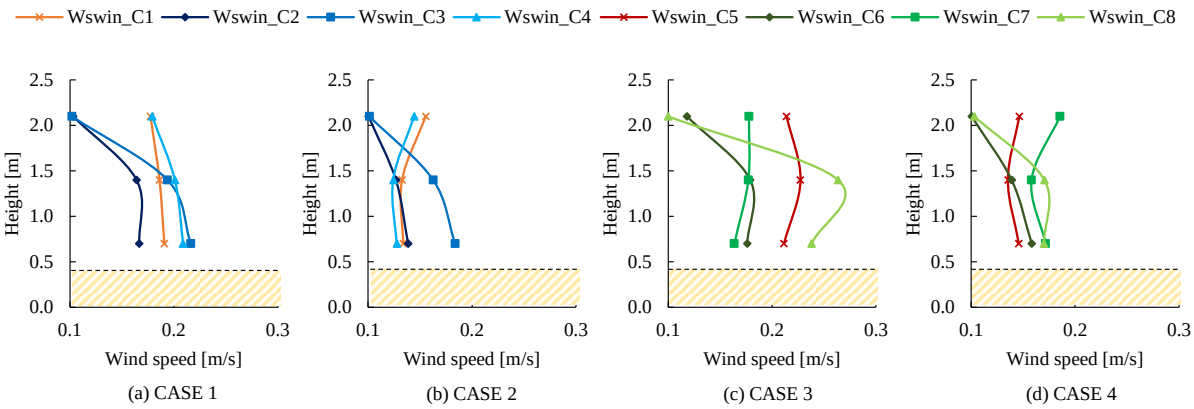

Figure 2.15. Wind speed inside the window before and after the louver is watered for each case.

2.5.8. Effect of ventilation settings and wind speed on the air temperature

Figure 2.14 and Figure 2.15 show the air temperature difference and wind speed inside the window for each case based on the ventilation settings. The air temperature difference is defined as the difference between the air temperature inside the window (T_{win}) and the ambient temperature (T_{amb}). Figure 2.14a-c show that the T_{win} values are higher when the window is half open (subcases C2, C3, C6, and C8) compared with those when the window is fully open (subcases C4 and C7) at points above GL + 2.0 m. This confirms that the presence of shutter increases the T_{win} values on both days due to the lack of ventilation. In contrast, there is a reduction of the T_{win} values when the window is fully open because there is ventilation across the window, which helps keep the air temperature inside the window cooler. Moreover, at points below GL + 1.5 m, the induction of cool air for CASE 1 is improved when the window is half open (subcase C3) and the WS_{win} is 0.22 m/s. This shows that the induction of cool air improves as the wind speed increases for CASE 1. For CASE 3, the indoor air is kept cooler when the window is half open (subcase C6) and the WS_{win} is less than 0.2 m/s. The T_{win} increases when WS_{win} exceeds 0.2 m/s, where the window is half open (subcase C8). This is because the cool air at T_{sop} is accumulated near the ground below GL + 0.5 m, thus when wind crossing the window is higher, the hot air is induced. This confirms cool outdoor microclimate is necessary in order to improve indoor microclimate.

2.6. Analysis of results

2.6.1. Cool microclimate formation in the semi-outdoor space.

2.6.1.1. Effect of solar radiation

The effect of solar radiation on the formation of cool microclimate at the semi-outdoor space is apparent by comparing the results for CASE 1 and CASE 3 (Figure 2.12a, c). For CASE 3 the T_{sop} values were higher than those for CASE 1 by 0.3–1.6 °C from GL + 0.5 m to GL + 2.0 m, even though the semi-outdoor space is fully surrounded by vegetation in both cases. Thus, the height of accumulated cool air is higher by 1.0 m for CASE 1 (low solar radiation) compared with that for CASE 3 (high solar radiation). The discrepancy between CASE 1 and CASE 3 is likely due to the difference in the amount of solar radiation, which heats both the sunscreen and window. Hence, the heated air accumulates in the semi-outdoor space, which limits the formation of cool air below GL + 0.5 m on Day 2. Hence, in order to accumulate cool air at higher levels

above the ground, it is essential to protect the semi-outdoor space from high solar radiation by applying an alternative horizontal shading device.

2.6.1.2. Effect of louver window distance

The effect of louver-window (L-W) distance on the formation of cool microclimate is evident by comparing the results for CASE 1 and CASE 2 on Day 1 because the space between T_{lo} (Figure 2.11) and T_{sop} (Figure 2.12) is surrounded by vegetation for both cases. However, the distance between the louver and center of the semi-outdoor space is different for both cases. Table 2.6 shows the air temperature difference ($T_{sop} - T_{lo}$) for CASE 1 and CASE 2. The results showed that the cooling effects are reduced by 0.3–1.3 °C and 0.6–2.0 °C for CASE 1 and CASE 2, respectively. This indicates that the cool air generated by the louver is dissipated when the distance between the louver and center of the semi-outdoor space is increased. Hence, in order to utilize the cool air generated by the PCMs for natural ventilation, a shorter L-W distance is recommended. Wong et al. (cited by [51]) found that the cooling effect increased with a temperature reduction of 3.3 °C when the distance between the living wall system (LWS) and the wall was 15 cm. In contrast, they found that the temperature reduction was reduced to 1.6 °C when the distance between the LWS and the wall was increased to 30 cm. Likewise, Chen et al. [52] found reducing the distance between the LWS and wall surface resulted in higher cooling effect. In contrast, a larger L-W distance was used in this work compared with those in previous studies, which indicates that the distance and surrounding vegetation also affects the accumulation of cool air at the semi-outdoor space. Furthermore, the combination of L-W distance and vegetation surrounding the semi-outdoor space has a direct effect on the formation of cool microclimate. Although the T_{sop} values for CASE 1 and CASE 2 are similar, the cool air in the semi-outdoor space does not reach the window for CASE 2 (Figure 2.14b) because Space B distance is larger and is partially surrounded by vegetation and thus, the cool air is dissipated. In contrast, Space A (which is fully surrounded by vegetation) is shown to have the highest accumulation of cool air generated by the louver. Moreover, as seen in Figure 2.13 the presence of vegetation reduces the wind speed, which confirms well with the results of Lee et al. [15], who concluded that the wind speed outside the window is reduced by placing potted plants close to the window. The presence of plants and watering created a cool air which flowed into the indoor space during the daytime. Similarly, the results obtained in this study showed that the formation of cool microclimate is significantly improved significantly when the semi-outdoor space is fully

surrounded by vegetation. This might be owed to the fact that the vegetation may be prevent the cool air from dissipating.

2.6.1.3. Effect of the wind speed

In a previous research Hirayama et al. (2018) analyzed the individual effects of the louver and vegetation on the wind speed and air temperature reductions [25]. Results showed that wind speed reduction was approximately 20 % when using the individual louver and vegetation, and the reduction in air temperature was 0.8-1.1°C when watered. It was concluded that the louver and vegetation contribute toward a decrease in air temperature, rather than the wind speed. In this study, the wind conditions inside the semi-outdoor space were only recorded inside Space A. Therefore, the effect of wind speed on the air temperature could be seen in CASE 1 and CASE 3. In CASE 1, the wind speed reduced from 0.6 m/s to 0.3 m/s between the outside and inside of the semi-outdoor space, and a reduction in air temperature was observed below GL + 1.5 m in the semi-outdoor space when the louver was watered. In contrast, in CASE 3, the wind speed did not change between the inside and outside of the semi-outdoor space, and the reduction in air temperature was observed only below GL + 0.5 m in the semi-outdoor space. Therefore, there was a trade-off relation between the reduction in wind speed and that of the air temperature for these cases. However, despite CASE 1 and CASE 3 being configured with surrounding vegetation; the amount of solar radiation was different. Hence, if compared, the effect of wind speed cannot be definite. This is because solar radiation is already affecting the formation of cool air and the air temperature inside the window in Space A, as seen above in GL+0.5 m in Figure 2.12c and GL+2.5 m in Figure 2.14c, respectively.

2.6.2. **Induction of cool air**

Based on the results shown in Figure 2.14, induction of cool air can be seen for CASE 1 and CASE 3, where both semi-outdoor spaces have a short L-W distance and is fully surrounded by vegetation, which facilitates the formation of cool air until the window. The induction of cool air is most pronounced for CASE 1 (subcase C3), where the window is half open and a blower door is used. This results in the highest reduction of T_{win} while the WS_{win} is increased to 0.22 m/s at the point nearest to the floor (GL + 1.5 m or FL + 0.1 m). However, the T_{win} increases at the points above GL + 1.5 m, which indicates that the lack of ventilation worsens the indoor air temperature. The best results are obtained when the window is fully open (subcase C4), which provides ventilation through the window. This provide a cooler vertical T_{win} distribution unlike

where the window is half open. Based on the results for CASE 1, the induction of cool air can be improved if the wind speed of the air across the window is more than 0.2 m/s. However, for CASE 3, the high solar radiation reduces the cool air formed in the semi-outdoor space. Thus, the indoor air is kept cooler when the WS_{win} is less than 0.2 m/s and the window is half open (subcase C6). According to Toe and Kubota [42], the indoor air temperature can be reduced during the daytime by minimizing cross ventilation with the hot outdoor air, which maintains a relatively low indoor air temperature. Hence, in order to maintain a cool indoor air temperature at all times, it is necessary to monitor the air temperature outside the window. The wind speed of the air crossing the window needs to be increased in order to induce cool air into the house, which can be achieved by promoting cross ventilation indoors with the window fully open. However, to prevent the induction of hot outdoor air into the house, it is crucial to restrict cross ventilation indoors by closing the doors and leaving the shutter or window half open. This reduces the wind speed of the air crossing the window, which helps maintain a cooler air distribution indoors. Moreover, shutting the window completely is undesirable on sunny days with high solar radiation because this will significantly increase the indoor air temperature. This is confirmed by the T_{win} values at points above GL + 2.0 m when the window is half open. Shutting the windows completely can also affect the indoor air quality.

2.7. Summary

A field measurement was carried out to find the best configuration of PCMs to improve the outdoor and indoor microclimate of a passive cooling house during hot and humid summer in Japan. The PCMs included an evaporative cooling louver, vegetation, and sunscreen installed outside two windows in the southwest façade of the house. In addition, ventilation settings were implemented simultaneously to evaluate the induction of cool air into the indoor space. Among the cases studied, CASE 1 exhibited the best PCMs configuration to create a cool microclimate at the semi-outdoor space, with the combined effect from (1) watered louver (2) semi-outdoor space fully surrounded by vegetation, (3) shorter louver-window distance (1 meter), (4) sunscreen, and (5) low solar radiation. In contrast, the worst results were obtained in CASE 4, which was expected as the semi-outdoor space was exposed to high solar radiation, was not surrounded by vegetation, and had a large louver-window distance (2.8 m). Moreover, for CASE 1, the air passing through the watered louver was decreased by approximately 1.0-4.0 °C from 1.5 m to 0.1 m above the ground,

respectively. In addition, low solar radiation showed a better cool microclimate formation, 0.5-3.0 °C, up to 1.5 meters at the center of the semi-outdoor space. In contrast, when exposed to high solar radiation, the cooling effect of the louver was 1.0−3.0 ° C, up to 0.5 m above the ground. This demonstrates that protecting the semi-outdoor space from solar radiation can significantly improve the formation of cool air. This includes surrounding the semi-outdoor space with vegetation. The presence of vegetation reduced the air temperature passing through the louver by 0.1−3.5 ° C (CASE 3) compared with those for the case with no surrounding vegetation (CASE 4). Hence, no cool air was formed in CASE 4. Moreover, the cooling effect of the louver is dissipated as the louver-window distance increase (from CASE 1 to CASE 2). Thus, a shorter louver window distance (1-m) showed to be more effective for cool microclimate formation because the cool air generated by the louver could be accumulated until the window.

With respect to ventilation settings, their effects varied according to the microclimate formed at the semi-outdoor space. For cool outdoor air (CASE 1), opening the window fully and a wind speed above 0.2 m/s induced cool air. However, a minimal wind speed and half-open window was preferable when the outdoor air was hot (CASE 3) which kept the indoor air temperature cooler. The ventilation settings showed that it is possible to control the wind speed passing through the window, with improving indoor cross ventilation which increased the wind speed passing through the window. This indicates the importance of indoor cross ventilation in improving natural ventilation and induction of cool air.

CHAPTER 3. MODELING AND VALIDATION OF PASSIVE COOLING METHODS FOR CFD SIMULATION

3.1. Background

3.1.1. Limitations of the field measurement

In this chapter, the data obtained in the field measurement is used to validate a CFD model. Previous field measurements (Chapter 2) showed that cool microclimate can be formed in a semi-outdoor space using combined PCMs under certain conditions (e.g. CASE 1). However, the cool outdoor microclimate formed at the semi-outdoor space was not properly induced for improving the indoor microclimate with natural ventilation. Therefore, further studies need to be carried out in order to evaluate in detail the effects of the outdoor microclimate generated by PCMs and effects of indoor conditions. Field measurements are generally performed at a limited number of points, thus only the investigated variables can be analyzed. Meanwhile, numerical simulation can provide detailed information on any investigated variable in the entire computational domain [cited by [33]. Field measurements can be used for validating the CFD model. Therefore, the validated CFD model can be used to performed comparative analyses based on different scenarios.

3.1.2. Previous studies using numerical simulation to evaluate the effects of outdoor and indoor microclimates.

There has been considerable research focusing on urban microclimate modeling and its validation. Microclimates formed by surrounding buildings [53,54], vegetation [55,56], and cool materials [57] have been simulated using numerical models in urban spaces; this enables the assessment of their effects on human thermal comfort [58]. However, most the microclimate simulations target a specific height around 1–2 m from the ground and discuss the two-dimensional (2D) horizontal distribution of these microclimates.

Numerical simulations have been also applied to assess the thermal and energy performance of buildings, including the effects of envelope materials (e.g., wall materials, phase change materials) [59–61]. There has also been intensive research into numerical simulations to evaluate the effects of outdoor microclimates on the indoor environment as passive cooling techniques [62]. This includes evaluation of the

effects of the outdoor radiation environment on the solar heat gain of buildings [3,63], the outdoor wind environment on the natural ventilation of buildings [64–66], the outdoor microclimate on building thermal performance [67–69] and energy demands [2,70–75], and outdoor overheating, including urban heat islands, on the energy demand of buildings [5,76]. In particular, vegetation models have been applied to numerical simulations to evaluate solar shading [16,77–79], wind break [6], and overall cooling effects [80,81] derived from vegetation on the indoor thermal environment. The effects of cool pavements and materials on building energy use and thermal environment have also been evaluated [82,83]. However, there has been limited discussion on the effects of cool microclimates for a spatial scale less than 1 m, with the detailed vertical distribution formed by vegetation and cool materials. Furthermore, the combined effect of multiple elements (e.g., vegetation and cool materials) has received less attention [15]. This is primarily due to the complexity of calculating two semi-independent spaces (outdoor and indoor) simultaneously, whilst considering the physical phenomena at the surface and in the vicinity of space components. Thus, there is clearly a gap of numerical simulations that study outdoor and indoor microclimate simultaneously. There has been insufficient modeling and validation of CFD simulation of microclimate formed by combined PCMs.

3.2.Methodology

3.2.1. **CFD simulation**

A numerical CFD technique was chosen to conduct the simulations. scSTREAM (MSC software, Tokyo, Japan) commercial software is used to solve the steady Reynolds-averaged Navier–Stokes (RANS) equations in order to evaluate the average flow and temperature fields during the target evaluation time. Most natural ventilation studies presented in the past have used the RANS approach [38]. To assess the performance of RANS, detailed validation studies are required using high-resolution, well-defined and well-documented reduced-scale or full-scale experiments [38]. The non iso-thermal calculation is conducted with a buoyancy effect by using the Boussinesq approximation. Our research uses the coupled indoor–outdoor CFD simulation (Figure 3.1); i.e., performed at multiple scales by combining building and indoor scales, because it resolves the outdoor and indoor wind flow within the same computational domain and is able to capture the dynamic interaction between the outdoor and indoor environment at the window openings [84] – ideal to conduct natural ventilation studies [33]. A study by Straw et al. (2000) [85] reported in their publication that coupled indoor–outdoor CFD simulation provided more accurate results.

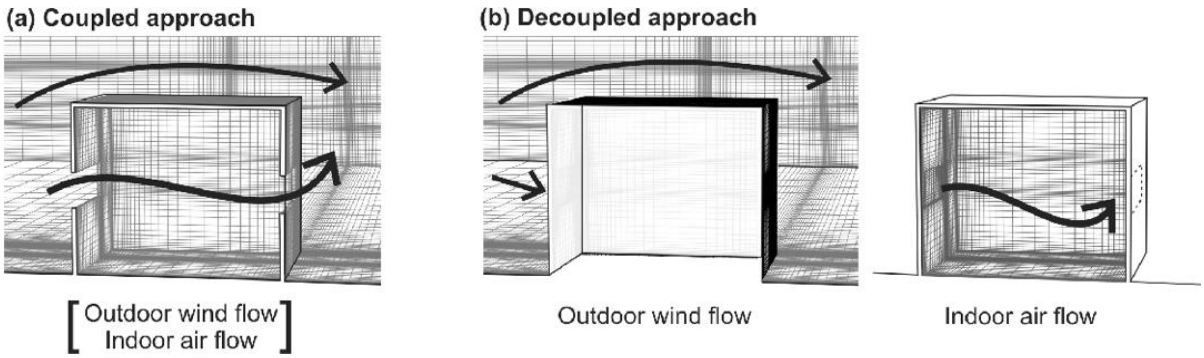

Figure 3.1. (a) Coupled and (b) decoupled approach for analysis of natural ventilated buildings [86]

3.2.2. Field experiment case selected for the validation of the CFD model

Among the several cases reported in the field measurements (Chapter 2), CASE 1 CASE 2 subcase C4 (Table 2.3) was used to validate the CFD simulation. This experimental case was selected as the PCMs and the ventilation settings with windows fully open were set to maximize the cooling effect with natural ventilation. Figure 3.2 shows the floor plan of the case study with the experimental settings of the selected case as follows: (1) the analysis area where air flows inside the house; (2) the openings for inflow (sliding windows), flow between rooms (kitchen door), and outflow (ceiling window); (3) the target area, comprised of the semi-outdoor spaces (Spaces A and B) and the indoor space. The air passing across the rooms and the kitchen door would flow out through the ceiling window located on the stair hall (Figure 3.2b). These conditions were used to validate the numerical simulation (Figure 3.3).

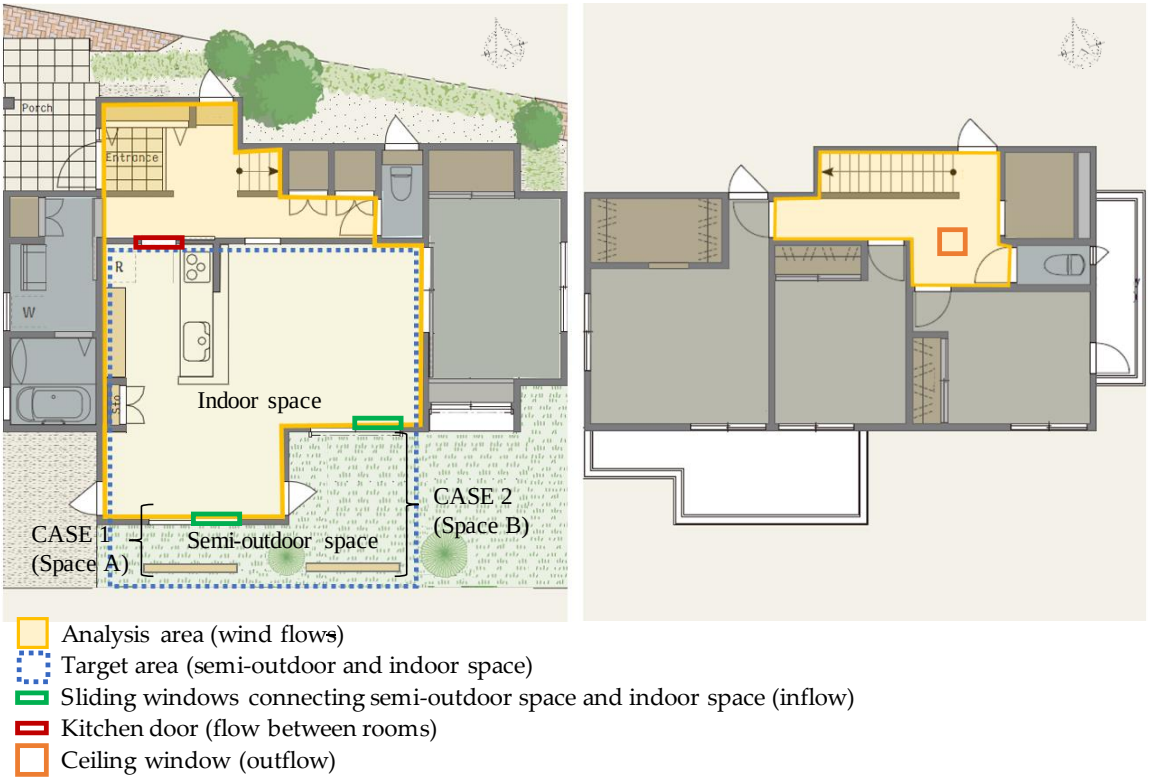

Figure 3.2. Experimental settings of CASE 1 and CASE 2 subcase C4 selected for validation of CFD model.

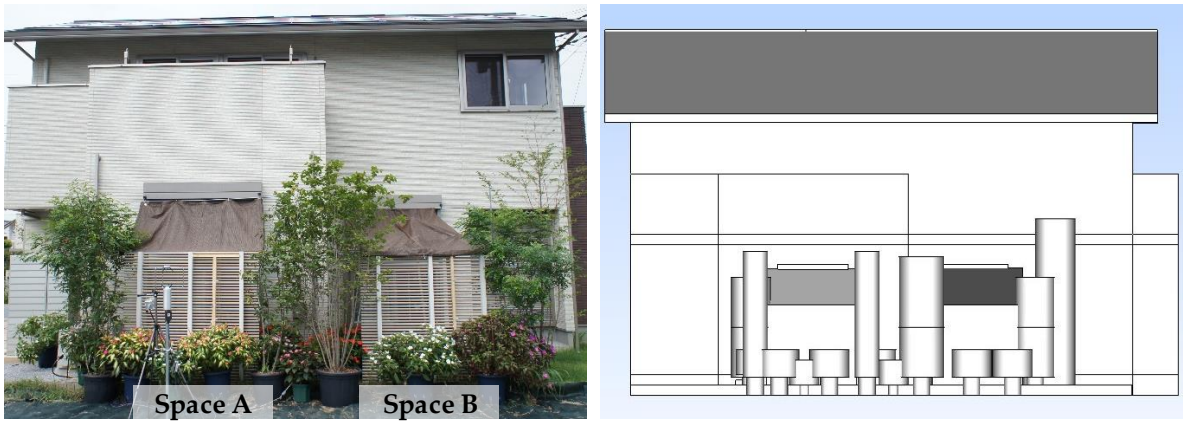

(a) **(b)**

Figure 3.3 View of PCMs in semi-outdoor spaces: (a) the field measurement and (b) the simulation.

3.2.3. **Modeling the building inside CFD software.**

Figure 3.4 shows the flow chart of the research method for the validation. As observed collected information such floor plans of the house, photography and in situ measurement were used to build the 3D building model. The building in the case study was modeled directly into the CFD software, combining building and indoor scales (multiple scale) which enables researchers to conduct coupled analysis – for natural ventilation studies [cited by [33]. Figure 3.5b shows the building model (exterior walls, roof, indoor partitions, kitchen counters, and PCMs. In addition, the measurement points are placed in similar locations to the field experiment for comparison of air temperature and wind speed. After the trial and error process showed in the appendix section (Figure 0.14) it is found that using multiple measurement points instead of single measurement points has a better accuracy when comparing field measurement data with validation data because it captures the actual air temperature around the measurement point.

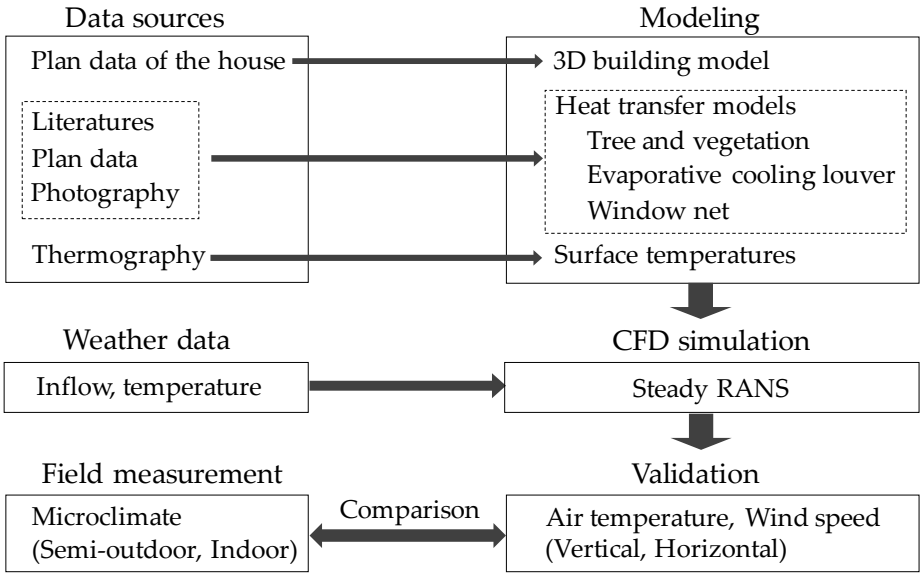

Figure 3.4. Flow chart of research method.

3.2.4. **Computational geometry, domain and grid**

Table 3.1 lists the calculation conditions used for the simulation. The size of the computational domain (calculation area), shown in Figure 3.5, was based on the best practice guidelines for CFD set by Franke et

al. [87], Tominaga et al. [88], and Blocken [89], that is, a distance of 5H from the building to the top and sides of the computational domain and a distance of 15H between the building and the outlet boundary downstream of the building [38]. The resulting dimensions of the domain are shown in Table 3.1. To predict the flow field around a building with acceptable accuracy, a fine grid arrangement is required to resolve the flows near the corners, with a stretching ratio of the adjacent grid of 1.3 or less [88]. A relationship also exists between the size of the mesh and convergence. Moreover, because the building model is complex and there are some materials with large aspect ratio 100-mm mesh was used, as shown in Table 3.1. Furthermore, the computational domain was discretized by a hexahedral mesh containing approximately 12 million elements, with an expansion ratio of 1.1.

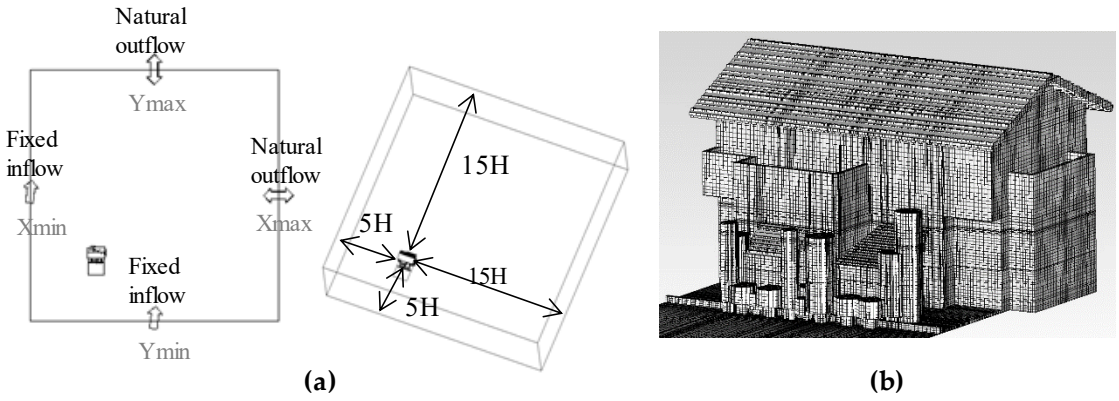

Figure 3.5. (a) Computational domain and flow boundaries; (b) building model and cell division.

Table 3.1. Computational settings.

Calculation area	133.9 m (x) x 123.9 m (y) x 43.2 m (z)
Expansion ratio	1.1
Mesh size	0.1 m x 0.1 m x 0.1 m
Number of elements	12,723,092
Turbulence model	Standard k-model
Inflow boundary	Fixed velocity X component: 0.29 m/s Y component: 0.95 m/s Z component: 0 m/s
Outflow boundary	Natural outflow
Wall boundary	Upper boundary: Freeslip Ground boundary: Nonslip
Scheme for convection terms	QUICK
Convergence criteria	1E-5 for all variables
Cycles	1000

3.2.5. **Boundary conditions**

3.2.5.1. Setting the inflow conditions

Setting the inflow conditions for an isolated building is one of the most crucial parts because of the replication of flow fields. The simulation for an isolated building condition can be comparable to the experiment in the site because at the moment the field experiment was conducted, there was no building facing the semi-outdoor space and windward windows – thus there was no obstruction of air flow. In order to evaluate the microclimate in the semi-outdoor space and cooling effects into indoor thermal environment using CFD simulation, wind conditions (direction and speed) at these spaces are important. Therefore, in order to find the most optimal wind direction and speed, the rose wind shown in Figure 3.6 and Figure 3.7 are analyzed (for location of measurement points refer to Table 2.5). As observed the average outdoor wind speed and direction is 0.6 m/s at SSE (164 degrees). Several simulations for validation (Appendix Section A.2) of the case were carried out with average wind directions, however this did not replicate the outdoor and indoor microclimates. In contrast to the results from the field experiment shown in Figure 3.7, when SSE was set as the fixed inflow, the window for Space B acted as windward and Space A as leeward. Moreover, during the validation process using average wind speed for fixed inflow did not replicate the value at WS_{out}. Thus, using predominant outdoor wind speed and directions for an isolated building was not a good approach. Several trials and errors were conducted to find the appropriate wind direction that replicates incoming wind for windows in Space A and Space B, together with the formation of cool microclimate at the semi-outdoor space. Therefore, in the CFD simulation, appropriate inflow boundary conditions were set to fit the wind conditions in both spaces (i.e., WS_{out},WS_{win}) to the field experiment. As a result, it was found that setting the inflow conditions to SSW at 1 m/s replicates the accumulation of cool air at the semi-outdoor space and the induction of cool air in the field experiment (result section). Thus, fixed inflow is set at the inflow boundary (Xmin, Ymin). A velocity of 1 m/s (maximum WS_{out} recorded during the case) is set at a height of 1.5m. The wind direction is SSW (197 degrees) the coordinates for X and Y are 0.29 m/s and 0.95 m/s, respectively, for obtaining a velocity of 1 m/s (see Table 3.1). Moreover, 197 degrees is the average value of the maximum and minimum WD_{out} value recorded in the selected case from the field measurement. In addition, the average relative humidity recorded of 56% is set. For the turbulence model, the standard k-ε model is used, thus the turbulent kinetic energy and dissipation is set as 0.173 m2/s2 and 0.0069 m2/s3, respectively. Natural outflow is set at the outlet boundary (Xmax and Ymax).

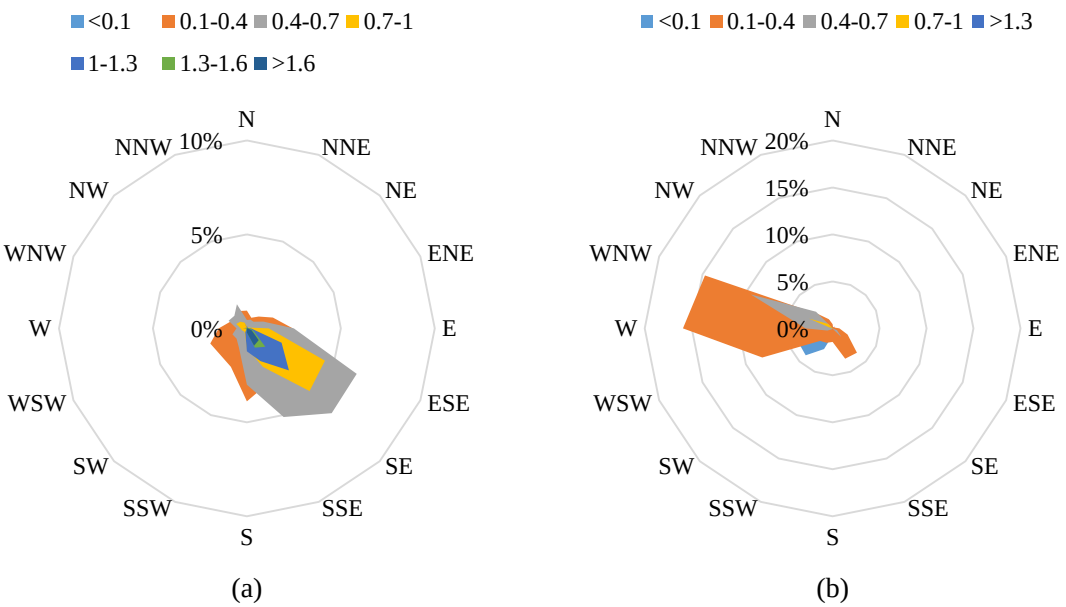

Figure 3.6. Rose wind for the (a) outdoor space and (b) semi-outdoor space for CASE 1 CASE 2 subcase C4.

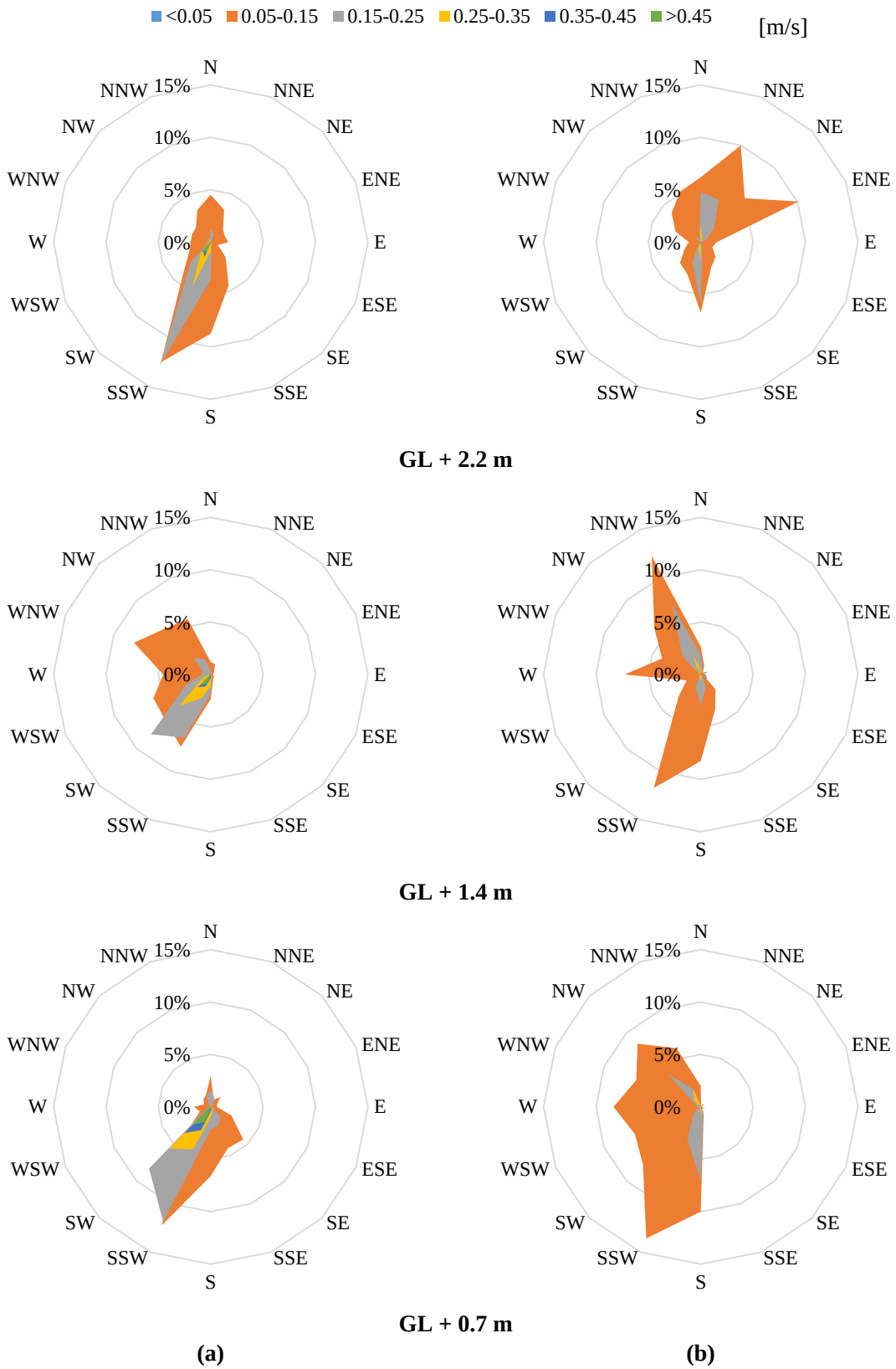

Note: Air velocity at 0.05 m/s is stagnant.

Figure 3.7. Rose wind for the incoming wind speed to the indoor space for (a) Space A and (b) Space B for CASE 1 CASE 2 subcase C4.

3.2.5.2. Setting wall boundary conditions

For the ground boundary, the log law condition was applied to the flow fields. For the top boundary of the computational domain, a symmetry boundary condition (slip wall) was used.

3.2.5.3. Setting thermal boundary conditions

The surface temperature of the building elements was based on thermal images (Figure 3.8) taken by an infrared camera (Thermo GEAR G100, Nippon Avionics Co., Ltd., Tokyo, Japan) during the experiment. The heat transfer coefficients used for the outdoor and indoor geometry were 11.6 W/m^{2}k and 9.5 W/m^{2}k, respectively [90], which included the effect of solar radiation. Appendix section 2.3 (Table 0.2) shows how the thermal boundary conditions were set for each part of the building.

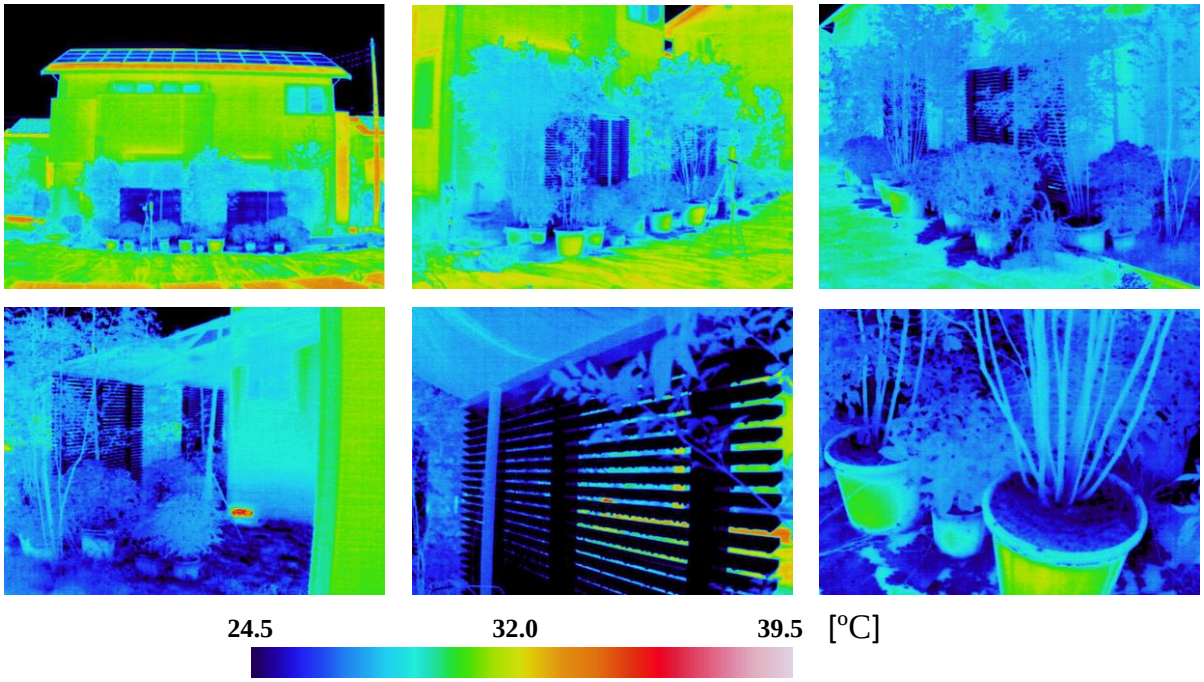

Figure 3.8. Thermal image used to estimate the surface temperature. Left to right: Southwest façade; Space A; Space B; Inside Space B; Louver and sunscreen; pots, soil and vegetation.

3.2.6. **Detailed modeling**

3.2.6.1. Modeling of plants

Plants were modeled with the same sizes and locations as the experiment using a cylindrical shape, as shown in Figure 3.9 and Table 3.2. As shown in Table 3.2, the leaf area density (LAD) and drag coefficient (C_d) were estimated by observing the foliage density of each type of plant using photos taken during the experiment. Accordingly, different LAD and C_d were assigned to each foliage density found (high-density

type 1 (HD1), high-density type 2 (HD2), low-density type 1 (LD1), high-density type 3 (HD3), and low-density type 2 (LD2). The values used for LAD and Cd of plants and trees were based on the resistance [91] and turbulent model B by Mochida (2008) [92] (see Table 3.3). For the ground cover inside the semi-outdoor space (HD3 and LD2), as the surface temperature is significantly lower than that of plants (refer to Figure 3.9), LAD and Cd were estimated to achieve a higher cooling effect than the plants due to the watered soil. A previous study [93] showed that the average porosity for various tree densities was 0.91, 0.69, and 0.42 for one, two, and three trees, respectively. When porosity is reduced, more flow is forced around the plant. Moreover, the fitting equation of permeability in turbulent flow has high accuracy when the vegetation porosity ranges from 0.9 to 1.0 [94]. Thus, for HD and LD types, porosities of 0.90 and 0.99 were assigned, respectively. The average surface temperatures, shown in Figure 3.9, were derived from thermal images taken during the experiment. As observed, the T_s of the vegetation was 28.0 °C with direct solar radiation (dashed black), 27.5 °C when semi-shaded, and 26.5 °C when shaded (inside white square) during the evaluation time. In addition, the T_s of the ground cover was 23.0 °C inside the semi-outdoor space and 25.5 °C near the window in Space B. Furthermore, the model constant 1.8 was chosen because it can accurately reproduce the velocity deficit effect downwind of the trees and has been shown to result in good correspondence between calculations and measurements [92]. The convective heat transfer coefficient of plants and trees (CHTC) is based on Asawa et al. [95] and estimated by the following equation:

$$CHTC = 7.9v + 17.2, \quad \text{(Equation 3.1)}$$

where v [m/s] is the inflow fixed velocity for the entire crown. The CHTCs are double the value given by the Jürges relation formula [95]. The CHTCs of the ground cover were derived from Hagishima et al. (2000) [96] and are shown in Table 3.2. Moreover, a constant moisture flux of 0.1 g/m2s was set for the vegetation with high foliage density, that is, HD1, HD2, and HD3.

Table 3.2. Size of vegetation and plant canopy settings.

Type of vegetation	Plant parameters	Density	Cd	LAD [m2/m3]	CHTC [W/m2k]	Porosity
		Potted flowers				
	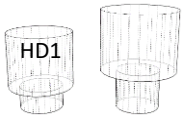 Ø: 0.60–0.70 m Height: 0.50–0.55 m	HD1	0.50	5.34	25.1	0.90
		Potted trees: Fraxinus griffithii and Quercus glauca				
	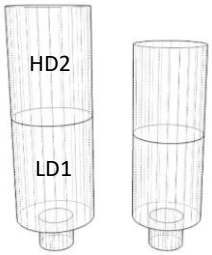 Ø: 0.80–0.90 m Height: 2.00–2.40 m	HD2	0.59	5.59	25.1	0.90
		LD1	0.63	3.61	25.1	0.99
	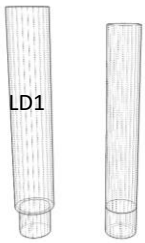 Ø: 0.40–0.50 m Height: 2.30–2.50 m	LD1	0.63	3.61	25.1	0.99
		Existant trees: Amelanchier canadensis, Styrax japanicus				
	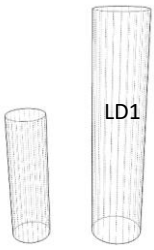 Ø: 0.60–0.80 m Height: 2.00–3.50 m	LD1	0.63	3.61	25.1	0.99
		Ground cover: Semi-outdoor space				
		HD3	0.80	0.70	20	0.90
		LD2	0.50	5.0	20	0.99

HD1: high-density type 1; HD2: high-density type 2; HD3: high-density type 3; LD1: low-density type 1; LD2: low-density type 2. Model constant Cp1: 1.8

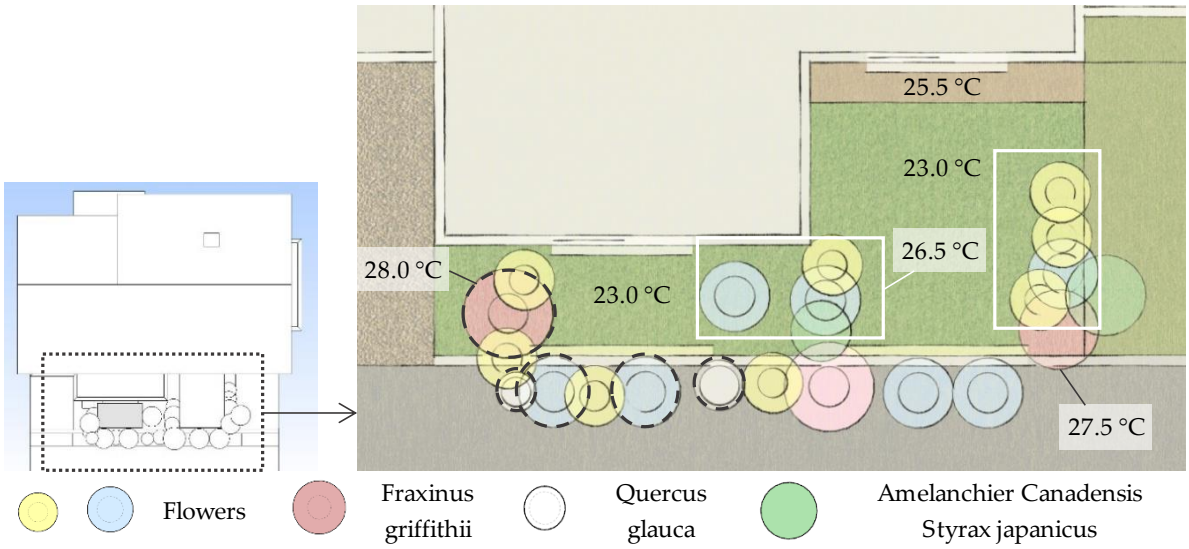

Figure 3.9. Location and surface temperature of vegetation in Space A and Space B.

Table 3.3. Model B: Resistance (drag) and turbulence caused by planted area

Type	F_i	F_k	F_ε	Model constant
Model B	$\rho LADC_d u_i V$	$\rho LADC_d V^3$	$\frac{\varepsilon}{\kappa} C_{pi} F_k$	$C_{p1} = 1.8$

3.2.6.2. Modeling of porous media: evaporative cooling louver and window net

The evaporative cooling louver has a complex geometry with an acute angle toward the windward direction, which is considered to result in less drag with a higher evaporative cooling effect [24]. To save calculation load and time with appropriate drag and cooling effects, the evaporative cooling louver was modeled as a porous media anisotropic model containing a solid and fluid as an alternative to generating fine mesh elements. As shown in Figure 3.10a, the length and height of the louver were 1.8 m, and the louver thickness was set to 0.1 m to match the mesh size. Similarly, the window net was modeled as porous media, with length and height based on one panel of the sliding window (0.70 m × 2.10 m), and a thickness of 0.1 m. The inputs of the porous media (louver and window net), which include the CHTC, surface area ratio (surface area / volume mesh), porosity (volume ratio / volume mesh), fixed temperature, cross-sectional area ratio (area / area mesh), and pressure loss are shown in Table 3.4. For the CHTC of the louver, the heat transfer model of the louver developed by Hirayama et al. (2018) [97] was employed. The CHTC [W/m2k] of the louver was based on the following equation:

$$CHTC = 22.17v + 16.22, \quad \text{(Equation 3.2)}$$

where v is the inflow fixed velocity [m/s].

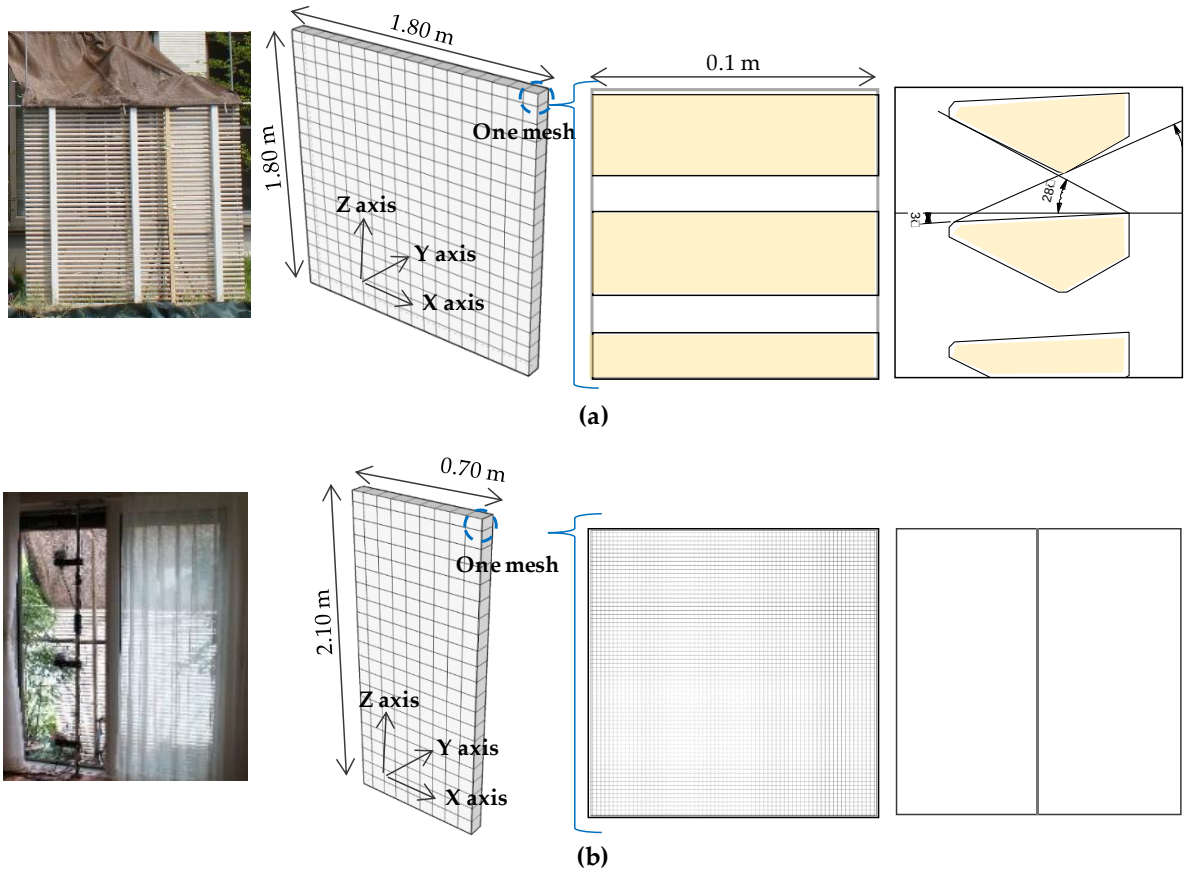

Figure 3.10. Model inputs for porous media (surface area ratio, porosity, and cross-sectional area ratio) for (a) the louver model and (b) the window net model. Left to right: photo; dimensions; front view (Y axis); side view (X axis).

Table 3.4. Model inputs for the porous media: anisotropic model.

Porous media	**CHTC [W/m2k]**	**Surface area ratio [m2/m3]**	**Porosity**	**Fixed temperature [°C]**	**Cross-sectional area ratio**		**Pressure loss [Pa]**
					Front	Side	
Louver	38.39 (2)	39.2	0.79	23.5	0.66	0.21	Table 5
Window net	11.6	2.60	0.99	No heat generation	0.26	0.002	Table 5

As seen in Table 3.4, a fixed surface temperature of 23.5 °C (watered) was assigned to the louver, and no heat generation was assigned to the window net in order to avoid affecting the surrounding air temperature. For the surface area ratio, porosity, and cross-sectional area ratio, the data of one mesh was inputted as shown in Figure 3.10. Therefore, the front view (Y axis) and side view (X axis) of one mesh were used to calculate the surface area, volume ratio, and cross-sectional area ratio. For the louver, the surface area used to calculate the ratio was obtained by multiplying the circumference of one slat (0.153 m) by the number of slats in one mesh (2.5 slats) and the thickness of the mesh (0.1 m). The volume ratio of one mesh used to calculate the porosity was obtained by multiplying the volume of one slat by the number of slats in one mesh and the thickness of one mesh. Similarly, the same data was calculated for the window net by assuming an area of one hole of the net of 1.2 mm^2 and a wire thickness of 0.2 mm. The results are shown in Table 3.4; and details of the calculations are shown in the Appendix (section A.2).

Moreover, the pressure loss variations of the louver and window net are shown in Table 3.5. The pressure loss of the louver was obtained from the analysis model of Hirayama et al. (2018) [97], and the window net was estimated from the model of Noda et al. (2014) [46], which used a similar net size (i.e., net4). Moreover, a moisture of 1.177 g/s was set for the louver based on the evaporation rate of the louver (Figure 3.11) at the time of the field experiment; i.e., 16:00-16:25.

Table 3.5. Model inputs for the porous media: pressure loss variation

Evaporative cooling louver [97]		Window net [98]	
Wind speed [m/s]	Pressure loss variation [Pa]	Wind speed [m/s]	Pressure loss variation [Pa]
0.00	0.00	0.00	0.00
0.25	0.20	0.75	2.50
1.00	3.11	1.90	8.00
4.00	38.77	2.90	16.00
		4.00	25.00

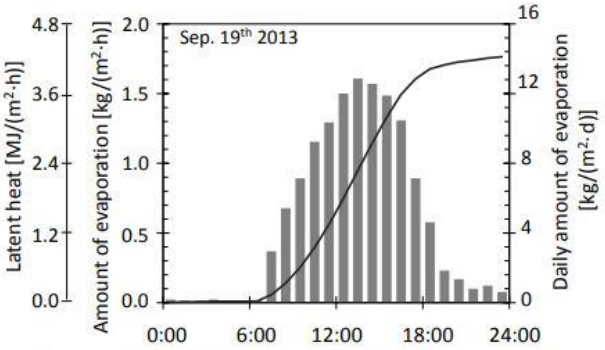

Figure 3.11. Evaporation rate of the louver [24]

The porous media uses the following equations for momentum (Equation 3.3), energy for fluid media (Equation 3.4) and solid media (Equation 3.5):

Momentum equation for porous media:

$$\frac{\partial \rho_F u_i}{\partial t} = -\frac{\partial u_j \rho_F u_i}{\partial x_j} - \frac{\partial \sigma_{ij}}{\partial x_j} + \rho_F g_i + \varsigma_i \qquad \text{(Equation 3.3)}$$

Energy equation for fluid media:

$$\frac{\partial \alpha_F \rho_F C_{PF} T_F}{\partial t} = -\frac{\partial u_j \rho_F C_{PF} T_F}{\partial x_j} + \frac{\partial}{\partial x_j} K_F \frac{\partial T_F}{\partial x_j} + \chi h (T_s - T_F) + \alpha_F q_F \qquad \text{(Equation 3.4)}$$

Energy equation for solid media:

$$\frac{\partial \alpha_S \rho_S C_S T_S}{\partial t} = \frac{\partial}{\partial x_i} K_S \alpha_{ij} \frac{\partial T_S}{\partial x_j} + \chi h (T_F - T_S) + (1 - \alpha_F) q_S \qquad \text{(Equation 3.5)}$$

where u_i is the mean velocity in the *i* direction [m/s]; u_j is the mean velocity for the *j* direction [m/s]; σ_{ij} is the stress tensor [Pa] ; g_i is the gravitational acceleration in the *i* direction [m/s^2]; ς_i is the pressure loss in the *i* direction per unit length [Pa/m]; α_F is the porosity of porous media [-]; ρ_F is the fluid density [kg/m^3]; ρ_S is the solid density [kg/m^3]; C_{PF} is the specific heat of fluid at constant pressure [J/(kg K)]; C_S is the specific heat of solid [J/(kg K)]; K_F is the heat conductivity of fluid [W/m]; K_S is the heat conductivity of solid [W/m]; T_F is the fluid temperature [K]; T_S is the solid temperature [K]; q_F is the heat generation in fluid per unit volume [W/m^3]; q_S is the heat generation in solid per unit volume [W/m^3]; α_{ij} is the tensor of area ratio [-]; χ is the surface area ratio (contact ratio between the fluid and solid per unit volume) [m^2/m^3]; and h is the convective heat transfer coefficient [W/(m^2 K)].

3.2.7. Solver settings

The three dimensional (3D) steady RANS equations were solved with a standard k-model. Second-order upwind discretization schemes were used for the momentum and turbulence equations. The Quadratic Upstream Interpolation for Convective Kinematics (QUICK) scheme was used for convection terms. This scheme solves advection terms by using both upwind and downwind values, resulting in a more accurate calculation compared with using the 1st order upwind values alone. Convergence is obtained when all variables reached and are stable at 1 x10^{-5}, i.e., 1000 cycles, because calculation needs to be finished after sufficient convergence of the solution [88]. Therefore, stricter convergence criteria are required to check that there is no change in the solution.

3.3. Results

3.3.1. Vertical temperature distribution for each measurement point between experiment and validation.

Figure 3.12 compares the vertical temperature distribution for each measurement point for the semi-outdoor and indoor spaces between the results of the experimental case selected for the validation (CASE 1 CASE 2 subcase C4) and the simulation results. Table 3.6 and Figure 3.14 shows the correlation and deviation between the experiment and simulation at each measurement point. Figure 3.13 compares the wind speed for the outdoor, semi-outdoor, and indoor spaces between the experiment and simulation. According to the vertical temperature distribution in Figure 3.12, cool air formation occurs near the ground in the semi-outdoor spaces (Space A and Space B) both in the experiment and simulation, indicating that the cooling effects of the PCMs are replicated in the simulation. In general, the results for Space A and Space B show a good correlation between the experiment and simulation (Table 3.6). The coefficient of determination (R^2) for all points lies between 0.93 and 0.99, and the root mean square error (RMSE) is between 0.2 and 0.5 except T_{win} , demonstrating that the model accurately predicts the data. However, for the point T_{win} at Space A, an RMSE of almost 0.9 is obtained. This is because the model overpredicts the wind speed through the window (WS_{win}). The WS_{win} is approximately 0.2 m/s (Figure 3.13) higher than that recorded during the experiment. It is assumed that this causes T_{win} to be slightly cooler because more cool air flows through the window, resulting in a maximum air temperature difference of 0.7–1.0 °C for GL + 0.5 m to GL + 2.5 m (Figure 3.12a). Nevertheless, good correlation is observed for T_{cin}(air temperature in the center of the indoor

space / representative indoor air temperature) in both Space A and Space B, indicating that the model accurately predicts the indoor air temperature. Overall, the vertical air temperature distribution shows a good trend between the experiment and simulation, demonstrating that the model can effectively predict the conditions observed during the experiment.

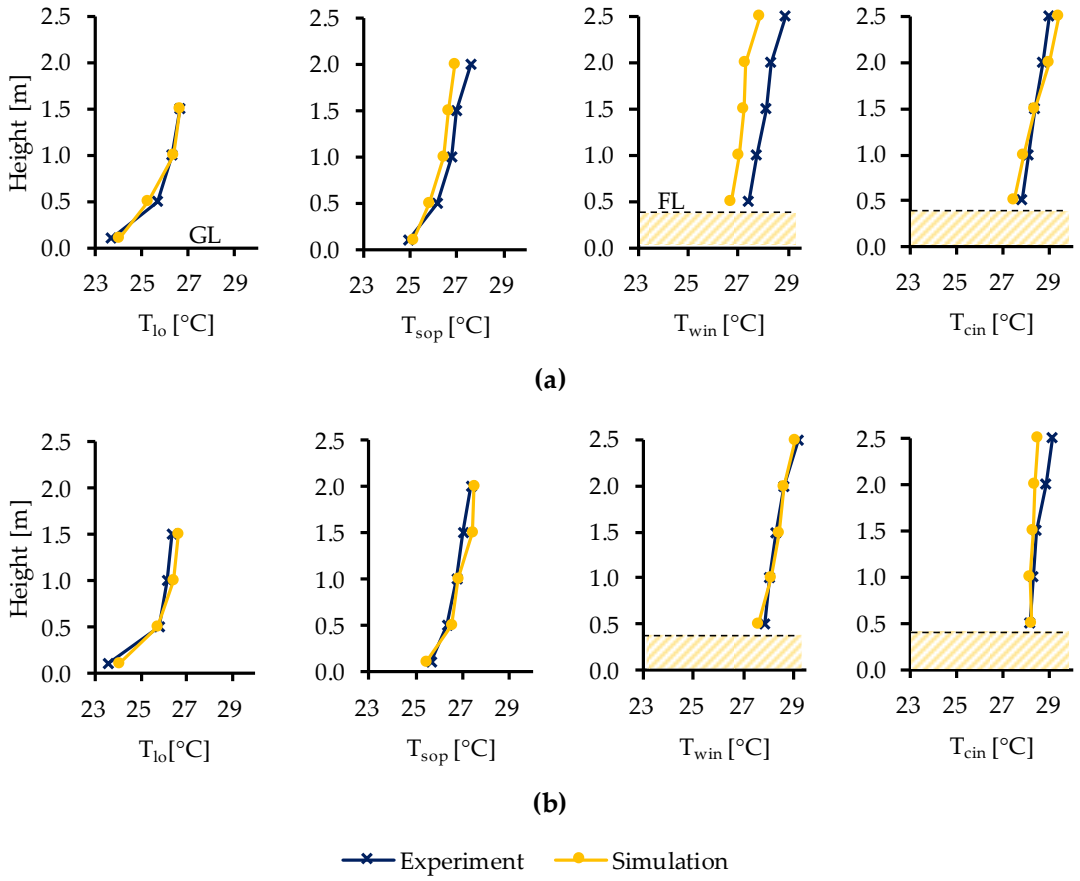

Figure 3.12. Vertical air temperature distribution between the experiment and simulation in semi-outdoor and indoor space for (a) Space A and (b) Space B.

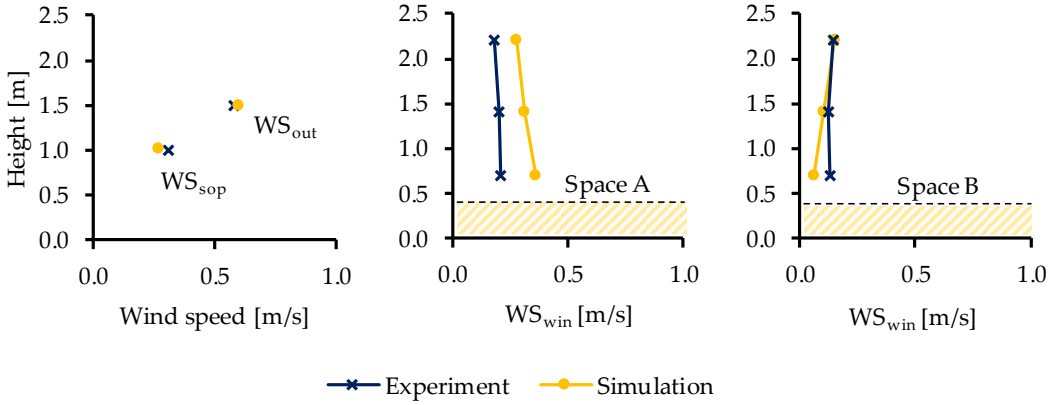

Figure 3.13. Wind speed in the outdoor (WS_{out}), and semi-outdoor (WS_{sop}), and indoor space (WS_{win}) between the experiment and simulation.

Table 3.6. Correlation and deviation between the experiment and simulation.

	Space A			Space B		
Point	RMSE	MSE	R2	RMSE	MSE	R2
Tlo	0.27	0.07	0.95	0.32	0.10	0.97
Tsop	0.40	0.16	0.98	0.25	0.06	0.96
Twin	0.89	0.79	0.97	0.14	0.02	0.93
Tcin	0.29	0.09	0.99	0.35	0.12	0.94

R2, coefficient of determination; RMSE, root mean square error; MSE, mean squared error

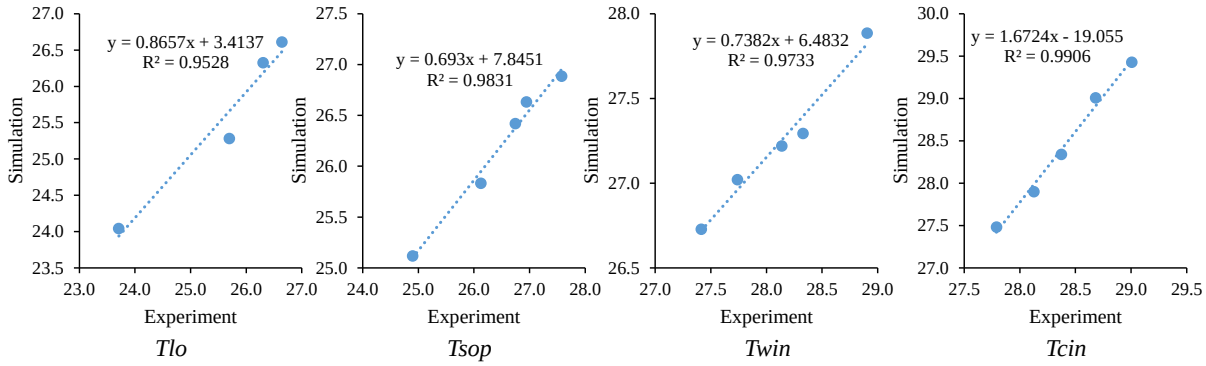

(a)

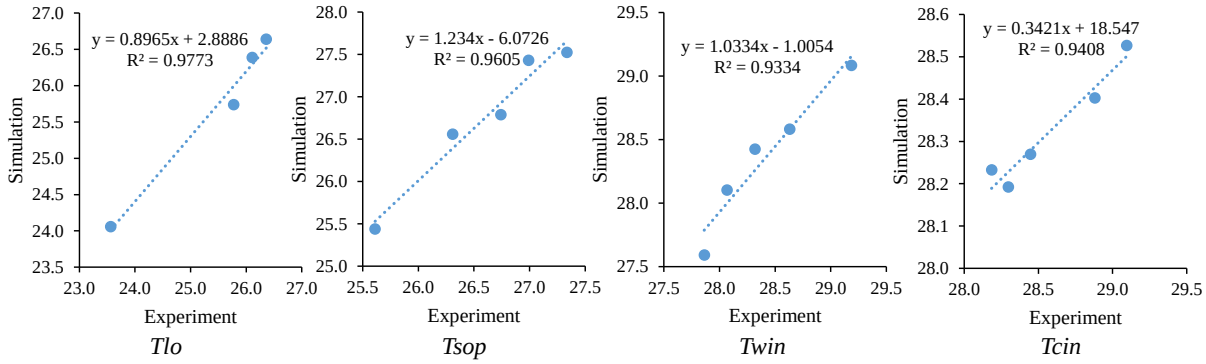

(b)

Figure 3.14. Correlation plot between exper iment and validation

3.3.2. Contour images: Air temperature, relative humidity and wind speed.

Figure 3.15 shows different contour images of the air temperature, relative humidity and wind speed of the validation case at GL + 1.5 m, Space A and Space B. The contour images clearly show the tradeoff between the air temperature and relative humidity where the cooling effect of the watered louver and vegetation reduces the air temperature and increases the relative humidity. At the center of the semi-outdoor Space A, the relative humidity increased from 56% to about 62% at a height of 1.5 m above the ground (GL + 1.5m). In contrast, the air temperature was reduced from 27.5 °C to 26.6°C at GL + 1.5m. Thus, relative humidity increased by 6% while air temperature was reduced by 0.9 °C. As observed the evaporation is higher near the ground (below GL + 0.5 m) due to the combined effect of the watered louver, ground floor and surrounding vegetation in Space A. Thus, the coolest air tend to accumulate near the ground. Meanwhile the cool air accumulation between GL + 0.5 m and GL + 2.0 m flows through the window and slightly cools the indoor space. For Space B, the coolest air similar to Space A was accumulated near the ground up to GL + 0.5 m. However, cool air above GL + 0.5 m did not reach the window mostly due to the large L-W distance, half surrounding vegetation and wind direction which dissipated cool air through the sides. These results match to the conclusions found in the field measurement (Chapter 2) where for Space B the cool air generated by the louver could have potentially dissipate through the side prior to reaching the window. Therefore, to obtain a higher cooling effect (cool breeze) in the indoor space, the watered louver should be installed close to the window.

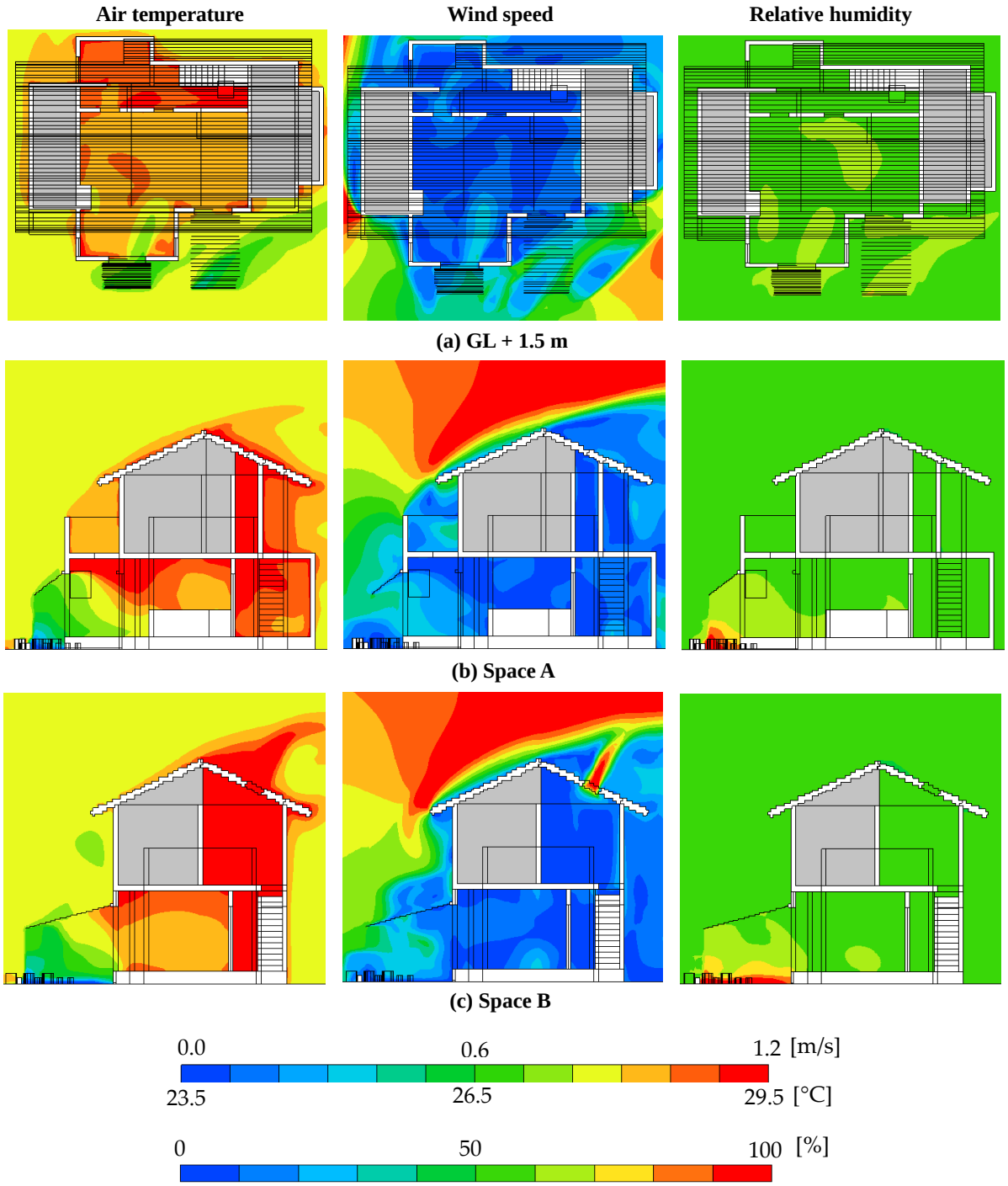

Figure 3.15. Contour image sections for the air temperature, wind speed and relative humidity of the validation case: (a) GL + 1.5 m, (b) Space A and (c) Space B

3.4. Analysis of results

The validation results of the CFD simulation with detailed modeling of PCMs show that this model can effectively predict the cooling effect of PCMs for a semi-outdoor spaces. The maximum difference in air temperature between the experiment and simulation was obtained at T_{win} (0.7–1 °C) in Space A. This difference is considered acceptable for CFD simulations, considering the model simplification and assumptions (i.e., average steady-state flow calculations in the CFD, limited boundary conditions, imperfect agreement with experimental conditions), and considering the following points. Previous studies that compared experimental and simulated air temperatures in outdoor spaces with cool materials and vegetation reported a mean absolute error of 1.34 °C on average, 3.67 °C as a maximum, and 0.27 °C as a minimum [57]. The reported R^2 was 0.92 on average, 0.99 as a maximum, and 0.66 as a minimum. In this validation, the R^2 was between 0.93 and 0.99 for all measurement points. Therefore, these results show better accuracy than that previously reported in the literature.

CHAPTER 4. SENSITIVITY ANALYSIS OF PASSIVE COOLING METHODS USING VALIDATED CFD MODEL.

4.1. Introduction

Previous chapter showed that the CFD model can accurately predict the conditions of the field experiment. Accordingly, the CFD model can be used to investigate the individual effect of the PCMs. Therefore, in this chapter a sensitivity analysis is conducted to observe if the CFD model can also predict the watering conditions of the louver. Moreover, to investigate the effectiveness of each PCMs on the formation of cool microclimate at the semi-outdoor space.

4.2. Methodology

Simulation cases for the sensitivity analysis**Table 4.1** shows the simulation conditions between the base case (case S-0), presented in the previous chapter, and simulation cases for the sensitivity analysis cases S-0–S-5. As observed in Table 13, to ensure controlled conditions, only one variable was changed at a time. The sensitivity analysis mainly focuses on replicating and analyzing the formation of cool air in a semi-outdoor space. Thus, the settings in the semi-outdoor space were changed whereas the settings in the indoor space were kept constant. Case S-0 was used as the base case for the sensitivity analysis to analyze the cooling effects of the PCMs under various conditions, including louver watering conditions and the amount of PCMs. The effect of louver watering conditions is represented by cases S-0–S-2. The effect of the amount of PCMs on the formation of cool air is represented by cases S-3–S-5. Only the sunscreen was kept installed in the semi-outdoor space in order to maintain the initial thermal boundary conditions for the building elements and ground cover. In order to simulate different watering louver conditions, the surface temperature of the louver (T_s) was modified. For the watered louver condition, according to the results of the field measurement (Figure 2.9), the T_s of the watered louver was approximately 4 °C lower than T_{amb}; thus, 23.5 °C was applied. Moreover, when the louver was wet, T_s was approximately 2 °C lower than T_{amb}; thus, 25.5

°C was applied. For the dry louver, T_s was set to 29 °C because solar radiation during the experiment was relatively low.

Table 4.1. Simulation cases for the sensitivity analysis

Simulation cases		PCMs in the semi-outdoor space	Louver watering	Louver T_s [°C]	Vegetation watering
Validation	case S-0	louver, vegetation[1], sun screen	watered	23.5	watered
Sensitivity analysis	case S-1	louver, vegetation sun screen	wet	25.5	watered
	case S-2	louver, vegetation, sun screen	dry	29.0	watered
	case S-3	louver, sun screen	watered	23.5	-
	case S-4	vegetation, sun screen	-		watered
	case S-5	sun screen	-		-

[1]Vegetation: Potted flowers and trees. The ground cover was watered at all times. The vegetation T_s is shown in Figure 3.9.

4.3. Results and analysis

Figure 4.1 to Figure 4.8 show the sensitivity analysis results for the formation of cool air in the semi-outdoor space and the subsequent cooling effect in the indoor space for different louver watering conditions (case S-0 - S-2) and amount of PCMs (case S-3 - S-5).

Figure 4.1 and Figure 4.2 shows the vertical air temperature distribution results in semi-outdoor and indoor spaces for Space A and Space B. Figure 4.3, Figure 4.4, Figure 4.5 shows the air temperature, wind speed and relative humidity contours, respectively, for each case at the measurement point GL + 1.5 m, that is, 1.5 m above the outdoor ground or 1.0 m above the indoor floor level. In addition, Figure 4.6, Figure 4.7 and Figure 4.8 show the air temperature, wind speed and relative humidity contours section, respectively, for Space A and Space B.

4.3.1. Watering conditions of the evaporative cooling louver

The results in Figure 4.1 for cases S-1 and S-2 show that, when the watering stops and the T_s of the louver is increased, the evaporative cooling effect of the louver, shown in the T_{lo}, is significantly reduced. In case S-1, when the louver is wet, the cooling effect of the T_{lo} from GL + 0.1 m to GL + 1.5 m is reduced by approximately 1.8–0.6 °C for Space A and 1.7–0.5 °C for Space B, in contrast to the initial case S-0. Moreover, when the louver is dry in case S-2, the cooling effect at the T_{lo} from GL + 0.1 m to GL + 1.5 m is further reduced by approximately 3.4–1.3 °C for Space A and 4.3–1.2 °C m for Space B. The evaporative cooling effect between the watered and dry louver is also shown in the results of the relative humidity in Figure 4.5 and Figure 4.8. As expected when the louver is dry the evaporative cooling effect is lost and thus

the relative humidity does not increases. In contrast, when the louver is watered, the air temperature is reduced and relative humidity increases. This confirms that the model can also reproduce the evaporative effect of the watered louver by increase in relative humidity.

For the T_{sop} (measurement point at the center of the semi-outdoor space), the reduction of the cooling effect differs greatly between Space A and Space B because of the louver-window (L-W) distance. The L-W distance is 1 m for Space A and 2.8 for Space B. Thus, for Space A in case S-1, the cooling effect at the T_{sop} is reduced by approximately 1.3–0.4 °C from GL + 0.1 m to GL + 2.0 m. In contrast, for Space B in case S-1, the cooling effect at T_{sop} is only reduced by approximately 0.35–0.1 °C from GL + 0.1 m to GL + 2.0 m. This demonstrates that the cooling effect is reduced with increasing distance from the evaporative cooling louver. Thus, a shorter L-W distance is preferable when the evaporative cooling louver (watered) is used for the formation of cool air in a semi-outdoor space. This is confirmed when observing the air temperature contours at GL + 1.5 m in Figure 4.3, and Figure 4.6 for cases S-0 and S-1, where the formation and cooling effect (watered and wet louver) is better for Space A than for Space B. For Space B, the combination of factors such as the L-W distance, amount of vegetation, and wind direction directly affects the chances of cool air reaching the window – indoor space. Thus, at a larger L-W distance, the generation of cool air in the semi-outdoor space and flow of cool air into the indoor space is more difficult than at a shorter L-W distance in Space A. Furthermore, according to Figure 4.1, for case S-2, the cooling effect at T_{sop} from GL + 0.1 m to GL + 2.0 m is reduced by 2.3–0.9 °C for Space A and 0.5–0.4 °C for Space B. In addition, when the louver is dry (case S-2), there is no formation of cool air in the semi-outdoor space (Figure 4.3, Figure 4.6 case S-2); thus, T_{lo} and T_{sop} at point GL + 1.5 m are similar to the ambient temperature. Furthermore, Figure 4.1 (point T_{cin}), Figure 4.3, Figure 4.6 (cases S-0 and S-1) show that the generation of cool air in the semi-outdoor Space A cannot be effectively extend into the indoor space with the current indoor variables (window-opening conditions, indoor door opening, and leeward openings; see Figure 22). This is clearly seen by comparing cases S-0, S-1, and S-2, where no significant difference is observed in T_{cin}. Even though there is a difference for the T_{win} value in Space A, in reality, this point cannot be properly reproduced, as described in the previous section. Thus, only points T_{lo}, T_{sop}, and T_{cin} are appropriate for a comparative analysis.

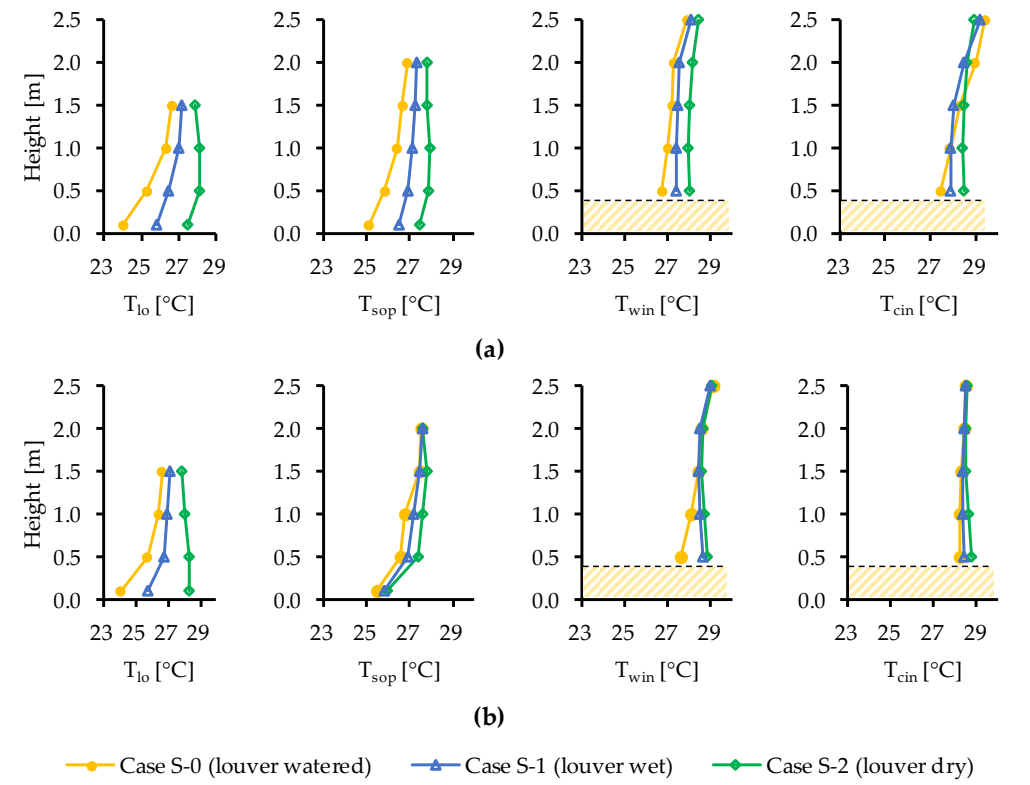

Figure 4.1. Vertical air temperature distribution in semi-outdoor and indoor spaces between watered, wet, and dry louvers for (a) Space A and (b) Space B.

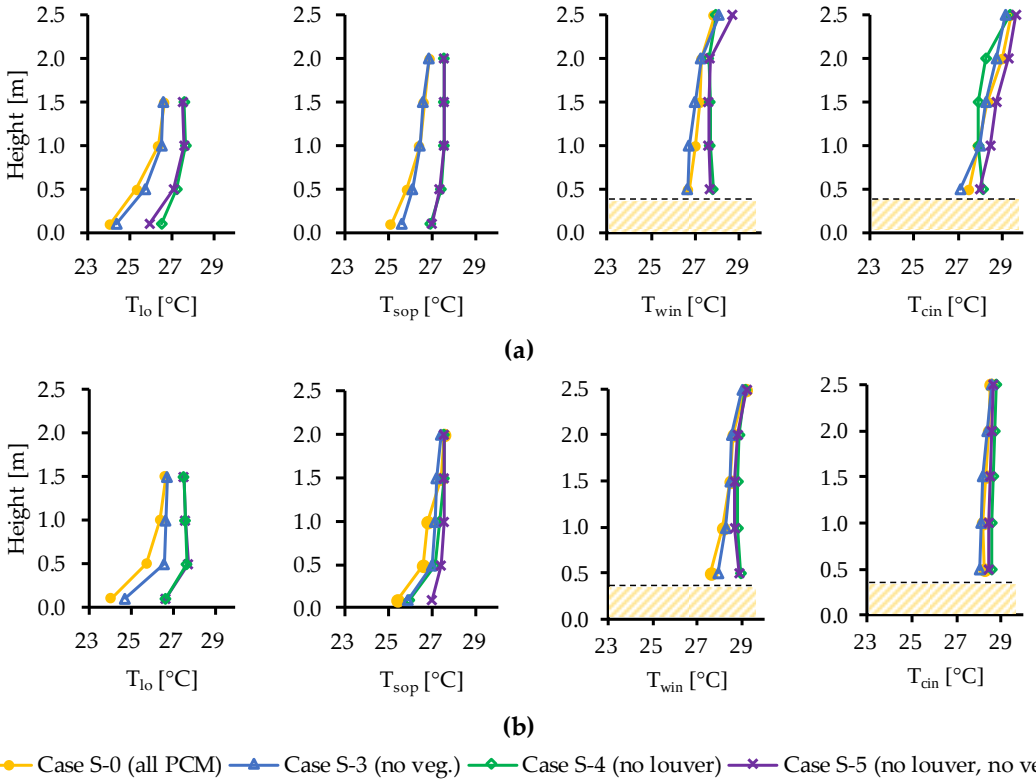

Figure 4.2. Vertical air temperature distribution in semi-outdoor and indoor spaces for different amounts of PCMs in (a) Space A and (b) Space B.

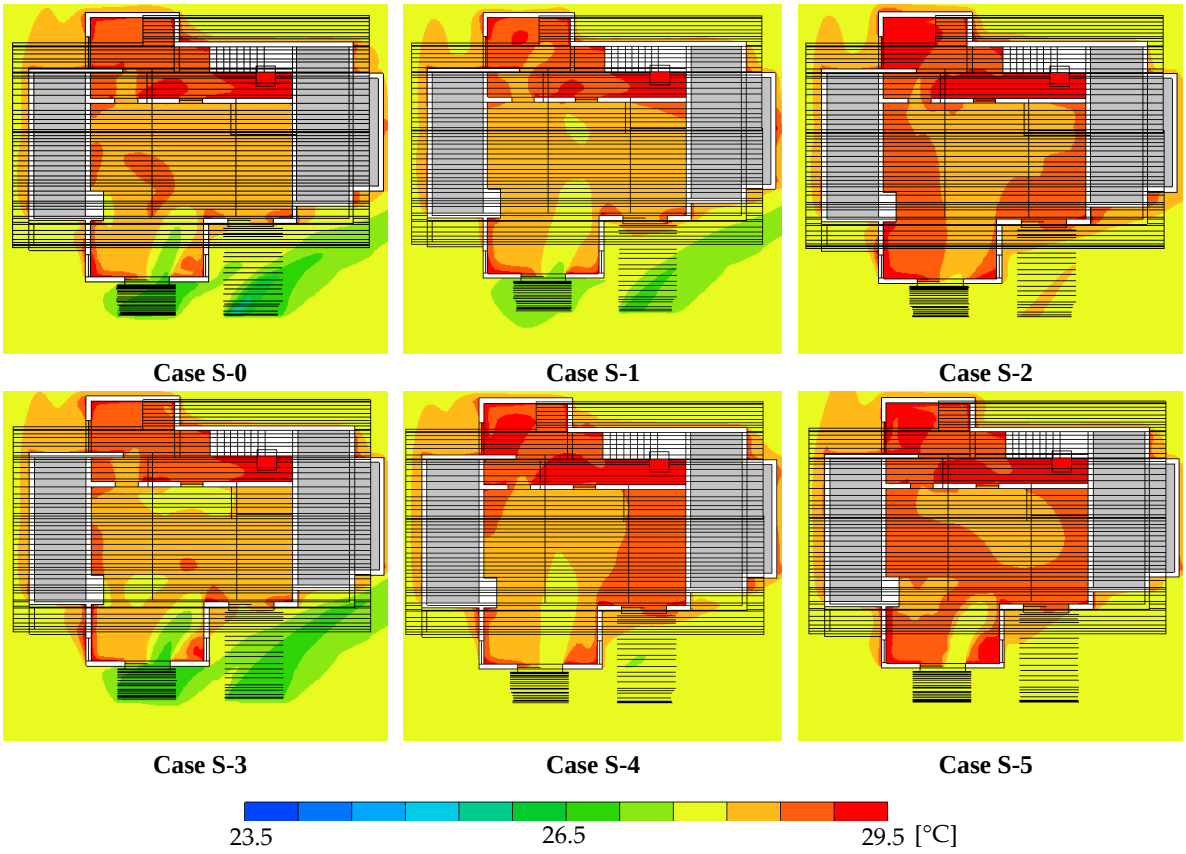

Figure 4.3. Horizontal air temperature contour section at GL + 1.5 m for cases S-0 – S-5.

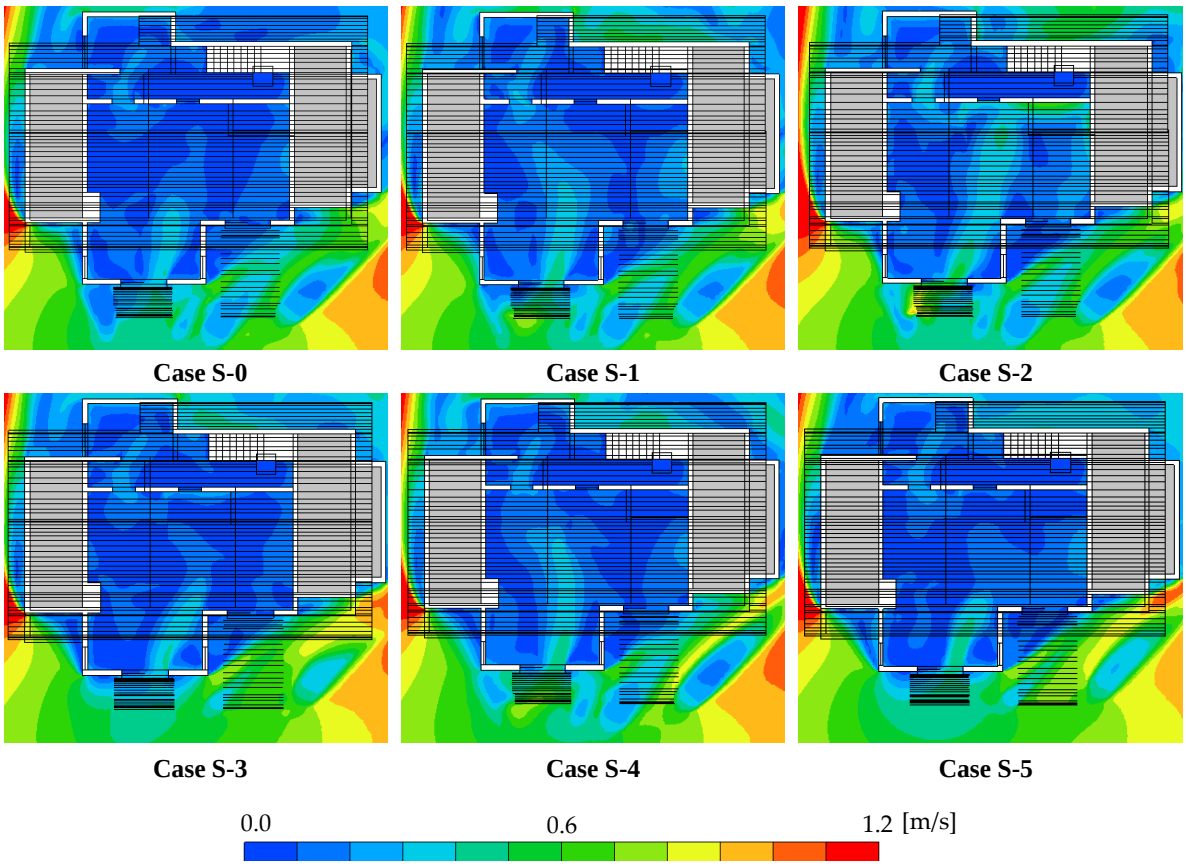

Figure 4.4. Horizontal wind speed contour sections at GL + 1.5 m for cases S-0 – S-5.

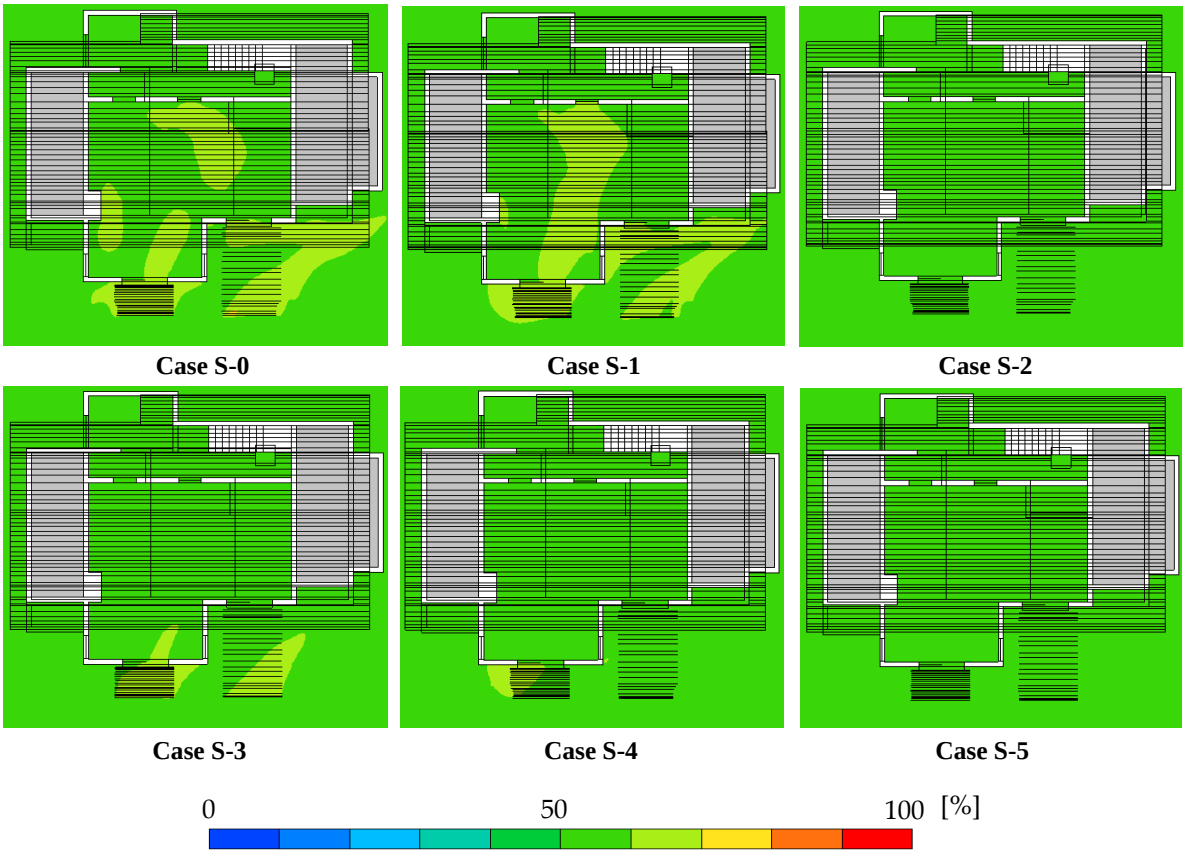

Figure 4.5 Horizontal relative humidity contour sections at GL + 1.5 m for cases S-0 – S-5

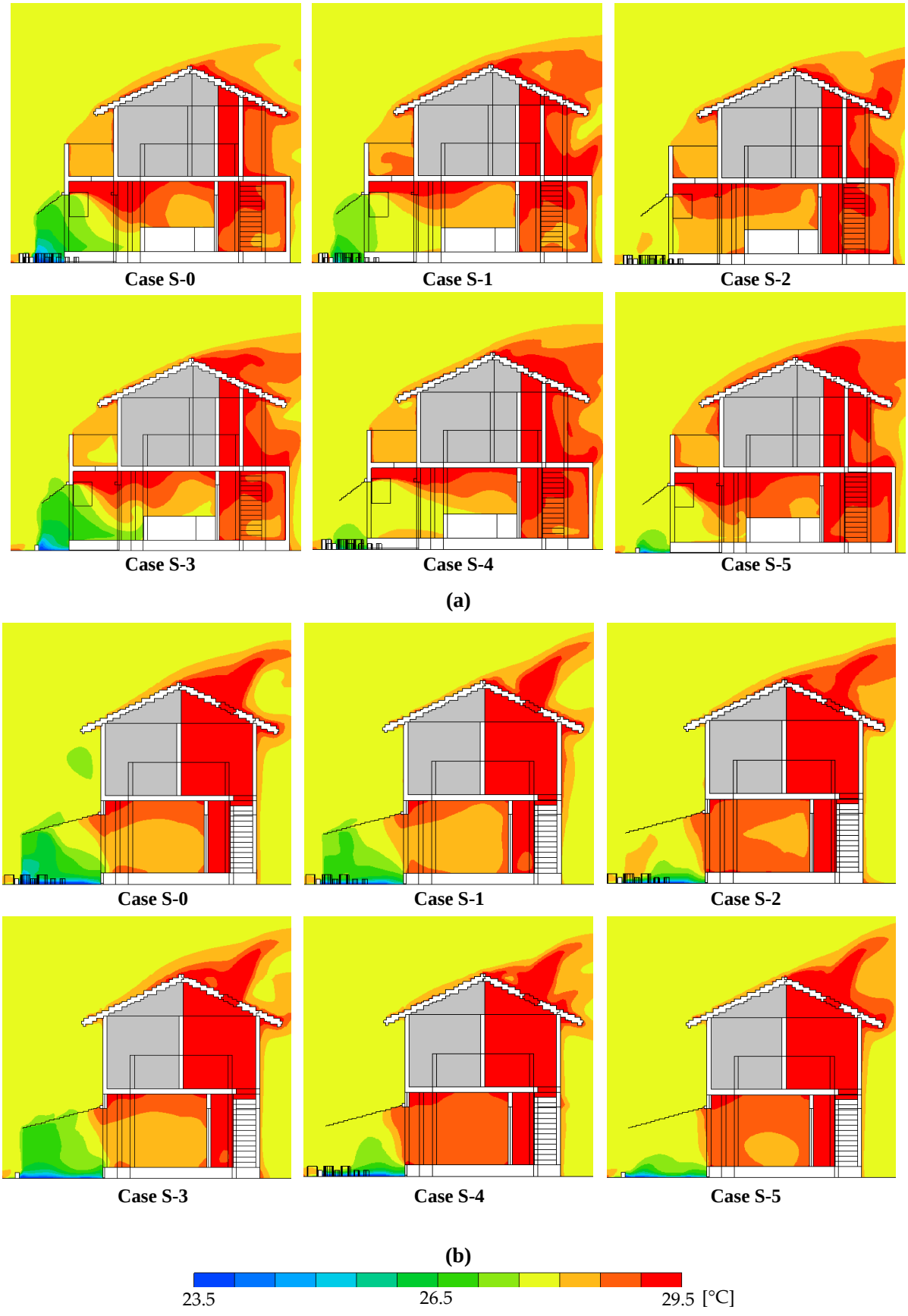

Figure 4.6 Vertical air temperature contour section at (a) Space A and (b) Space B for cases S-0 – S-5.

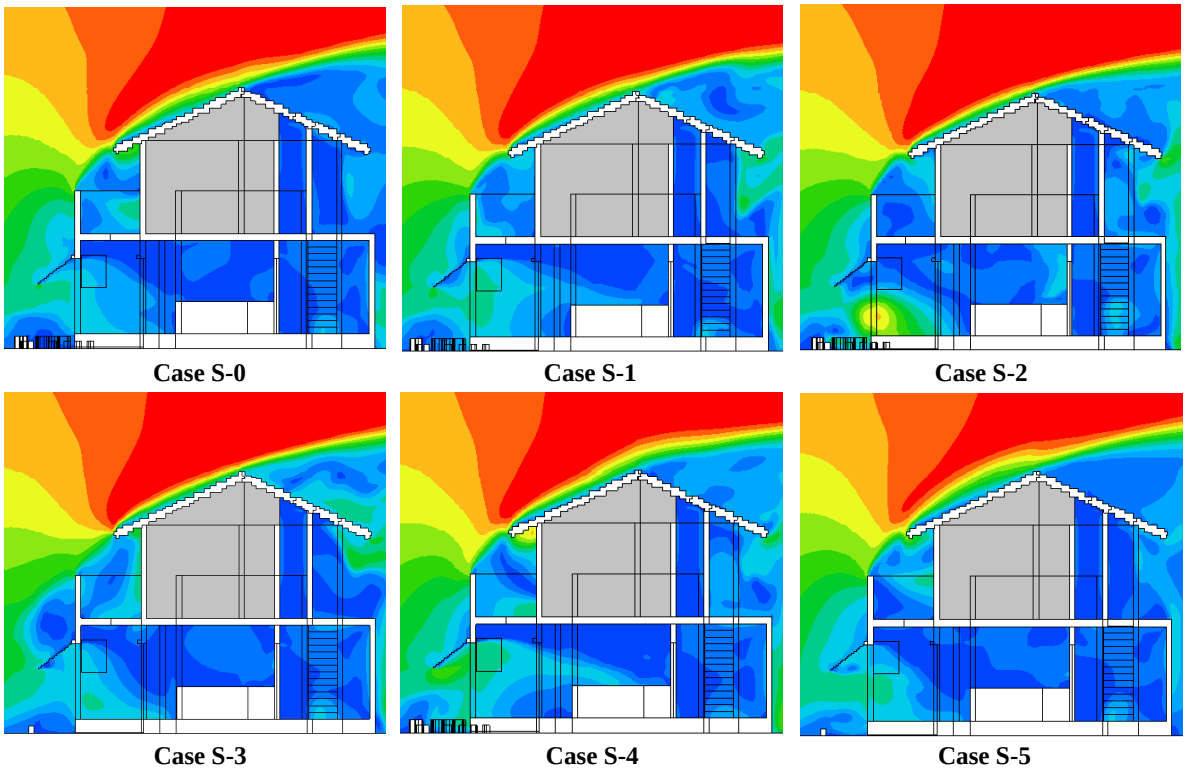

(a)

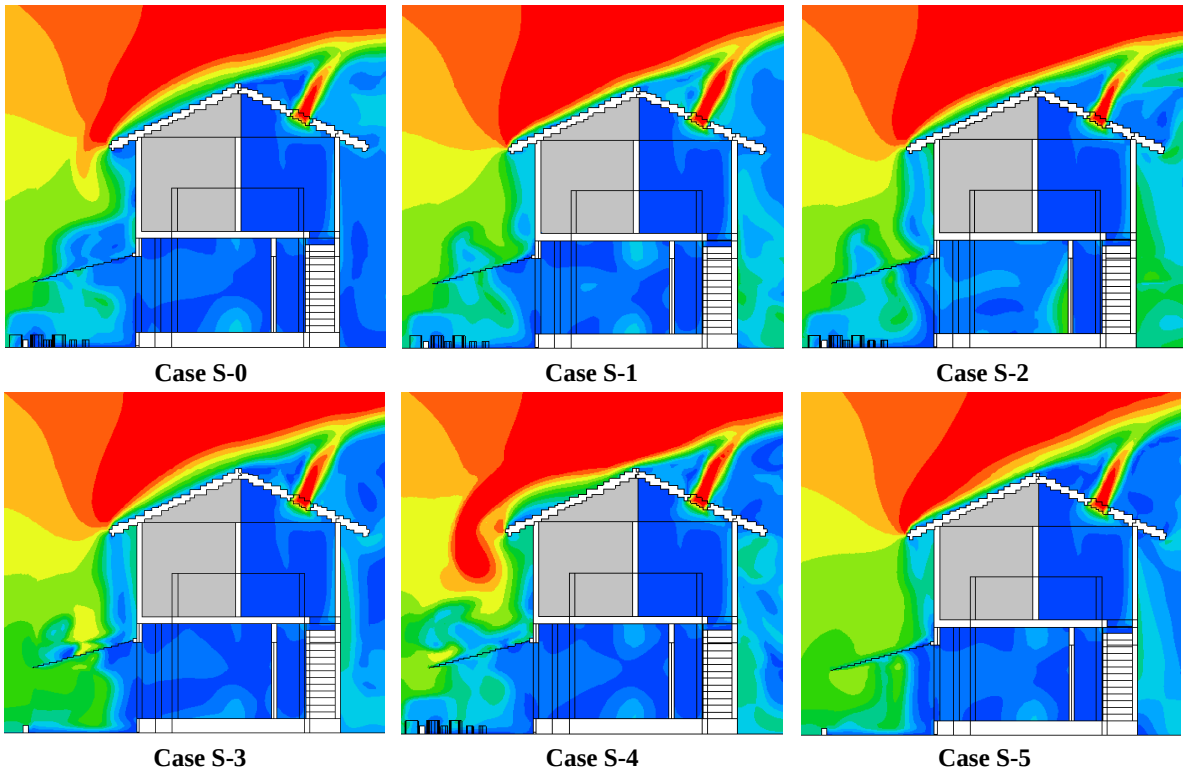

(b)

Figure 4.7 Vertical wind speed contour sections at (a) Space A and (b) Space B for cases S-0 – S-5.

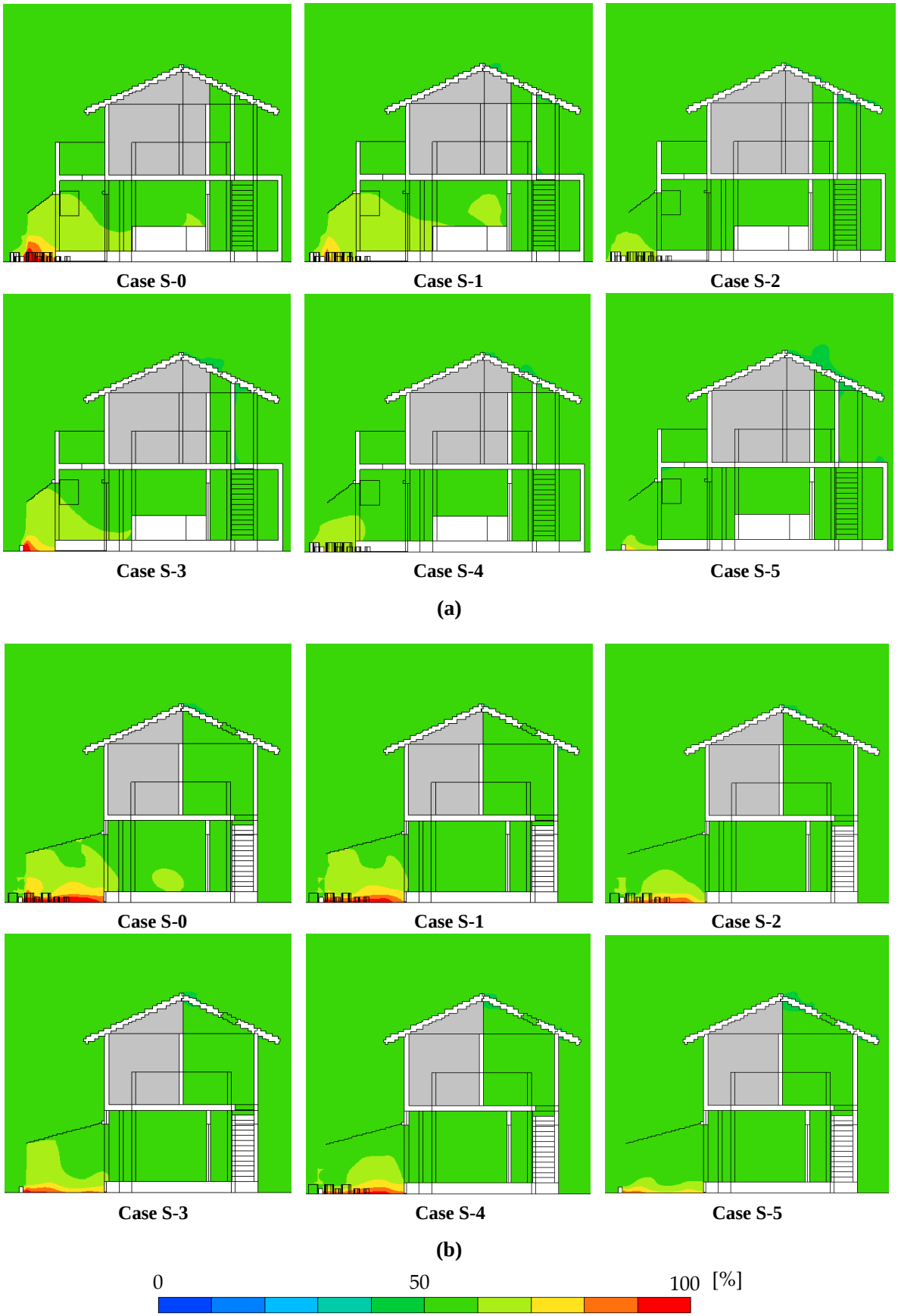

Figure 4.8 Vertical relative humidity contour sections at (a) Space A and (b) Space B for cases S-0 – S-5.

4.3.1. **Amount of passive cooling methods in the semi-outdoor space**

This section analyzes the individual effect of each PCMs. As shown in Table 4.1, all PCMs were applied to case S-0; case S-3 had no vegetation, case S-4 had no louver, and case S-5 had no louver and no vegetation. The vertical air temperature distribution in these cases is presented in Figure 4.2. As expected, for cases S-0 and S-3, a shorter L-W distance and use of the evaporative cooling louver results in a higher cooling effect (T_{lo}) and better formation of cool air (T_{sop}) in Space A. Moreover, when the vegetation is removed in case S-3, the air temperature at T_{lo} in Space A only increases by approximately 0.3–0.1 °C for GL + 0.1 m to GL + 1.0 m in contrast to when the louver is removed in cases S-4 and S-5, where the air temperature at T_{lo} increases by 2.5–1.0 °C and 1.9–0.9 °C for GL + 0.1 m to GL + 1.5 m, respectively. In contrast, for Space B, the lack of vegetation in case S-3 results in a further increase at T_{lo} of approximately 0.7–0.1 °C for GL + 0.1 m to GL + 1.5 m, which is twice the cooling effect lost in Space A at all points.

Furthermore, the comparison of the results in Figure 4.6 and Figure 4.7 for Cases S-0 (louver + vegetation) and Case S-3 (louver only) show that when the vegetation is removed the wind speed crossing the window in Space A increases. Moreover, even though the vegetation is removed the cooling effect is not lost. This is because the evaporative cooling effect of the louver is higher than the vegetation. The surface temperature of the watered louver (23.5°C) was closer to the wet bulb temperature owing to the higher evaporation rate, in contrast to that of the vegetation (26.5°C) was 3°C higher owing to the lower transpiration rate through stomata. Therefore, removing the vegetation installed in a short L-W distances (Space A) allowed for the cool air generated by the louver to be induced into the indoor space. In contrast, for a large louver window distance (Space B), the presence of vegetation is beneficial as it prevents the cool air from dissipating near the louver thus extending its cooling effect.

This suggests that the use of surrounding vegetation is more beneficial for obtaining a higher cooling effect and generating more cool air at a larger L-W distance than at a shorter L–W distance in Space A. This is more explicitly shown in Space B for cases S-4 and S-5, where the air temperature at case S-4 T_{sop} increases by 0.5–0.1 °C for GL + 0.1 m to GL + 1.5 m, in contrast to case S-5, where the air temperature in T_{sop} increases by 1.5–0.1 °C.

4.3.2. Cooling the indoor space

For cases with wet and watered louvers, the accumulation of cool air in the semi-outdoor space for case S-0, S-1 and S-3 is evident in Space A (Figure 4.3, and Figure 4.6). In contrast, the cool air formed by the louver does not reach the window in Space B mostly due to the large L-W distance and wind, which clearly contributes to dissipation of cool air through the side. Regarding the presence of vegetation, a comparison of case S-3 and case S-0 shows that the cool air generated in the semi-outdoor space is more easily dissipated when the vegetation is removed in both Space A and Space B. Moreover, comparing cases S-0 and S-3 (Figure 4.3, Figure 4.4, Figure 4.6 and Figure 4.7), the wind speed through the window is higher in case S-3 due to the lack of vegetation, which allows more cool air to flow through the window, further cooling the indoor space. Thus, although vegetation enhances the cooling effect near the louver, it can prevent cool air from further dissipating into the indoor space. This suggests that vegetation is not necessary for a shorter L-W distance. For cases S-0 and S-4 (Figure 4.3, Figure 4.4, Figure 4.6, Figure 4.7), vegetation has different effects on the wind speed and flow of air because the combination of vegetation and louver significantly reduces the wind speed in case S-0, unlike in case S-4 without the louver, where only vegetation results in a higher wind speed through the window. Generally, the use of solar shading (sunscreen) alone (case S-5) results in the worst-case scenario. As seen in the indoor space, a better cooling effect is observed when using the watered louver (cases S-0 and S-3). In addition, a comparison between Space A and Space B reveals that a shorter L-W distance is more beneficial for cooling the indoor space than a longer L-W distance, where controlling the wind direction and inducing cool air is more difficult. Moreover, the results for all cases reveal that the ventilation strategies employed during CASE 1 CASE 2 subcase C4 (Table 2.3, Figure 22) restricted indoor flow due to a lack of more leeward openings. Moreover, all the cases in the field measurement had the same indoor conditions for leeward; i.e., ceiling window open, which confirms the reason why in all the results the induction of cool air was restricted. In general, the results show that the louver is effective for indoor cooling if a combination of proper installation (shorter L-W distance) and indoor ventilation strategies are applied.

4.4. Summary

A sensitivity analysis was carried out to analyze the cool microclimate formation at the semi-outdoor space using the validated CFD model case S-0. Thus, case S-0 was used as the base case. For case S-1 and case S-2 the louver watering conditions were changed to wet and dry, respectively. For case S-3 to case S-5 the amount of PCMs were changed by removing the surrounding vegetation, louver and both, respectively. The comparison of results between cases S-0 and S-2 showed a significant difference on the formation of cool microclimate at the semi-outdoor spaces: Space A and Space B. As expected, the watered louver resulted in a higher cooling effect, however, Space A had a better performance due to the short louver window (L-W) distance which facilitated the cool air formation at the semi-outdoor space. This demonstrated that the cooling effect is reduced with increasing distance from the evaporative cooling louver. Moreover, comparison between case S-0 and S-3 showed that for a short L-W distance vegetation might not be beneficial because it limits the dissipation of cool air into the indoor space. In general, cool microclimate is formed when: (1) louver is continuously watered; (2) L-W distance is short; (3) horizontal shading device is applied to shade the semi-outdoor space and window. And (4) appropriate indoor condition are applied to induce the cool air (results showed that current ventilation settings are not good for inducing the cool air). For this chapter the variables at the indoor space were not investigated.

CHAPTER 5. OPTIMIZATION OF OUTDOOR AND INDOOR MICROCLIMATES USING CFD SIMULATION

5.1. Introduction

Chapter 2, and Chapter 4 confirmed that the best configuration of PCMs to form a cool microclimate in the semi-outdoor space is when the evaporative cooling louver is watered and closer to the window, i.e., Space A. Also, results for Space B showed difficulties forming a cool microclimate at a longer distance from the window. Moreover, for both indoor spaces the cool microclimate formed at the semi-outdoor space was not properly utilized for indoor cooling. Thus in this chapter, we investigate the best PCMs and indoor condition configurations to improve the formation of cool air at the semi-outdoor space and induction of cool into the indoor space using the validated CFD model (base case S-0).

5.2. Methodology

5.2.1. Optimization cases

Table 5.1 shows the base case (case S-0) and the cases studied in this chapter (case S-6–S-10) to find the best PCMs and indoor condition configuration for optimizing the outdoor and indoor microclimates of the case study. As observed the variables studied at the semi-outdoor space included L-W distance for Space B; GL (ground level) – FL (floor level) distances; and wing wall (refer to Figure 5.1). Wing walls are vertical solid panels placed alongside of windows perpendicular to the wall on the windward side of the house. They are used to accelerate the natural wind speed due to the pressure differences created by the wing wall and direct wind flow through windows. Moreover, indoor conditions investigated included type of window used (windward ventilation); increasing indoor porosity of the building / cross ventilation (opening indoor doors); and leeward ventilation. As noticed variables such louver watering conditions; sunscreen; L-W distance for Space A; amount of vegetation; do not appear in Table 5.1 because these are constants used throughout all cases in this chapter. The variables changed for each of the cases are shown in Table 5.1. As observed, variables applied to Case S-6 modify the air flow of the house; variables for Case S-7 shortens the L-W distance of Space B by 1 m; variables for Case S-8 shortens the ground level floor level (GL – FL) distance for both Space A and Space B; variables for Case S-9 proposes to change the window type; and variable for

Case S-10 proposes to use the same L-W distance of Space A for Space B. The cases shown in Table 5.1 were carefully selected after several trial and error cases (Appendix Table 0.3) were conducted to find the variables that influence the formation of cool microclimate at the semi-outdoor space and the induction of cool air into the indoor space.

Table 5.1. Cases for improving the passive cooling design using CFD model.

Simulation cases	Semi-outdoor space			Indoor conditions		
	L-W distance Space B [m]	GL – FL distance [m]	Wing wall	Windward ventilation	Cross ventilation	Leeward ventilation
Case S-0	2.8	0.4	No	Sliding window	Open kitchen door	Ceiling window
Case S-6	2.8	0.4	Yes	Sliding window	Open kitchen and living room doors	Ceiling window + entrance door open
Case S-7	1.8	0.4	Yes			
Case S-8	1.8	0.2	Yes			
Case S-9	1.8	0.2	Yes	Casement window		
Case S-10	1.0	0.2	Yes			

Sunscreen, L-W distance for Space A, louver watering conditions and amount of vegetation at each space are kept constant.

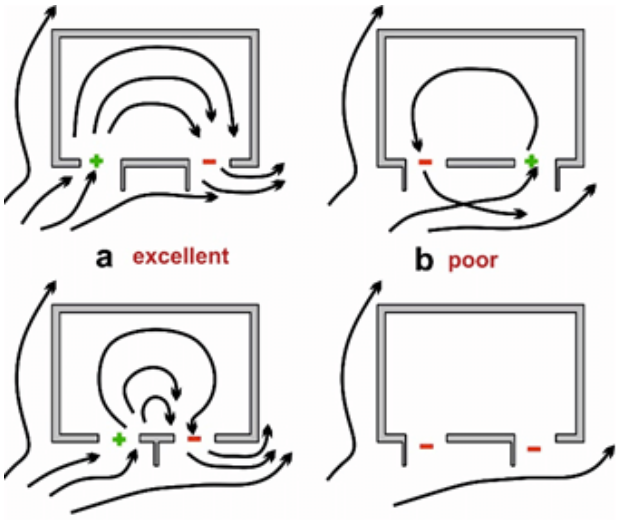

Figure 5.1. Example of (a) excellent and (b) poor cross ventilation performance by location of wing walls [99].

5.2.2. **Design process for optimization**

This section explains the decision process for each of the variables applied in each case for improving the passive cooling design of the CFD model. In general, to ensure good ventilation, openings should be parallel to the axis of the prevailing wind [100]. As shown in case S-0 Figure 4.3, the window in Space A received most of the prevailing wind – acting as a windward (positive pressure). Therefore, the cool air generated by the louver was easily accumulated at the semi-outdoor space and induced. In contrast, for Space B, since the cool air follows the same movement as the wind direction, it was dissipated and did not reach the window due to the large "louver to window distance" and air flow derived from the building geometry. As seen in case S-0 Figure 4.3 the wind speed crossing the window is nearly null. Moreover, the indoor space was not effectively cooled, demonstrating different requirements for optimization of Space A and Space B.

The following sections explain the design process (Figure 5.2) in detail and the results obtained after each optimization. The design process consists of the following steps of analysis, problem identification, implementation of hypothetical solution, and verification improvement of model. Each simulation is optimized in each step (by trial and error) until the desired outcome is reached. For this study, the optimized design was achieved when the averaged indoor air temperature was reduced to a minimum of 1 °C (i.e., 27 °C) as the criteria, in contrast to the field measurement results. Previous studies (T. Sawachi et al., 1987; H. Habara et al., 2005; H. Habara, 2015) have shown that the usage of air conditioners by building users decreases by less than 20% when the air temperature is kept below 28 ºC.

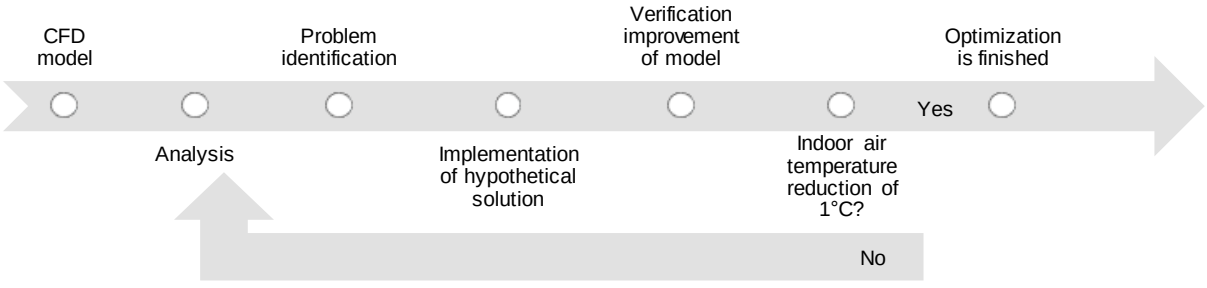

Figure 5.2. Flow chart of the process for passive cooling design using CFD simulation.

5.2.2.1. Optimization in case S-6: natural ventilation design.

Natural ventilation design is the first priority because it can instantly change airflow patterns inside buildings. Since this is a case study, variables such as architectural design of the house, window placement, orientation of the house, among others, could not be modified. Thus, for case S-6 the natural ventilation is improved by pressure difference. According to the simulation results, the most noticeable issues in case S-0 included nearly null WS_{win} for Space B and low cross ventilation inside the house. Therefore, to improve wind-driven ventilation, there is a need to force positive pressure at the window in Space B and increase the overall cross ventilation inside the house. Therefore, for case S-6, the following variables are used: (1) a wing wall added to Space B – wing walls increase the pressure difference and facilitate the motion of air through building openings [100]. (2) Living room door – found at the wall parallel to windward windows – is opened to facilitate the airflow inside the house. This adds one more negative pressure, increasing the porosity inside the building and improving the inflow through the window in Space B. Also (3) the entrance door is opened for easier exit of the hot air trapped inside the house. Results are shown in the section 3.1 of this chapter.

5.2.2.2. Optimization in case S-7 and S-8: semi-outdoor space design

After improving the natural ventilation design, the second priority is to improve the formation of cool air at the semi-outdoor space, especially for Space B. According to the results from case S-0 and case S-6, Space A has a better performance. However, for Space B, the large louver-window distance (2.8 m) reduces the cooling effect into the indoor space. Therefore, for the second optimization case S-7 the PCMs were shifted one meter closer to the window, resulting in a louver-window distance of 1.8 m. Potted vegetation and sunscreen was moved along, too, while planted trees were kept in their original position. In addition, to further improve the availability of cool air outside the windows in Space A and Space B, the ground level-floor level distance was reduced. Thus, for the third optimization case S-8 – a floor slab was added to the semi-outdoor space and the PCMs were shifted vertically 0.2 m. Results are shown in section 3.2 of this chapter.

5.2.2.3. Optimization in case S-9: Induction of cool air

Currently, the window has a simple opening – horizontal sliding – where only 50% of the airflow is induced (Figure 5.3). These types of windows do not affect the pattern or velocity of airflow except near the window as the airstream flows through the opening [100].Thus, because only 50% of the airflow is induced,

most of the cool air at the semi-outdoor space is not used for indoor cooling. Therefore, to improve the induction of cool air, the window is opened 100% in Space A and Space B. Large windows are required to maximize natural ventilation, but at the same time, any sunlight that enters through these large windows increases discomfort [4]. For this study, it is possible to open the window 100% since the PCMs provide a shelter from direct exposure of strong winds during summer. The effectiveness of windows in controlling air movement depends not only on the opening size but also on the type of window [100]. Vertical-vane openings influence both the pattern and velocity, with a particular effect on the airflow pattern [100]. Double casement windows are versatile, as the sashes can be inswinging or outswinging. In addition, sashes can be open one at a time, or both, allowing better control of the desired airflow. Thus, for the fourth optimization case S-9 a double casement window was applied. In this case the type of double casement window opens outwards (outswinging) to direct the maximum of cool air into the indoor space.

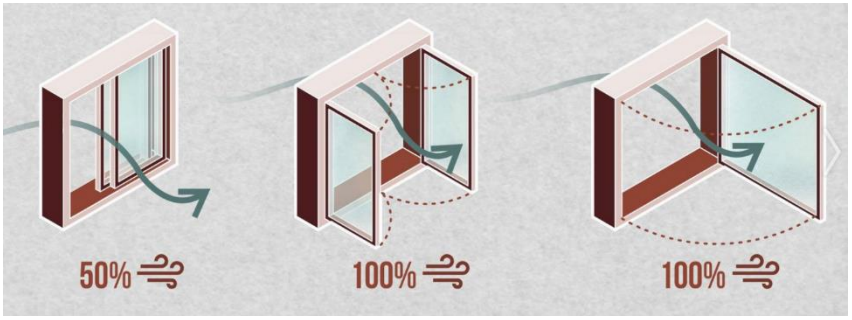

Figure 5.3. Example of percentage of incoming inflow according to window type.

5.2.2.4. Optimization in case S-10: Equal L-W distance for both semi-outdoor spaces.

In order to make a fair comparison of the cooling effect between Space A and Space B into the indoor space, an equal L-W distance is needed. Therefore, for the last optimization – case S-10, the PCMs were shifted 0.8 m closer to the window for Space B, so that both semi-outdoor spaces had the same L-W distance of 1.0 m.

5.3. Results

Figure 5.4 and Figure 5.5 show the vertical air temperature and wind speed distribution at the semi-outdoor and indoor space; and Figure 5.6, Figure 5.7, and Figure 5.8 show the air temperature and wind speed contours for GL + 1.5 m, Space A and Space B, respectively, for each case investigated in this chapter (Table 5.1).

5.3.1. Results for the optimization in case S-6

As observed in Figure 5.6 and Figure 5.8 for case S-6, when the case S-0 is modified to case S-6 with the variables in Table 5.1, the airflow through window in Space B significantly improves. Moreover, the air movement from windward windows to the entrance door is clearly observed (Figure 5.6b). Furthermore, Figure 5.5 shows that most of the improvement was observed for the indoor air temperature (T_{cin}) in Space B with an average reduction of 0.7 °C. This clearly demonstrates the importance on prioritizing natural ventilation design, which improved the airflow through the window thus inducing the cool air (available outside the window) into the indoor space. This case proves that the way air moves in and around a building is an unsteady, complex phenomenon, being highly affected by design choices and very much dependent on the dynamics of both the internal and the external environment [30].

5.3.2. Results for the optimization in case S-7 and case S-8

Results show that shifting the PCMs in Space B closer to the window allowed: (1) Space A to be more exposed to the outdoor wind resulting in a slight increase on the wind speed through the window (Figure 5.5); and (2) to improve the formation of cool microclimate in Space B (Figure 5.8). This resulted in an improvement on the induction of cool air into the indoor space for Space A and Space B. The average indoor air temperature (T_{cin}) was reduced 0.4 °C and 0.8 °C for Space A and Space B, respectively, in contrast to case S-0. Moreover, most of the cool air is accumulated near the ground (Figure 5.4, Figure 5.7, Figure 5.8). Therefore, for case S-8 a floor slab was added (explained in section 2.2.2) to investigate if there is a further reduction in the air temperature. Results show that the WS_{win} increased to an average of 0.6 m/s and 0.4 m/s for Space A and Space B, respectively, which resulted in an average T_{cin} reduction of 0.7 °C for Space A and 1.3 °C for Space B, in contrast to case S-0.

5.3.3. Results for the optimization in case S-9

After analyzing results from case S-8, it is seen that one of the major factors affecting the effective usage of cool microclimate formed in the semi-outdoor space, is the window type. Results in Figure 5.6 shows a significant improvement after the window type is changed. Not only is the cool air effectively induced (reducing T_{cin} to an average of 1.0 °C for Space A and 1.2 °C for Space B – in contrast to case S-0), but the wind speed through the window is also decreased to 0.4 m/s and 0.2 m/s for Space A and Space B, respectively, as shown in Figure 5.5. Even though the wind speed through the window was slightly lower – 0.2 m/s which is barely noticeable but comfortable [4] – the induction of cool air was obtained through natural convection. In addition, increasing the windward window area allowed more cool air to be induced into the indoor space. Case S-9 shows that increasing the window area can improve the induction of cool air by increasing the amount of air that enters the house.

5.3.4. Results for the optimization in case S-10

In addition, in order to compare the cooling effects of Space A and Space B into the indoor space with similar PCMs configurations, Space B was adjusted to have the same L-W distance as Space A. Results in Figure 5.4 shows that for the indoor space in Space A, the average indoor air temperature reduction in T_{cin} was maintained at 1 °C. Whereas for Space B the average T_{cin} was significantly reduced (in contrast to S-0) from 1.2 °C (Case S-9) to 1.6 °C. As observed in Figure 5.6, Space A is twice the size of the indoor space connected to Space B. Thus, this could be the reason why different T_{cin} reductions were obtained. This demonstrates that the cooling effect of PCMs into the indoor space is more likely to be more efficient if installed outside a smaller indoor space. In addition, case S-9 and case S-10 demonstrated that different L-W distance can be applied to obtain the desired cooling effect. For instance (case S-9) showed that a shorter L-W distance (1.0 m) is effective in cooling a larger indoor area, while a larger L-W distance (1.8 m) – which can be used as an outdoor patio – has the same indoor cooling effect with a smaller indoor area.

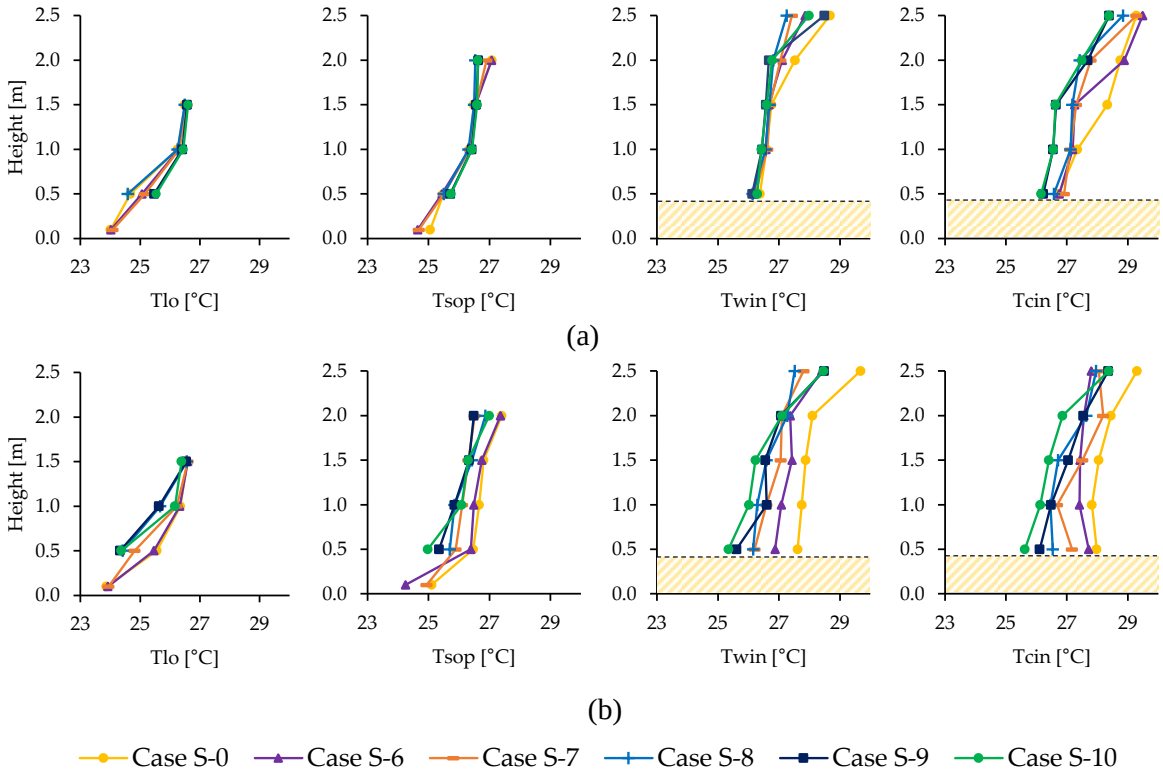

Figure 5.4. Vertical air temperature distribution at the semi-outdoor and indoor spaces at (a) Space A and (b) Space B for case S-0 and cases S-6-S-10.

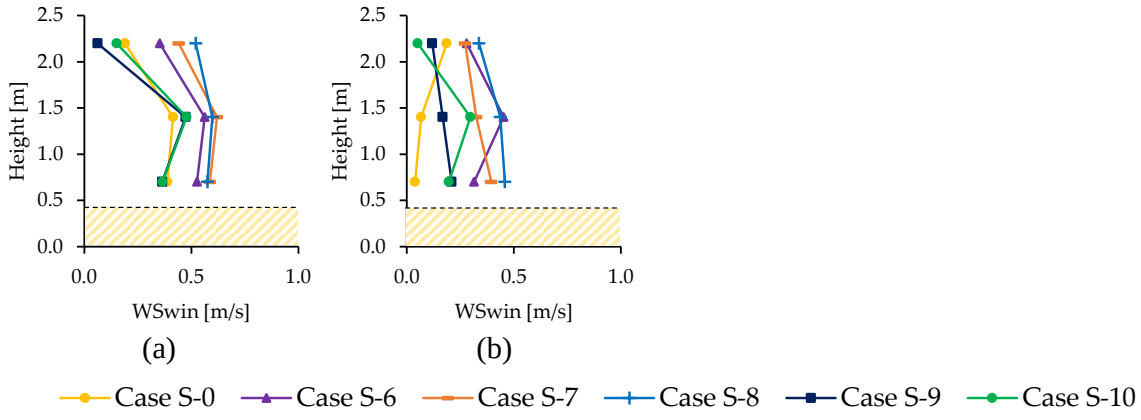

Figure 5.5. Vertical wind speed distribution at the indoor space (WS_{win}) for (a) Space A and (b) Space B for case S-0 and cases S-6-S-10.

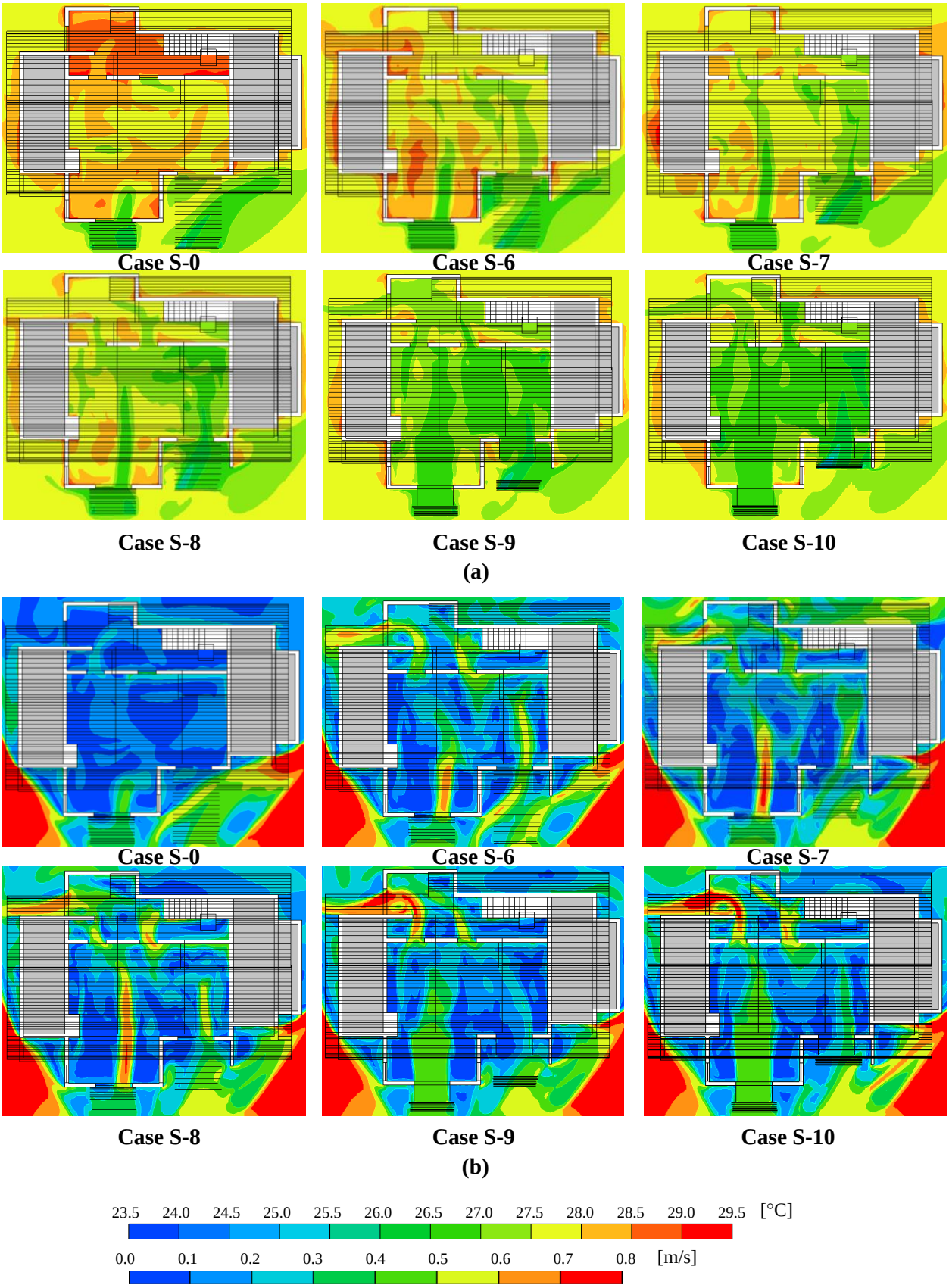

Figure 5.6. Horizontal (a) air temperature and (b) wind speed contour sections at GL + 1.5 m for Cases S-0, S-6 – S-10.

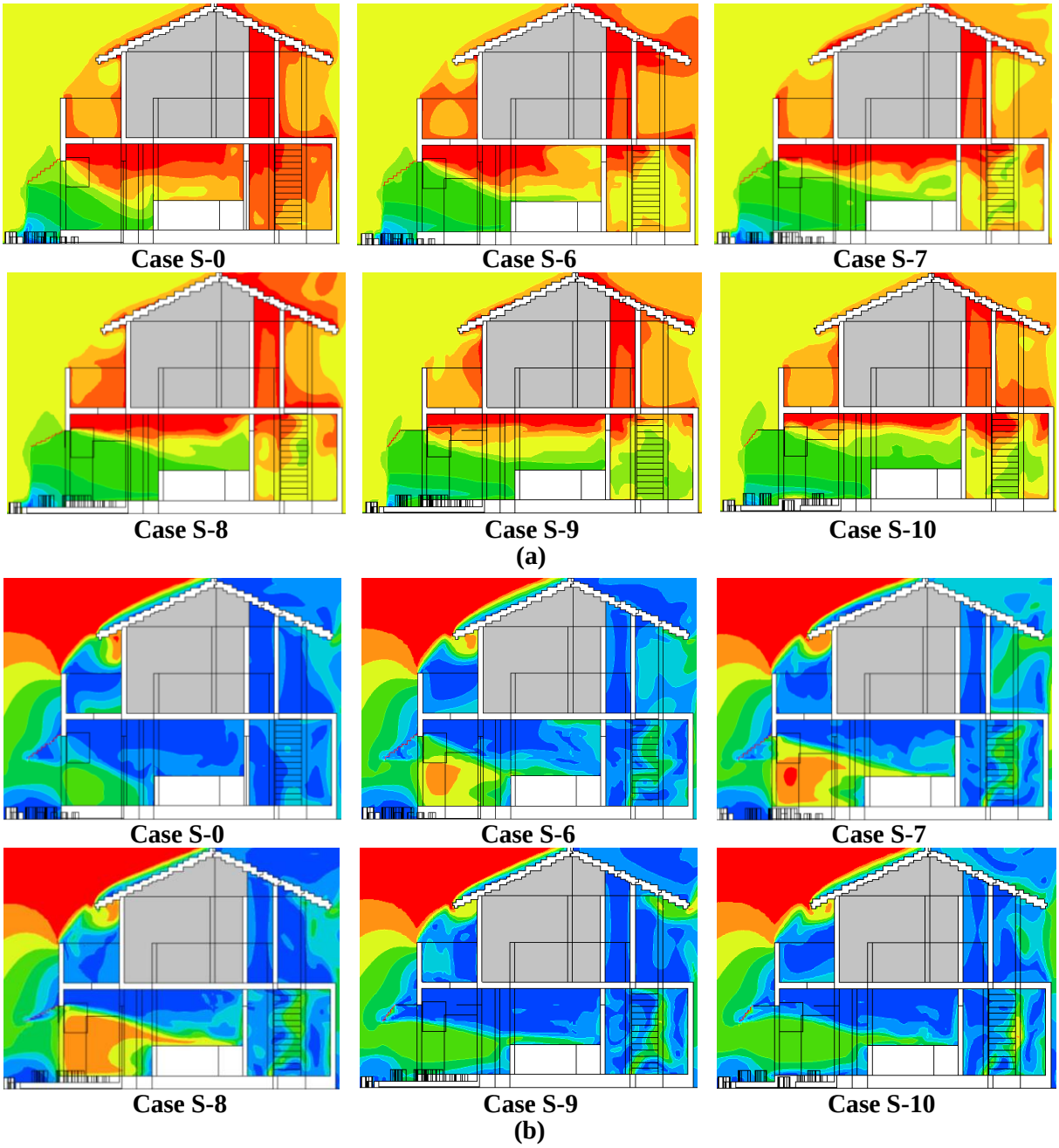

Figure 5.7. Vertical (a) air temperature and (b) wind speed contour sections for Space A for cases S-0, S-6 – S-10.

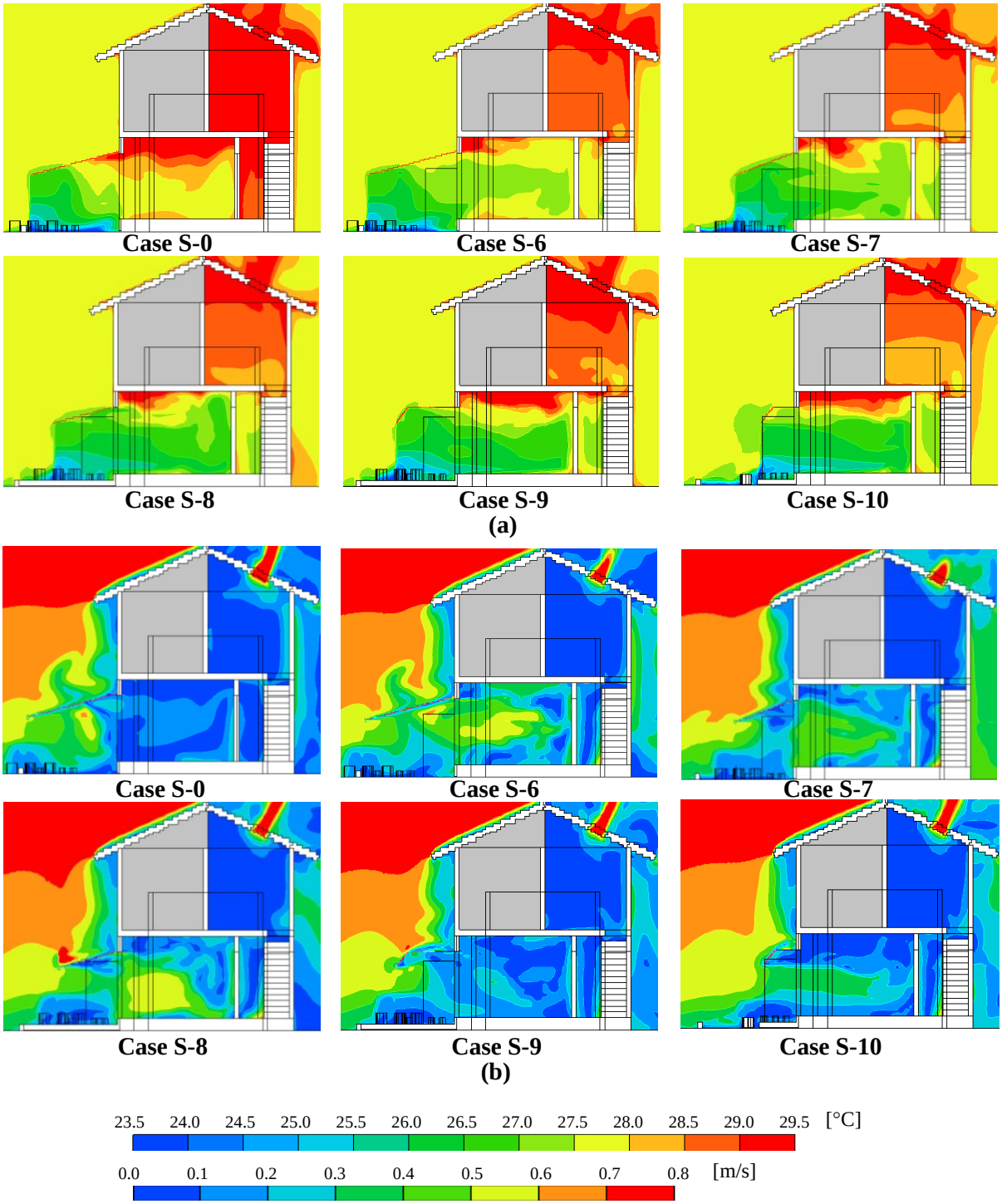

Figure 5.8. Vertical (a) air temperature and (wind speed) contour sections for Space B for case S-0 and cases S-6 – S-10.

5.4. Summary of optimization

This chapter investigates the improvement of the outdoor and indoor microclimate of a house using CFD simulation. The study consisted in modifying variables in the CFD model of case S-0 to find the best PCMs configuration and indoor conditions that will reduce the indoor air temperature to about 1 °C. The cases were optimized from case S-6 to case S-10 (Table 5.1). Case S-6 studied the pressure differences by adjusting the windward ventilation; ventilation between indoor rooms; and leeward ventilation with the variables (wing wall, opening indoor doors and opening the entrance door) in order to induce the cool air already available with the existent PCMs configurations. The results of case S-6 demonstrated that in order to utilize the cool microclimate by the PCMs; firstly proper natural ventilation techniques needs to be implemented – thus natural ventilation should be the first investigated variable when passive cooling designing with CFD simulation. Case S-7 utilized the same configurations of case S-6; where induction of cool air is already improved; to additionally tackle the L-W distance issues of Space B – which has a large L-W distance. Therefore, for case S-6 the PCMs in Space B were shifted 1.0 m closer to the window in order improve the cool microclimate formation. Results showed that the indoor air temperature for Space A and Space B was reduced to about 0.4 and 0.8 °C, respectively. Moreover, Figure 5.4 shows that most of the cool air is accumulated near the ground. Therefore, it was important to investigate the improvement of the indoor microclimate if this air is utilized. Thus, for case S-8 the PCMs were shifted 0.2 m above the ground by adding a floor slab in order to have less height difference between the semi-outdoor space and indoor space. Results showed that the indoor air temperature was reduced 0.7 °C for Space A and 1.3 °C for Space B, in contrast to case S-0. For indoor space A, the cooling effect of the PCMs are not as strong as with Space B, even though the cool microclimate formation is better in Space A due to the short L-W distance. Thus, to further induce the cool air available outside the window for both Space A and Space B, the window type was changed to casement window in case S-9 because the current window type is sliding and only allows 50% of the cool air to be induced. Thus, for case S-9 the induction of cool air by window type is investigated. Results shows that the indoor air temperature is reduced to 1.0 °C for Space A and 1.2 °C for Space B, in contrast to case S-0. This showed that the casement window (1) slightly decreased the wind speed, however (2) induced more cool air – increasing ventilation by natural convection. Moreover, results for case S-9 showed that the right combination of variables at the semi-outdoor and indoor space (Table 5.1) can improve the outdoor and indoor microclimates of the house. Furthermore, one more case was investigated in order to

study the formation of cool microclimate with similar PCMs configuration – L-W distances. Thus for case S-10 the PCMs in Space B were shifted 0.8 m so both Space A and Space B have the same L-W distances. Results showed that the indoor air temperature for Space B was further reduced from 1.2 (case S-9) to 1.6 °C in contrast to case S-0. This case demonstrated that cooling efficiency of the PCMs is determined not only by L-W distance but also by size of the indoor space adjacent to the PCMs; where, a smaller indoor space is easier to cool. This study demonstrates that is possible to use CFD simulation for passive cooling design during early stages of a project.

5.5. Performance of case S-9 with different wind directions.

In the previous section the case S-0 (base CFD model validated in Chapter 3) was optimized in order to tackle problems such as formation of cool microclimate in Space B and the induction of cool air into the indoor space. Moreover, the natural ventilation design of the house was optimized as well. Results were based on the best optimization for a stable wind direction and wind speed. Thus, in this section the design of Case S-9 will be evaluated under different wind direction conditions in order to observe how the cool outdoor and indoor microclimate formed by the current PCMs and ventilation conditions perform under different wind direction conditions. The case S-9 was selected because it shows the best application of PCMs according to semi-outdoor space size and indoor space size.

5.5.1. Wind direction settings

Table 5.2 shows the simulation cases that will be evaluated in this section. As observed, the initial case S-0 has a wind direction of SSW. Thus, the remaining wind directions that fall between 90 degrees perpendicular to the window; i.e., SE to SW is evaluated. The variable settings for Case S-9 are used. Thus, the base case used in this chapter is Case S-9 with SSW wind direction; Case S-11 is the case S-9 with changed wind direction to South; and so on, as observed in Table 5.2. For cases S-14 and S-15, one side of the window for Space A was removed to allow wind to be induced into the indoor space because the wind direction is not perpendicular to the window, i.e., SE and SW, respectively.

Table 5.2. Simulation cases for evaluation of performance of Case S-9 under different wind directions.

Simulation case	Wind direction	Flow boundary conditions		Variables
		Fixed inflow	Natural outflow	
Case S-9	SSW (197 degrees)	(Xmin, Ymin) X component =0.29 m/s Y component = 0.95 m/s Z component = 0 m/s	(Xmax, Ymax)	Case S-9
Case S-11	S (180 degrees)	(Ymin) X component =0 m/s Y component = 1 m/s Z component = 0 m/s	(Ymax)	Case S-9
Case S-12	SSE (163 degrees)	(Xmax, Ymin) X component =-0.29 m/s Y component = 0.95 m/s Z component = 0 m/s	(Xmin, Ymax)	Case S-9
Case S-13	SE (135 degrees)	(Xmax, Ymin) X component =-0.7 m/s Y component = 0.7 m/s Z component = 0 m/s	(Xmin, Ymax)	Case S-9
Case S-14	SE (135 degrees)	(Xmax, Ymin) X component =-0.7 m/s Y component = 0.7 m/s Z component = 0 m/s	(Xmin, Ymax)	Case S-9 + no right side of the window for Space A
Case S-15	SW (225 degrees)	Xmin and Ymin X component =-0.7 m/s Y component = 0.7 m/s Z component = 0 m/s	(Xmax, Ymax)	Case S-9 + no left side of the window for Space A

5.5.2. Results for Case S-9 under different wind directions

5.5.2.1. Formation of cool air at the semi-outdoor spaces

Figure 5.9, Figure 5.10, and Figure 5.11 shows the air temperature and wind speed contours for Case S-9 under different wind directions. As observed formation of cool air at the semi-outdoor space was easier to obtain for Space B under all wind directions in contrast to Space A. For Space A, the cases that performed the best were under SSW and S wind direction. This implies that for Space A, locating the louver in front of the window does not guarantee that the cool air will be induced or dissipated into the indoor space. The main difference from Space A and Space B is the building geometry; where, Space A has no walls blocking or affecting the wind direction, thus the cool air follows the wind direction. In contrast for Space B, there are walls to the left and right which protects the semi-outdoor from unstable winds which makes the formation of cool air easier.

5.5.2.2. Induction of cool air into the indoor spaces

Wind speed crossing the window is necessary in order to induce the cool air accumulated at the semi-outdoor space. This is confirmed and observed more clearly for Space B; where despite there is accumulation of cool air at the semi-outdoor space in Case S-15, the cool air was not induced into the indoor space. Among all cases for Space B, only case S-15 (SW) showed difficulties for inducing the cool air. Moreover, among all cases for Space A and Space B, more induction of cool air was obtained for Space B in contrast to Space A. This confirms that the performance of the evaporative cooling louver will vary according to where it is installed; where factors such as predominant wind direction; and building geometry are crucial. For this case in particular, the case study is placed in a residential area where the predominant wind direction during summer is SSE. Thus this study demonstrates that the best placement for the evaporative cooling louver for this particular house is for Space B because the evaporative cooling effect into the indoor space can be obtain in most of the wind directions.

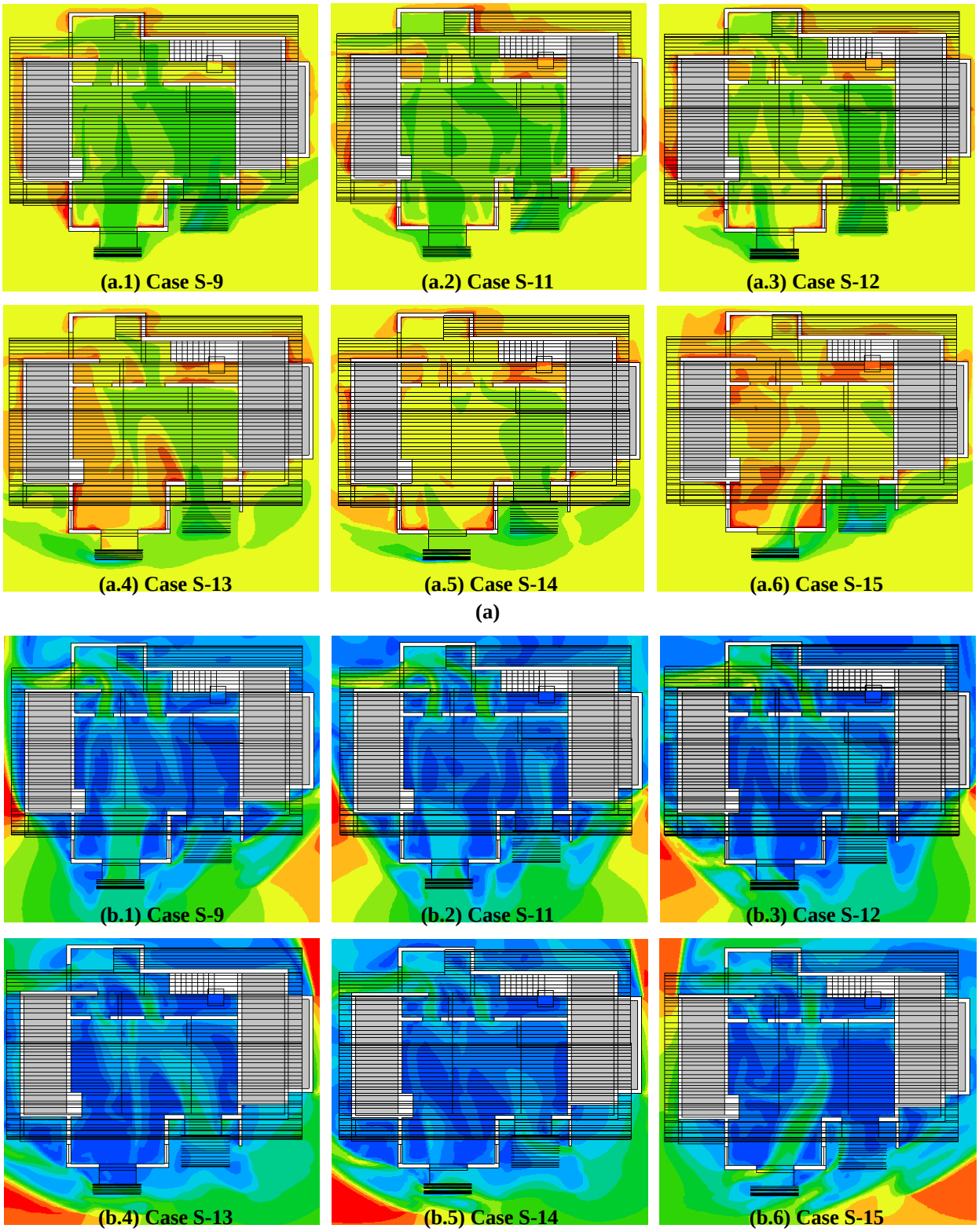

Figure 5.9. Horizontal (a) Air temperature and (b) wind speed contour sections at GL + 1.5 m for optimized Case S-9 under different wind directions.

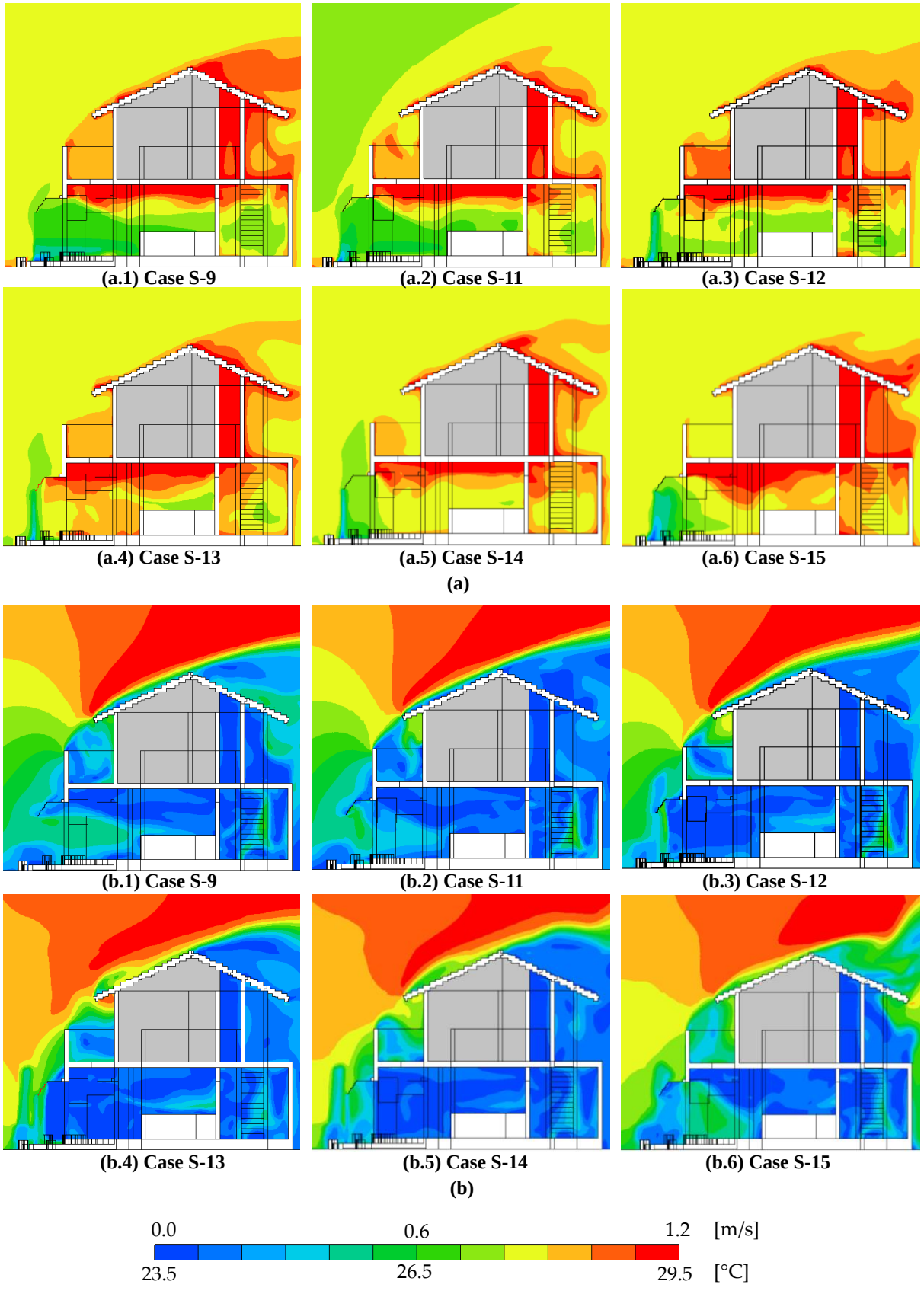

Figure 5.10. Vertical (a) Air temperature and (b) wind speed contour sections for Space A for Case S-9 under different wind directions.

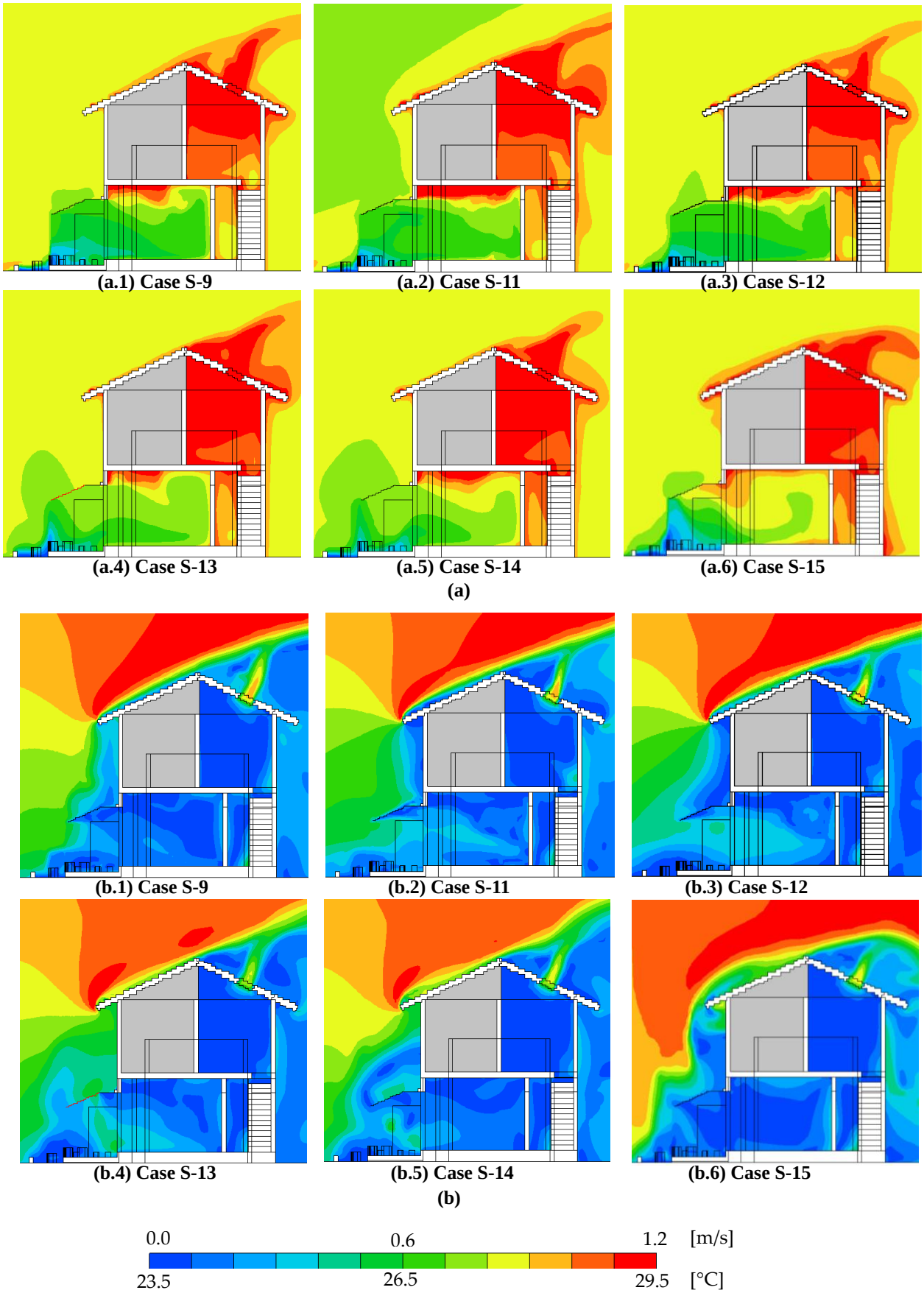

Figure 5.11. Vertical (a) Air temperature and (b) wind speed contour sections for Space B for Case S-9 under different wind directions.

Figure 5.12. Summary of all cases and variables.

Cases		WD_{out}	PCMs	Semi-outdoor space			GL – FL [m]	Wingwall	Indoor conditions		
				Louver watering	L-W distance [m] Space A	Space B		1 m Space B	Windward ventilation	Cross ventilation	Leeward ventilation
Validation	Case S-0	SSW	Louver (L), vegetation (V), sunscreen (S)	watered	1	2.8	0.4	No	Sliding window	Open kitchen door	Sky window
Sensitivity analysis	Case S-1	SSW	L, V, S	wet	1	2.8	0.4	No	Sliding window	Open kitchen door	Sky window
	Case S-2		L, V, S	dry	1	2.8					
	Case S-3		L, S	watered	1	2.8					
	Case S-4		V, S	-	-	-					
	Case S-5		S	-	-	-					
Optimization	Case S-6	SSW	L, V, S	watered	1	2.8	0.4	Yes	Sliding window	Open kitchen and living room doors	Sky window + entrance door open
	Case S-7					1.8	0.4				
	Case S-8					1.8	0.2				
	Case S-9					1.8	0.2		Casement window		
	Case S-10					1.0	0.2				
Evaluation with different wind directions	Case S-11	S	L, V, S	watered	1	1.8	0.2	Yes	Casement window	Open kitchen and living room doors	Sky window + entrance door open
	Case S-12	SSW									
	Case S-13	SE									
	Case S-14	SE									
	Case S-15	SW									

CHAPTER 6. CONCLUSION

In the hot-humid summer climate of Tokyo, a combination of factors such as reduced green spaces and increasingly compact house design in urban and suburban areas has made it difficult to maintain a comfortable indoor microclimate using only passive cooling methods such as natural ventilation and solar shading. In order to improve natural ventilation in urban residences, outdoor microclimate design using a combination of passive cooling methods (PCMs) is recommended. This study analyzes the formation of outdoor and indoor microclimates of a house located in one of the hottest cities in Japan by using combined PCMs and indoor conditions. The PCMs included an evaporative cooling louver, vegetation, and sunscreen installed outside two windows in the southwest facade of the house. The study was carried out in several parts in order to evaluate the best configuration of PCMs on forming a cool microclimate and best indoor conditions for inducing the cool air. First, a (1) field measurement was conducted. Among the cases in the field measurement studied, CASE 1 exhibited the best PCMs configuration and CASE 4 the worst. It was found that combination of watered louver, surrounding vegetation and shorter louver-window distance provided a better microclimate than when no vegetation and a large louver window distance was used. Induction of cool air was not fully obtained during the field measurement. Thus, in order to conduct a parametric study a (2) CFD simulation was conducted and validated using field measurement data. The results showed good correlation between the experiment and simulation for Spaces A and B. The R^2 for all points was between 0.93 and 0.99, and the RMSE was between 0.2 and 0.5 except for T_{win}, demonstrating that the model accurately predicts air temperature. The validated case was then used to conduct a (3) sensitivity analysis to reproduce the cooling effect between different louver watering conditions; and effect of different amount of PCMs in the formation of cool microclimate. (4) Finally an optimization of the validated case is conducted in order to find the best PCMs and indoor conditions that improves both outdoor microclimate and indoor microclimate simultaneously. Moreover, the best optimization method was evaluated under different wind directions.

6.1. Recommendations for generation of cool microclimates inside buildings

After analyzing all cases it was found that in order to generate cool microclimates inside buildings a combination of (1) reduction of ambient temperature and (2) improving the natural ventilation is necessary:

- (1) Reduce outdoor ambient temperature by shading walls and windows, using evaporative cooling materials (vegetation, louver).
- (2) Improve natural ventilation of the house by increasing the porosity of the building (windward and leeward openings). In general to guarantee natural ventilation windward openings should be located perpendicular to the prevailing wind during summer.

According to the results in this study the usage of evaporative cooling louver for cooling indoor spaces is limited. Table 6.1 shows the recommendations for using the louver for forming cool microclimates inside buildings. Evaporative cooling louver can reduce indoor air temperatures to about 1-2 °C, depending on the size of the indoor space, the smaller the indoor space the higher the cooling effect.

Table 6.1. Use of the evaporative cooling louver for cooling indoor spaces

	Recommended	Avoid
1	Install louver in a semi-enclosed* outdoor space.	Install louver in an open*outdoor space.
2	Shade surroundings (wall, window, floor)	
3	Install louver close to the target area. Up to 1.5 meters apart from the window.	Install louver far from the target area.
4	Use to aid mixed mode ventilation.	
5	Install louver parallel to the window and perpendicular to the predominant wind direction during summer.	Installing the louver without careful consideration of wind direction, and location of openings.
6	Use watered louver when the relative humidity is about 50-70% and outdoor temperatures below 29 °C (outdoor temperatures are not too hot).	Use watered louver when the relative humidity is above 70%, outdoor temperatures above 29 °C or very hot outdoor air temperature, in this case air conditioning is recommended.
7	Used during daytime.	Used during nighttime. More difficult to evaporate water and get high cooling effect.
8	House has indoor partitions, target area is enclosed.	House has an open floor plan; cool air is dissipated faster and cooling effect is lost.
9	Stack and cross ventilation. Windward + leeward ventilation (opposite sides of the room). Cool air travels further and cools the target indoor space.	Single sided ventilation. Cool air is not induced, it returns to same opening (windward and leeward opening are the same).

*Semi-enclosed: Space B (case S-9), *open: Space A.

An open floor plan is considered effective for houses located in countries with year round hot and humid climate and fully naturally ventilated. That said, Japan has four seasons and therefore houses in Japan need to be well insulated and airtight for high energy efficiency. They need to conserve heat during winter and cool during summer, thus a house with partitions will allow for each room to have a specific microclimate and thus conserve energy depending on its use. This said, a house with partitions can also be a well natural ventilated house (transition seasons) if a proper interior design and location of windows and indoor openings (doors) allow for optimal use of the differential pressure generated across the building, thus promoting cross and stack ventilation.

Figure 6.1 shows an example for recommended sizes for windward and leeward openings. As observed, for leeward openings these can be designed / installed around 1.5 meters above the floor level for cross ventilation and a clerestory window for stack ventilation in order to dissipate the hot air while maintaining the cool air inside the house.

The case study used has a compact design and obstacles (staircase / corridor) which impede smooth air movement. In addition, the case study did not count with many leeward openings, thus the optimization cases demonstrated that adding leeward openings improve natural ventilation. Therefore, the design of interior partitions and location of window is crucial to guarantee appropriate natural ventilation.

Figure 6.1 Example of sizes for windward and leeward opening for generating cool microclimates inside buildings

6.2.Future works

This study confirmed the formation of cool microclimates using PCMs and indoor conditions under certain conditions; i.e., building site, location of PCMs according to building geometry, location of windows, size of indoor space, and wind directions. Therefore, future studies can evaluate the PCMs when applied in other buildings located in dense suburban areas; i.e., with surrounding buildings. Results can be useful in the development of guidelines for installation of PCMs in semi-outdoor spaces to improve the outdoor microclimate of compact houses and thus the indoor microclimate. Moreover, thermal comfort with standard effective temperature (SET*) will be conducted to evaluate the improvement of indoor microclimate using best combined PCMs and indoor conditions.

Night purge ventilation

This study focused on evaluating the cooling effect of the evaporative cooling louver in the common area (kitchen, living room and dining room) with daytime ventilation. In general, the louver is recommended for daytime use - higher evaporative cooling effect – and window opening is safe. However, further studies can be carried out to analyze the extended effect of low surface temperature of outdoor elements (louver and vegetation) for night purge ventilation for rooms located in second floor or above (in balconies) because is more safe to keep windows open at nighttime (due to safety it is not recommended to open windows in the first floor). Moreover, the main purpose of night purge is inducing cool outdoor air into indoor spaces to store “coolness” in building structure and materials during night time. In this view, night purge needs higher heat capacity for building structure and materials (e.g. concrete). The target house of this study has wooden structure with less heat capacity. Therefore, it is important to add materials with higher heat capacity (e.g. phase change materials) into the house when applying night purge.

Bibliography

1. Iyendo, T. O.; Akingbaso, E. Y.; Alibaba, H. Z.; Özdeniz, M. B. A Relative Study of Microclimate Responsive Design Approaches to Buildings in Cypriot Settlements. *A/Z ITU J. Fac. Archit.* **2016**, *13* (1), 69–81. https://doi.org/10.5505/itujfa.2016.51423.

2. Liao, F. C.; Cheng, M. J.; Hwang, R. L. Influence of Urban Microclimate on Air-Conditioning Energy Needs and Indoor Thermal Comfort in Houses. *Adv. Meteorol.* **2015**, *2015*. https://doi.org/10.1155/2015/585623.

3. Allegrini, J.; Dorer, V.; Carmeliet, J. Impact of Radiation Exchange between Buildings in Urban Street Canyons on Space Cooling Demands of Buildings. *Energy Build.* **2016**, *127*, 1074–1084. https://doi.org/10.1016/j.enbuild.2016.06.073.

4. Lechner, N. *Heating, Cooling, Lighting: Sustainable Design Methods for Architects*; John wiley & sons, 2014.

5. Magli, S.; Lodi, C.; Lombroso, L.; Muscio, A.; Teggi, S. Analysis of the Urban Heat Island Effects on Building Energy Consumption. *Int. J. Energy Environ. Eng.* **2015**, *6* (1), 91–99.

6. Hong, B.; Qin, H.; Jiang, R.; Xu, M.; Niu, J. How Outdoor Trees Affect Indoor Particulate Matter Dispersion: CFD Simulations in a Naturally Ventilated Auditorium. *Int. J. Environ. Res. Public Health* **2018**, *15* (12), 2862. https://doi.org/10.3390/ijerph15122862.

7. Dimoudi, A. *Passive Cooling of Buildings*; Earthscan, 2013. https://doi.org/10.4324/9781315073668.

8. Santamouris, M.; Kolokotsa, D. Passive Cooling Dissipation Techniques for Buildings and Other Structures: The State of the Art. *Energy Build.* **2013**, *57*, 74–94. https://doi.org/10.1016/j.enbuild.2012.11.002.

9. Shahidan, M. F.; Jones, P. J.; Gwilliam, J.; Salleh, E. An Evaluation of Outdoor and Building Environment Cooling Achieved through Combination Modification of Trees with Ground Materials. *Build. Environ.* **2012**, *58*, 245–257.

10. Park, M.; Hagishima, A.; Tanimoto, J.; Narita, K. Effect of Urban Vegetation on Outdoor Thermal Environment: Field Measurement at a Scale Model Site. *Build. Environ.* **2012**, *56*, 38–46.

11. Srivanit, M.; Hokao, K. Evaluating the Cooling Effects of Greening for Improving the Outdoor Thermal Environment at an Institutional Campus in the Summer. *Build. Environ.* **2013**, *66*, 158–172.

12. Zhang, B.; Xie, G. di; Gao, J. xi; Yang, Y. The Cooling Effect of Urban Green Spaces as a Contribution to Energy-Saving and Emission-Reduction: A Case Study in Beijing, China. *Build. Environ.* **2014**, *76*, 37–43. https://doi.org/10.1016/j.buildenv.2014.03.003.

13. Santamouris, M. *Environmental Design of Urban Buildings: An Integrated Approach*; Routledge, 2013.

14. Yoshida, A.; Hisabayashi, T.; Kashihara, K.; Kinoshita, S.; Hashida, S. Evaluation of Effect of Tree Canopy on Thermal Environment, Thermal Sensation, and Mental State. *Urban Clim.* **2015**, *14*, 240–250.

15. Lee, T. C.; Asawa, T.; Kawai, H.; Sato, R.; Hirayama, Y.; Ohta, I. Multipoint Measurement Method for Air Temperature in Outdoor Spaces and Application to Microclimate and Passive Cooling Studies for a House. *Build. Environ.* **2017**, *114*, 267–280. https://doi.org/10.1016/j.buildenv.2016.12.030.

16. Calcerano, F.; Martinelli, L. Numerical Optimisation through Dynamic Simulation of the Position of Trees around a Stand-Alone Building to Reduce Cooling Energy Consumption. *Energy Build.* **2016**, *112*, 234–243. https://doi.org/10.1016/j.enbuild.2015.12.023.

17. Taleghani, M.; Tenpierik, M.; van den Dobbelsteen, A.; Sailor, D. J. Heat in Courtyards: A Validated and Calibrated Parametric Study of Heat Mitigation Strategies for Urban Courtyards in the Netherlands. *Sol. Energy* **2014**, *103*, 108–124.

18. Robitu, M.; Musy, M.; Inard, C.; Groleau, D. Modeling the Influence of Vegetation and Water Pond on Urban Microclimate. *Sol. Energy* **2006**, *80* (4), 435–447.

https://doi.org/https://doi.org/10.1016/j.solener.2005.06.015.

19. Do\ugramac\i, P. A.; Riffat, S.; Gan, G.; Ayd\in, D. Experimental Study of the Potential of Eucalyptus Fibres for Evaporative Cooling. *Renew. Energy* **2019**, *131*, 250–260.

20. Maerefat, M.; Haghighi, A. P. Natural Cooling of Stand-Alone Houses Using Solar Chimney and Evaporative Cooling Cavity. *Renew. Energy* **2010**, *35* (9), 2040–2052. https://doi.org/10.1016/j.renene.2010.02.005.

21. Wong, N. H.; Chong, A. Z. M. Performance Evaluation of Misting Fans in Hot and Humid Climate. *Build. Environ.* **2010**, *45* (12), 2666–2678. https://doi.org/10.1016/j.buildenv.2010.05.026.

22. URANO, Y.; WATANABE, T.; HAYASHI, T.; UCHIYAMA, A. Study on Thermal Environment of Traditional Vernacular Houses in Northern Kyushu. *J. Archit. Plan. Environ. Eng. (Transactions AIJ)* **1987**, *371* (0), 27–37. https://doi.org/10.3130/aijax.371.0_27.

23. He, J.; Hoyano, A. Experimental Study of Practical Applications of a Passive Evaporative Cooling Wall with High Water Soaking-up Ability. *Build. Environ.* **2011**, *46* (1), 98–108. https://doi.org/10.1016/j.buildenv.2010.07.004.

24. Hirayama, Y.; Ohta, M. I.; Hoyano, A.; Asawa, T. Thermal Performance of a Passive Cooling Louver System to Form Cool Microclimate in Urban Residential Outdoor Spaces. In *30th INTERNATIONAL PLEA CONFERENCE, CEPT University, Ahmedabad*; 2014.

25. Hirayama, Y.; Asawa, T.; Sato, R.; Ohta, I.; Sumi, N. Study on Design Method for Cool Spot Formation in a Semi-Outdoor Space by Combining Various Passive Cooling Techniques. *J. Environ. Eng.* **2018**, *83* (744), 193–203. https://doi.org/10.3130/aije.83.193.

26. Marui, M.; Hoyano, A.; Asawa, T. Proposal of an Evaporative Cooling Pavement System for the Improvement of Tropical Urban Thermal Environments. In *Proceedings of the second international conference on sustainable architecture and urban design in tropical regions, Jogjakarta, Indonesia*; 2006; pp P21--1.

27. Aflaki, A.; Mahyuddin, N.; Mahmoud, Z. A.-C.; Baharum, M. R. A Review on Natural Ventilation Applications through Building Façade Components and Ventilation Openings in Tropical Climates. *Energy Build.* **2015**, *101*, 153–162.

28. Chen, Y.; Tong, Z.; Malkawi, A. Investigating Natural Ventilation Potentials across the Globe: Regional and Climatic Variations. *Build. Environ.* **2017**, *122*, 386–396.

29. Fabi, V.; Andersen, R. V.; Corgnati, S.; Olesen, B. W. Occupants' Window Opening Behaviour: A Literature Review of Factors Influencing Occupant Behaviour and Models. *Build. Environ.* **2012**, *58*, 188–198. https://doi.org/10.1016/j.buildenv.2012.07.009.

30. Chenari, B.; Carrilho, J. D.; da Silva, M. G. Towards Sustainable, Energy-Efficient and Healthy Ventilation Strategies in Buildings: A Review. *Renew. Sustain. Energy Rev.* **2016**, *59*, 1426–1447.

31. Mumovic, D.; Santamouris, M. *A Handbook of Sustainable Building Design and Engineering:" An Integrated Approach to Energy, Health and Operational Performance"*; Routledge, 2013.

32. Toparlar, Y.; Blocken, B.; Vos, P.; Van Heijst, G. J. F.; Janssen, W. D.; van Hooff, T.; Montazeri, H.; Timmermans, H. J. P. CFD Simulation and Validation of Urban Microclimate: A Case Study for Bergpolder Zuid, Rotterdam. *Build. Environ.* **2015**, *83*, 79–90. https://doi.org/10.1016/j.buildenv.2014.08.004.

33. Toparlar, Y.; Blocken, B.; Maiheu, B.; van Heijst, G. J. F. A Review on the CFD Analysis of Urban Microclimate. *Renew. Sustain. Energy Rev.* **2017**, *80*, 1613–1640. https://doi.org/10.1016/j.rser.2017.05.248.

34. Tominaga, Y.; Sato, Y.; Sadohara, S. CFD Simulations of the Effect of Evaporative Cooling from Water Bodies in a Micro-Scale Urban Environment: Validation and Application Studies. *Sustain. Cities Soc.* **2015**, *19*, 259–270.

35. Yang, A.-S.; Juan, Y.-H.; Wen, C.-Y.; Chang, C.-J. Numerical Simulation of Cooling Effect of Vegetation Enhancement in a Subtropical Urban Park. *Appl. Energy* **2017**, *192*, 178–200.

36. Yuan, C.; Shan, R.; Adelia, A. S.; Tablada, A.; Lau, S. K.; Lau, S. S.-Y. Effects of Vertical Farming on Natural Ventilation of Residential Buildings. *Energy Build.* **2019**, *185*, 316–325.

37. Perén, J. I.; Van Hooff, T.; Leite, B. C. C.; Blocken, B. CFD Analysis of Cross-Ventilation of a Generic Isolated Building with Asymmetric Opening Positions: Impact of Roof Angle and Opening Location. *Build. Environ.* **2015**, *85*, 263–276.

38. van Hooff, T.; Blocken, B.; Tominaga, Y. On the Accuracy of CFD Simulations of Cross-Ventilation Flows for a Generic Isolated Building: Comparison of RANS, LES and Experiments. *Build. Environ.* **2017**, *114*, 148–165. https://doi.org/10.1016/j.buildenv.2016.12.019.

39. Borge-Diez, D.; Colmenar-Santos, A.; Pérez-Molina, C.; Castro-Gil, M. Passive Climatization Using a Cool Roof and Natural Ventilation for Internally Displaced Persons in Hot Climates: Case Study for Haiti. *Build. Environ.* **2013**, *59*, 116–126.

40. Michael, A.; Demosthenous, D.; Philokyprou, M. Natural Ventilation for Cooling in Mediterranean Climate: A Case Study in Vernacular Architecture of Cyprus. *Energy Build.* **2017**, *144*, 333–345.

41. Lapisa, R.; Bozonnet, E.; Salagnac, P.; Abadie, M. O. Optimized Design of Low-Rise Commercial Buildings under Various Climates--Energy Performance and Passive Cooling Strategies. *Build. Environ.* **2018**, *132*, 83–95.

42. Toe, D. H. C.; Kubota, T. Comparative Assessment of Vernacular Passive Cooling Techniques for Improving Indoor Thermal Comfort of Modern Terraced Houses in Hot--Humid Climate of Malaysia. *Sol. Energy* **2015**, *114*, 229–258.

43. He, J.; Hoyano, A. The Effects of Windbreak Forests on the Summer Thermal Environment in a Residence. *J. Asian Archit. Build. Eng.* **2009**, *8* (1), 291–298.

44. He, J.; Hoyano, A. Measurement and Evaluation of the Summer Microclimate in the Semi-Enclosed Space under a Membrane Structure. *Build. Environ.* **2010**, *45* (1), 230–242.

45. Kishore, K. N.; Rekha, J. A Bioclimatic Approach to Develop Spatial Zoning Maps for Comfort, Passive Heating and Cooling Strategies within a Composite Zone of India. *Build. Environ.* **2018**, *128*, 190–215.

46. Elshafei, G.; Negm, A.; Bady, M.; Suzuki, M.; Ibrahim, M. G. Numerical and Experimental Investigations of the Impacts of Window Parameters on Indoor Natural Ventilation in a Residential Building. *Energy Build.* **2017**, *141*, 321–332.

47. Manu, S.; Brager, G.; Rawal, R.; Geronazzo, A.; Kumar, D. Performance Evaluation of Climate Responsive Buildings in India-Case Studies from Cooling Dominated Climate Zones. *Build. Environ.* **2019**, *148*, 136–156.

48. Lin, F. The Development Path of Japanese Green Architecture under Energy Policy--Taking Misawa Home as an Example. *Energy Procedia* **2012**, *14*, 1305–1310.

49. Ohta, I.; Iijima, M.; Hirayama, Y. OBSERVATIONS ON THE NEWLY DEVELOPED ZERO-ENERGY-HOMES DISTRICT. In *Grand Renewable Energy proceedings Japan council for Renewable Energy*; 2018; p 111.

50. Office, K. M. On the Heat in Saitama Prefecture. 2018.

51. Raji, B.; Tenpierik, M. J.; van den Dobbelsteen, A. The Impact of Greening Systems on Building Energy Performance: A Literature Review. *Renew. Sustain. Energy Rev.* **2015**, *45*, 610–623.

52. Chen, Q.; Li, B.; Liu, X. An Experimental Evaluation of the Living Wall System in Hot and Humid Climate. *Energy Build.* **2013**, *61*, 298–307.

53. Crank, P. J.; Sailor, D. J.; Ban-Weiss, G.; Taleghani, M. Evaluating the ENVI-Met Microscale Model for Suitability in Analysis of Targeted Urban Heat Mitigation Strategies. *Urban Clim.* **2018**, *26*, 188–197.

54. Forouzandeh, A. Numerical Modeling Validation for the Microclimate Thermal Condition of Semi-Closed Courtyard Spaces between Buildings. *Sustain. cities Soc.* **2018**, *36*, 327–345.

55. Égerházi, L. A.; Kovács, A.; Unger, J. Application of Microclimate Modelling and Onsite Survey in Planning Practice Related to an Urban Micro-Environment. *Adv. Meteorol.* **2013**, *2013*.

56. Liu, Z.; Zheng, S.; Zhao, L. Evaluation of the ENVI-Met Vegetation Model of Four Common Tree Species in a Subtropical Hot-Humid Area. *Atmosphere (Basel).* **2018**, *9* (5), 198.

57. Tsoka, S.; Tsikaloudaki, A.; Theodosiou, T. Analyzing the ENVI-Met Microclimate Model's Performance and Assessing Cool Materials and Urban Vegetation Applications--A Review. *Sustain. cities Soc.* **2018**, *43*, 55–76.

58. Chatzinikolaou, E.; Chalkias, C.; Dimopoulou, E. URBAN MICROCLIMATE IMPROVEMENT USING ENVI-MET CLIMATE MODEL. *Int. Arch. Photogramm. Remote Sens. Spat. Inf. Sci.* **2018**, *42* (4).

59. Baglivo, C.; Congedo, P. M. Design Method of High Performance Precast External Walls for Warm Climate by Multi-Objective Optimization Analysis. *Energy* **2015**, *90*, 1645–1661.

60. Congedo, P. M.; Baglivo, C.; Centonze, G. Walls Comparative Evaluation for the Thermal Performance Improvement of Low-Rise Residential Buildings in Warm Mediterranean Climate. *J. Build. Eng.* **2020**, *28*, 101059.

61. Saffari, M.; de Gracia, A.; Ushak, S.; Cabeza, L. F. Passive Cooling of Buildings with Phase Change Materials Using Whole-Building Energy Simulation Tools: A Review. *Renew. Sustain. Energy Rev.* **2017**, *80*, 1239–1255.

62. Bhamare, D. K.; Rathod, M. K.; Banerjee, J. Passive Cooling Techniques for Building and Their Applicability in Different Climatic Zones-The State of Art. *Energy Build.* **2019**.

63. He, J.; Hoyano, A.; Asawa, T. A Numerical Simulation Tool for Predicting the Impact of Outdoor Thermal Environment on Building Energy Performance. *Appl. Energy* **2009**, *86* (9), 1596–1605. https://doi.org/10.1016/j.apenergy.2008.12.034.

64. Drach, P. R. C.; Karam-Filho, J. Increasing Ventilation by Passive Strategies: Analysis of Indoor Air Circulation Changes through the Utilization of Microclimate Elements. *Appl. Math.* **2014**, *05* (03), 442–452. https://doi.org/10.4236/am.2014.53044.

65. Yi, C. Y.; Peng, C. Microclimate Change Outdoor and Indoor Coupled Simulation for Passive Building Adaptation Design. *Procedia Comput. Sci.* **2014**, *32*, 691–698. https://doi.org/10.1016/j.procs.2014.05.478.

66. Elwy, I.; Ibrahim, Y.; Fahmy, M.; Mahdy, M. Outdoor Microclimatic Validation for Hybrid Simulation Workflow in Hot Arid Climates against ENVI-Met and Field Measurements. *Energy Procedia* **2018**, *153*, 29–34. https://doi.org/10.1016/j.egypro.2018.10.009.

67. de La Flor, F. S.; Dom\inguez, S. A. Modelling Microclimate in Urban Environments and Assessing Its Influence on the Performance of Surrounding Buildings. *Energy Build.* **2004**, *36* (5), 403–413.

68. Shirzadi, M.; Naghashzadegan, M.; Mirzaei, P. A. Developing a Framework for Improvement of Building Thermal Performance Modeling under Urban Microclimate Interactions. *Sustain. Cities Soc.* **2019**, *44*, 27–39.

69. Merlier, L.; Frayssinet, L.; Johannes, K.; Kuznik, F. On the Impact of Local Microclimate on Building Performance Simulation. Part I: Prediction of Building External Conditions. In *Building Simulation*; 2019; Vol. 12, pp 735–746.

70. Yang, X.; Zhao, L.; Bruse, M.; Meng, Q. An Integrated Simulation Method for Building Energy Performance Assessment in Urban Environments. *Energy Build.* **2012**, *54*, 243–251. https://doi.org/10.1016/j.enbuild.2012.07.042.

71. Gros, A.; Bozonnet, E.; Inard, C.; Musy, M. Simulation Tools to Assess Microclimate and Building Energy--A Case Study on the Design of a New District. *Energy Build.* **2016**, *114*, 112–122.

72. Gobakis, K.; Kolokotsa, D. Coupling Building Energy Simulation Software with Microclimatic Simulation for the Evaluation of the Impact of Urban Outdoor Conditions on the Energy Consumption and Indoor Environmental Quality. *Energy Build.* **2017**, *157*, 101–115.

73. Toparlar, Y.; Blocken, B.; Maiheu, B.; van Heijst, G. J. F. Impact of Urban Microclimate on Summertime Building Cooling Demand: A Parametric Analysis for Antwerp, Belgium. *Appl. Energy* **2018**, *228*, 852–872.

74. Dorer, V.; Allegrini, J.; Orehounig, K.; Moonen, P.; Upadhyay, G.; Kämpf, J.; Carmeliet, J. Modelling the Urban Microclimate and Its Impact on the Energy Demand of Buildings and Building Clusters. *Proc. BS* **2013**, *2013*, 3483–3489.

75. Natanian, J.; Maiullari, D.; Yezioro, A.; Auer, T. Synergetic Urban Microclimate and Energy Simulation Parametric Workflow. In *Journal of Physics: Conference Series*; 2019; Vol. 1343, p 12006.

76. Salvati, A.; Roura, H. C.; Cecere, C. Assessing the Urban Heat Island and Its Energy Impact on Residential Buildings in Mediterranean Climate: Barcelona Case Study. *Energy Build.* **2017**, *146*, 38–54.

77. Simpson, J. R. Improved Estimates of Tree-Shade Effects on Residential Energy Use. *Energy Build.* **2002**, *34* (10), 1067–1076.

78. Hes, D.; Dawkins, A.; Jensen, C.; Aye, L. A Modelling Method to Assess the Effect of Tree Shading for Building Performance Simulation. *Proc. Build. Simul. 2011 12th Conf. Int. Build. Perform. Simul. Assoc.* **2011**, 161–168.

79. Morakinyo, T. E.; Dahanayake, K. W. D. K. C.; Adegun, O. B.; Balogun, A. A. Modelling the Effect of Tree-Shading on Summer Indoor and Outdoor Thermal Condition of Two Similar Buildings in a Nigerian University. *Energy Build.* **2016**, *130*, 721–732. https://doi.org/10.1016/j.enbuild.2016.08.087.

80. Mochida, A.; Yoshino, H.; Miyauchi, S.; Mitamura, T. Total Analysis of Cooling Effects of Cross-Ventilation Affected by Microclimate around a Building. *Sol. Energy* **2006**, *80* (4), 371–382. https://doi.org/10.1016/j.solener.2005.08.014.

81. Morille, B.; Musy, M.; Malys, L. Preliminary Study of the Impact of Urban Greenery Types on Energy Consumption of Building at a District Scale: Academic Study on a Canyon Street in Nantes (France) Weather Conditions. *Energy Build.* **2016**, *114*, 275–282. https://doi.org/10.1016/j.enbuild.2015.06.030.

82. Gros, A.; Bozonnet, E.; Inard, C. Cool Materials Impact at District Scale - Coupling Building Energy and Microclimate Models. *Sustain. Cities Soc.* **2014**, *13*, 254–266. https://doi.org/10.1016/j.scs.2014.02.002.

83. Tsoka, S.; Tsikaloudaki, K.; Theodosiou, T. Coupling a Building Energy Simulation Tool with a Microclimate Model to Assess the Impact of Cool Pavements on the Building's Energy Performance Application in a Dense Residential Area. *Sustain.* **2019**, *11* (9), 2519. https://doi.org/10.3390/su11092519.

84. Tong, Z.; Chen, Y.; Malkawi, A. Defining the Influence Region in Neighborhood-Scale CFD Simulations for Natural Ventilation Design. *Appl. Energy* **2016**, *182*, 625–633.

85. Straw, M. P.; Baker, C. J.; Robertson, A. P. Experimental Measurements and Computations of the Wind-Induced Ventilation of a Cubic Structure. *J. Wind Eng. Ind. Aerodyn.* **2000**, *88* (2–3), 213–230.

86. Ramponi, R.; Blocken, B. CFD Simulation of Cross-Ventilation for a Generic Isolated Building: Impact of Computational Parameters. *Build. Environ.* **2012**, *53*, 34–48. https://doi.org/https://doi.org/10.1016/j.buildenv.2012.01.004.

87. Franke, J.; Baklanov, A. *Best Practice Guideline for the CFD Simulation of Flows in the Urban Environment: COST Action 732 Quality Assurance and Improvement of Microscale Meteorological Models*; Meteorological Inst., 2007.

88. Tominaga, Y.; Mochida, A.; Yoshie, R.; Kataoka, H.; Nozu, T.; Yoshikawa, M.; Shirasawa, T. AIJ Guidelines for Practical Applications of CFD to Pedestrian Wind Environment around Buildings. *J. Wind Eng. Ind. Aerodyn.* **2008**, *96* (10–11), 1749–1761. https://doi.org/10.1016/j.jweia.2008.02.058.

89. Blocken, B. Computational Fluid Dynamics for Urban Physics: Importance, Scales, Possibilities, Limitations and Ten Tips and Tricks towards Accurate and Reliable Simulations. *Build. Environ.* **2015**, *91*, 219–245.

90. YOSHIDA, S. Study on Effect of Greening on Outdoor Thermal Environment Using Three Dimensional Plant Canopy Model. *J. Arch. Plann. Environ. Eng., AIJ* **2000**, *536*, 87–94.

91. Kamiyama, K. Wind Tunnel Experiments on Drag Coefficient of Trees with the Leaf Area Density as a Reference Area. *J. Environ. Eng.* **2004**, *578*, 71–77.

92. Mochida, A.; Tabata, Y.; Iwata, T.; Yoshino, H. Examining Tree Canopy Models for CFD Prediction of Wind Environment at Pedestrian Level. *J. Wind Eng. Ind. Aerodyn.* **2008**, *96* (10–11), 1667–1677. https://doi.org/10.1016/j.jweia.2008.02.055.

93. Bitog, J. P.; Lee, I. B.; Hwang, H. S.; Shin, M. H.; Hong, S. W.; Seo, I. H.; Mostafa, E.; Pang, Z. A Wind Tunnel Study on Aerodynamic Porosity and Windbreak Drag. *Forest Sci. Technol.* **2011**, *7* (1), 8–16. https://doi.org/10.1080/21580103.2011.559939.

94. Zhao, M.; Fan, Z. Hydrodynamic Characteristics of Submerged Vegetation Flow with Non-Constant Vertical Porosity. *PLoS One* **2017**, *12* (4), e0176712. https://doi.org/10.1371/journal.pone.0176712.

95. Asawa, T.; Fujiwara, K.; Hoyano, A.; Shimizu, K. Convective Heat Transfer Coefficient of Crown of Zelkova Serrata. *J. Environ. Eng.* **2016**, *81* (720), 235–245. https://doi.org/10.3130/aije.81.235.

96. Hagishima, A.; Tanimoto, J. Field Measurements for Estimating the Convective Heat Transfer Coefficient at Building Surfaces. *Build. Environ.* **2003**, *38* (7), 873–881. https://doi.org/10.1016/S0360-1323(03)00033-7.

97. Hirayama, Y.; Asawa, T.; Hoyano, A. Development of Heat Transfer Model of a Passive Cooling Louver for Microclimate Simulation. In *Grand Renewable Energy proceedings Japan council for Renewable Energy*; 2018; p 105.

98. Minoru, N.; Shintarou, T.; Koumei, A.; Fumiaki, N. Decision Method of Pressure Loss Coefficient of Windbreak Nets For CFD. *Proc. Natl. Symp. Wind Eng.* **2014**, *23*, 445. https://doi.org/10.14887/kazekosymp.23.0_445.

99. Elwan, M.; Rizk, A.; El-Morsi, M. A Review on Wind - Driven Cross - Ventilation Techniques Inside Single Rooms. *Int. J. Sci. Eng. Res.* **2018**, *6*, 75 of 93.

100. Allard, F.; Allard, F. *Natural Ventilation in Buildings: A Design Handbook*; James & James London, 1998.

Other references

(TMG, 2017) Toyko Metropolitan Government. Final energy consumption and greenhouse gas emissions in Tokyo. Bureau of Environment. 2017. Last accessed June 30 2020. https://www.kankyo.metro.tokyo.lg.jp/en/climate/index.files/b0548c2a69e7883f1945aca50f606a92.pdf

(JMA, 2018) Japan Meteorological Agency. Climate change monitoring report 2018. Last accessed June 30 2020. https://www.jma.go.jp/jma/en/NMHS/ccmr/ccmr2018.pdf

T. Sawachi, Y. Matsuo, K. Hatano, H. Fuskushima, Determinants of heating and air conditioning behavior, and acceptable ranges of temperature based on behavior: Study on residents' behavior contributing formation of indoor climate, Part 1. J. Arch. Plann. Environ. Eng. (Trans AIJ) 382 (1987) 48-59. https://doi.org/10.3130/aijax.382.0_48. [In Japanese].

H. Habara, D. Narumi, Y. Shimoda, M. Mizuno, A study on determinants of air conditioning on/off control in dwellings based on survey. J. Environ. Eng. (Trans AIJ) 70 (589) (2005) 83-90. https://doi.org/10.3130/aije.70.83_1. [In Japanese with abstract in English].

H. Habara, Logistic regression analysis of factors affecting occupants' air conditioner/window operating behavior in living rooms. J. Environ. Eng. (Trans AIJ) 80 (715) (2015) 827-837. https://doi.org/10.3130/aije.80.827. [In Japanese with abstract in English].

APPENDIX

A.1 Field measurement

Air temperature results (1 minute average)

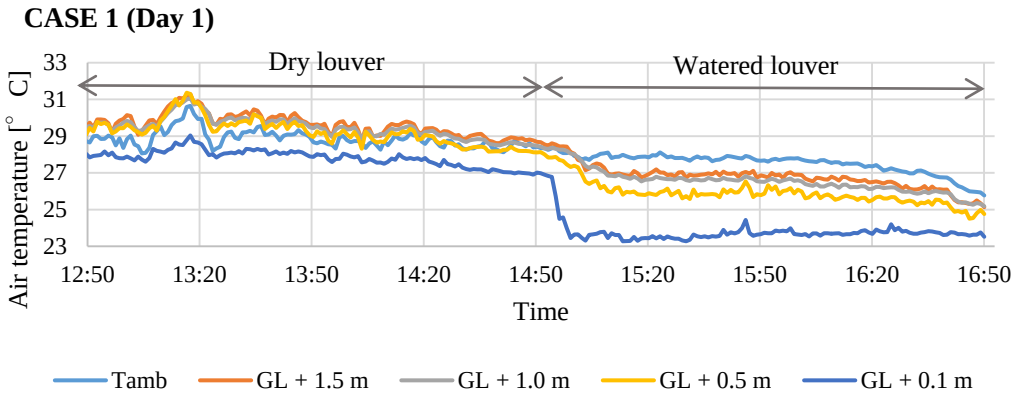

Figure 0.1. Air temperature at the back of the louver (T_{lo}) for CASE 1 (Space A) before and after the louver is watered.

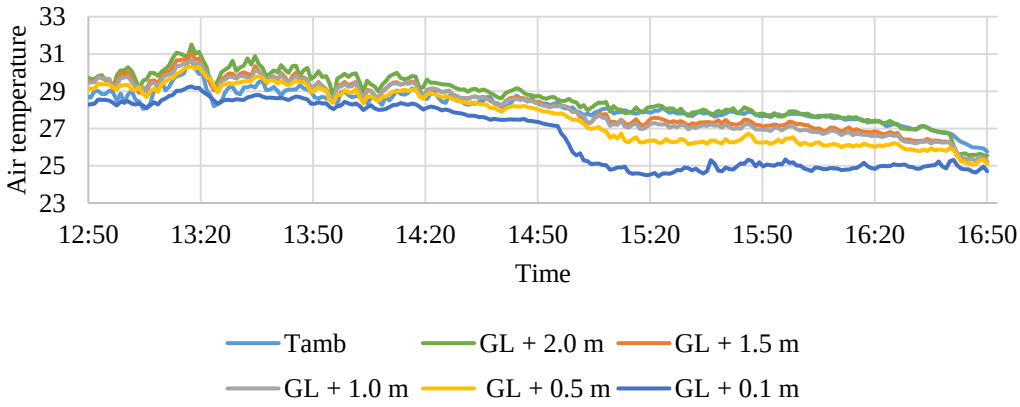

Figure 0.2. Air temperature at the center of the semi-outdoor space (T_{sop}) for CASE 1 (Space A) before and after the louver is watered.

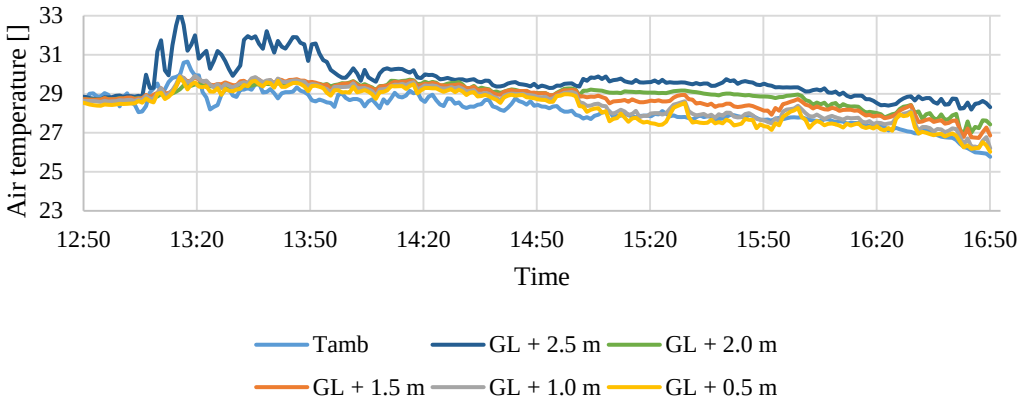

Figure 0.3. Air temperature inside the window (T_{win}) for CASE 1 (Space A) before and after the louver is watered.

CASE 2

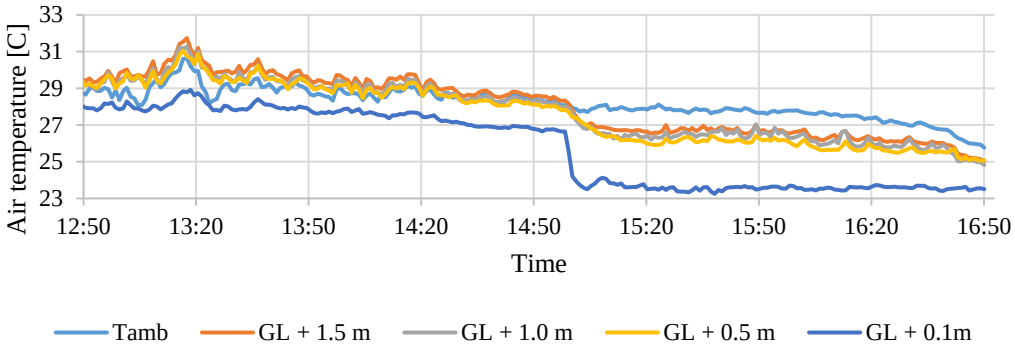

Figure 0.4. Air temperature at the back of the louver (T_{lo}) for CASE 2 (Space B) before and after the louver is watered.

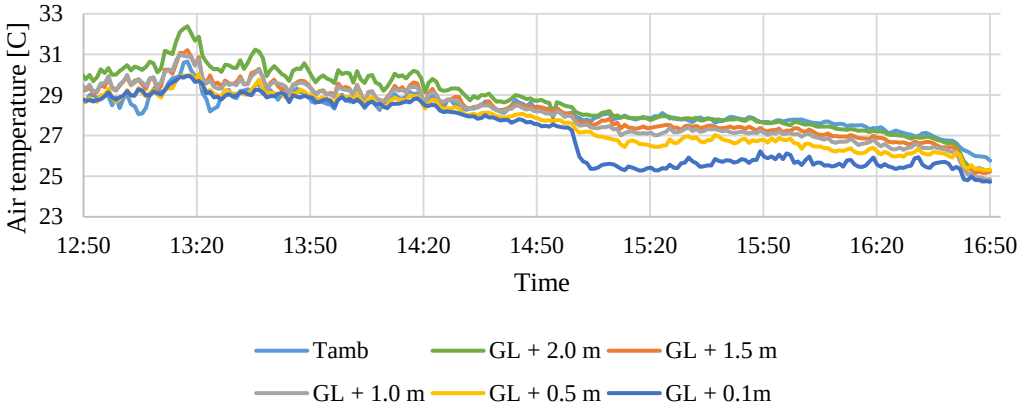

Figure 0.5. Air temperature at the center of the semi-outdoor space (T_{sop}) for CASE 2 (Space B) before and after the louver is watered.

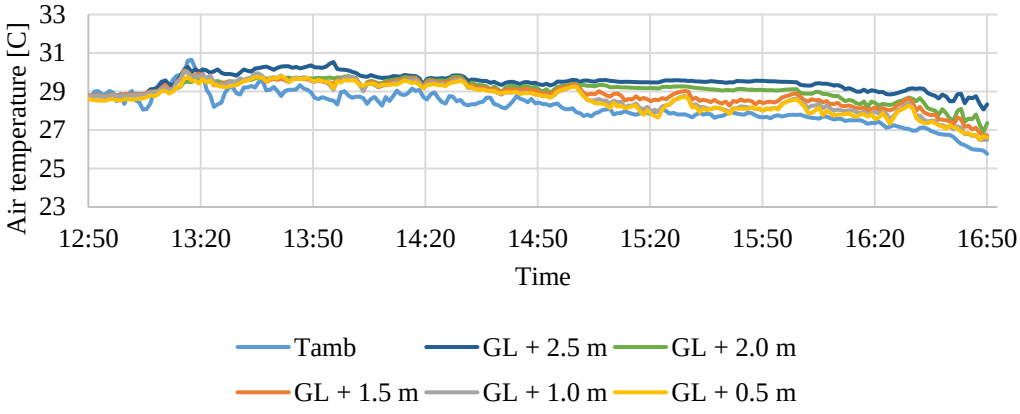

Figure 0.6. Air temperature inside the window (T_{win}) for CASE 2 (Space B) before and after the louver is watered.

CASE 3 (Day 2)

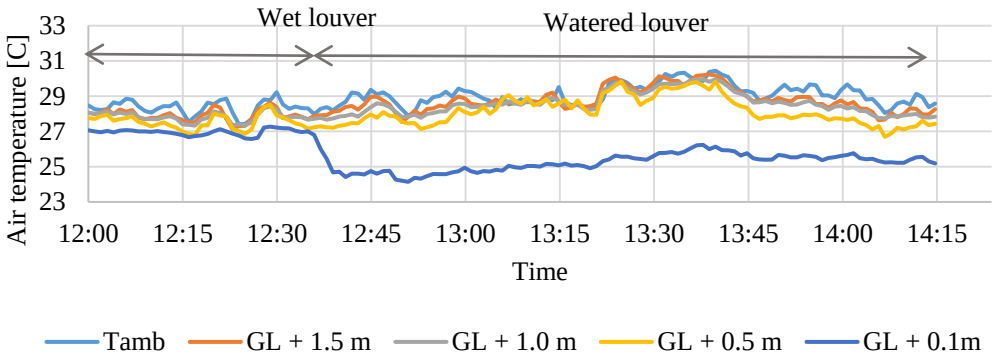

Figure 0.7. Air temperature at the back of the louver for CASE 3 (Space A) before and after the louver is watered.

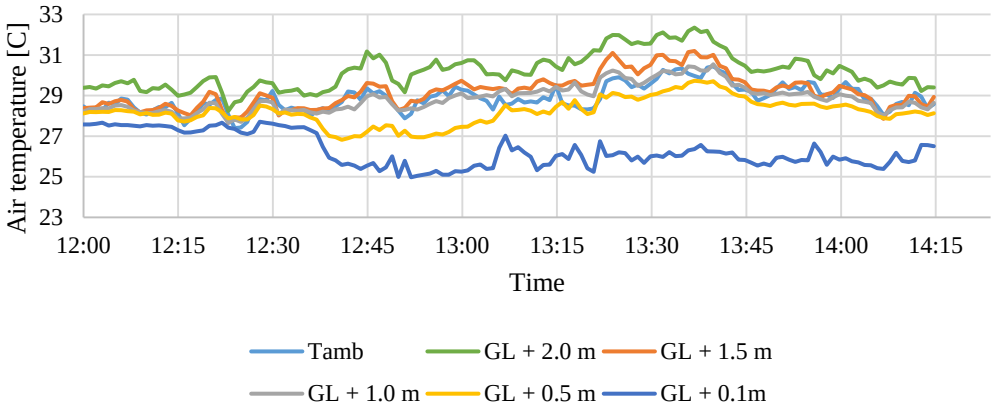

Figure 0.8. Air temperature in the center of the semi-outdoor space for CASE 3 (Space A) before and after the louver is watered.

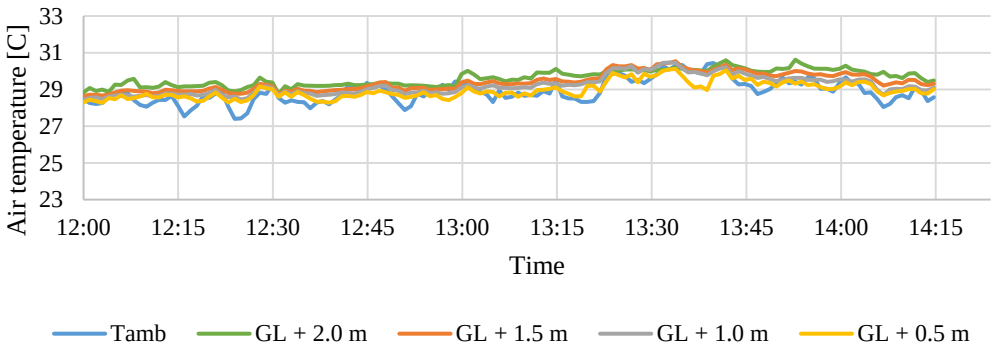

Figure 0.9. Air temperature inside the window for CASE 3 (Space A) before and after the louver is watered. (Data for Twin at GL + 2.5 m was defectuous)

CASE 4

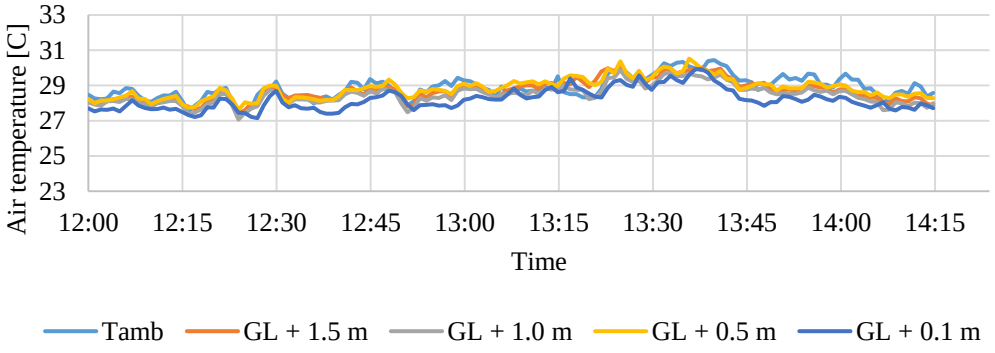

Figure 0.10. Air temperature at the back of the louver for CASE 4 (Space B) before and after the louver is watered.

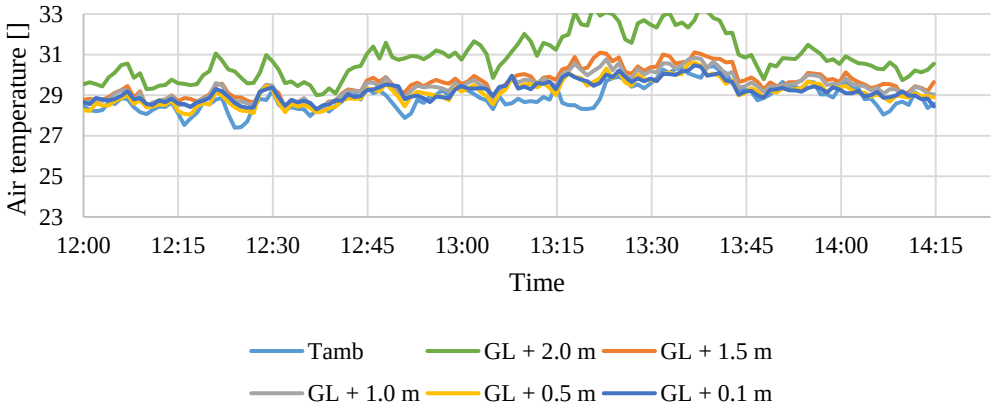

Figure 0.11. Air temperature in the center of the semi-outdoor space for CASE 4 (Space B) before and after the louver is watered.

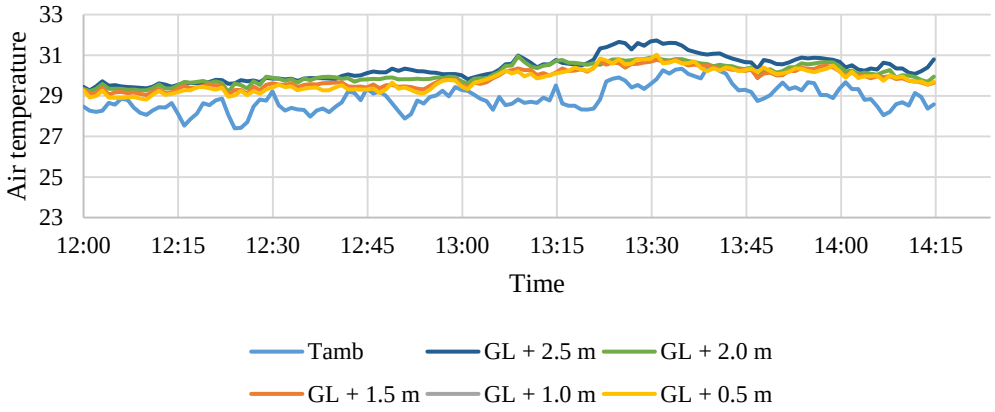

Figure 0.12. Air temperature inside the window for CASE 4 before and after the louver is watered.

A.2 CFD validation (case S-0)

Validation process

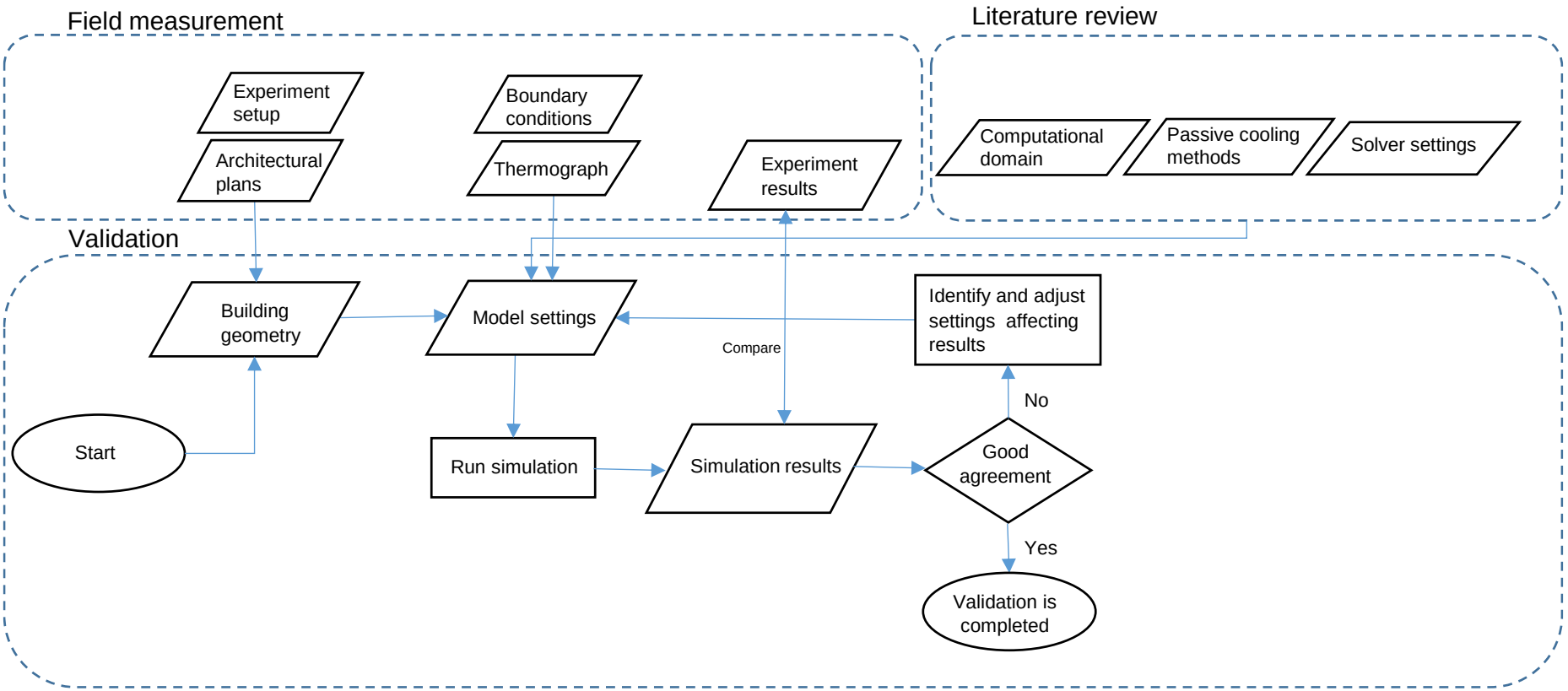

Figure 0.13. Flow chart of process for CFD validation

Trial and error validation cases

Table 0.1. Trial and error cases for validation.

Validation trials	Computational settings					Inflow boundary			Outflow boundary		Thermal boundary	Porous media - Window net	Measurement data points (Figure 0.14)
	Solver setting	Cycles	Convergence criteria	Computational domain size [mm]	Mesh size [mm]	Size	Fixed velocity	Tamb, WSout [m/s], WDout	Size	Natural outflow	CHTC (W/m2k)	without	Single
VT-1	Simple, 1st order upwind	300	1E-04	60000 x 100000 x 40000	200 x 200 x 200	3.5H	Ymin	29, 1, South	10H	Ymax	8 (inside), 23 (outside)	No	Single
VT-2	Simple, 1st order upwind	300	1E-04	60000 x 80000 x 25000	200 x 200 x 200	3.5H	Ymin	27.8, 1, SSE x=-0.3, y=1	7H	Ymax	8 (inside), 23 (outside)	No	Single
VT-3	Simple, 1st order upwind	300	1E-04	60000 x 85000 x 40000	100 x 100 x 100	3.5H	Ymin	27.9, 1, South	7H	Ymax	10.3 (inside) 11.4 (outside)	No	Single
VT-4	Simple, 1st order upwind	100	1E-04	75000 x 85000 x 40000	100 x 100 x 100	3H	Ymin, Xmax	27.9, 1.2, SSE x=-0.5, y=1.2	7H	Ymax	10.7 (inside), 11.8 (outside)	No	Single
VT-5	Simple, 1st order upwind	100	1E-04	75000 x 85000 x 30000	100 x 100 x 100	3H	Ymin, Xmax	27.9, 1.2, SSE x=-0.5, y=1.2	7H	Ymax	10.7 (inside), 11.8 (outside)	No	Single
VT-6	Simple, 1st order upwind	300	1E-04	84000 x 152000 x 42000	100 x 100 x 100		Ymin	27.9, 1.2, SSE x=-0.5, y=1.2		Ymax	10.3 (all)	No	Single

VT-7	Simple, 1st order upwind	300	1E-04	84000 x 152000 x 42000	100 x 100 x 100		Ymin	27.9, 1.2, SSE x=-0.5, y=1.2		Ymax	10.3 (all)	No	Single
VT-8	Simple, 1st order upwind	300	1E-04	84000 x 152000 x 42000	100 x 100 x 100		Ymin	27.9, 1.2, SSE x=-0.5, y=1.2		Ymax	9.5 (all)	No	Single
VT-9	Detail, QUICK	350	1E-06	152000 x 152000 x 42000	100 x 100 x 100	5H	Ymin, Xmax	27.5, 1.2, SSE x=-0.5, y=1.2	15H	Xmin, Ymax	9.5 (inside), 11.6 (outside)	No	Single
VT-10	Detail, QUICK	500	1E-06	84000 x 152000 x 42000	100 x 100 x 100	5H	Ymin	27.5, 1, South	15H	Ymax	9.5 (inside), 11.6 (outside)	No	Single
VT-11	Detail, QUICK	300	1E-06	152000 x 152000 x 42000	100 x 100 x 100	5H	Xmin, Ymin	27.5. 1, SSW x=0.17 m/s, y=0.98 m/s	15H	Xmax, Ymax	9.5 (inside), 11.6 (outside)	No	Multiple
VT-12	Detail, QUICK	350	1E-06	139600 x 139100 x 43200	100 x 100 x 100	3H	Xmin, Ymin	27.5, 0.9, SSW x = 0.1 m/s, y=0.9 m/s	15H	Xmax, Ymax	9.5 (inside), 11.6 (outside)	No	Multiple
VT-13	Detail, QUICK	350	1E-06	154000 x 290300 x 43200	100 x 100 x 100	5H	Xmin, Ymin	27.5, 0.9, SSW x = 0.1 m/s, y=0.9 m/s	15H	Xmax, Ymax	9.5 (inside), 11.6 (outside)	Yes	Multiple
VT-14	Detail, QUICK	1500	1E-05	154000 x 290300 x 43200	100 x 100 x 100	5H	Xmin, Ymin	27.5, 0.9, SSW x = 0.1 m/s, y=0.9 m/s	15H	Xmax, Ymax	9.5 (inside), 11.6 (outside)	Yes	Multiple
VT-15	Detail, QUICK	800	1E-05	154000 x 290300 x 43200	100 x 100 x 100	5H	Xmin, Ymin	27.5, 0.9, SSW x = 0.1 m/s, y=0.9 m/s	15H	Xmax, Ymax	9.5 (inside), 11.6 (outside)	Yes	Multiple

Case S-0	Detail, Quick	1000	1E-5		100 x 100 x 1000	5H	Xmin, Ymin	27.5, 1, SSW X=0.29, y=0.95	15H	Xmax, Ymax	9.5 (inside), 11.6 (outside	Yes	Multiple

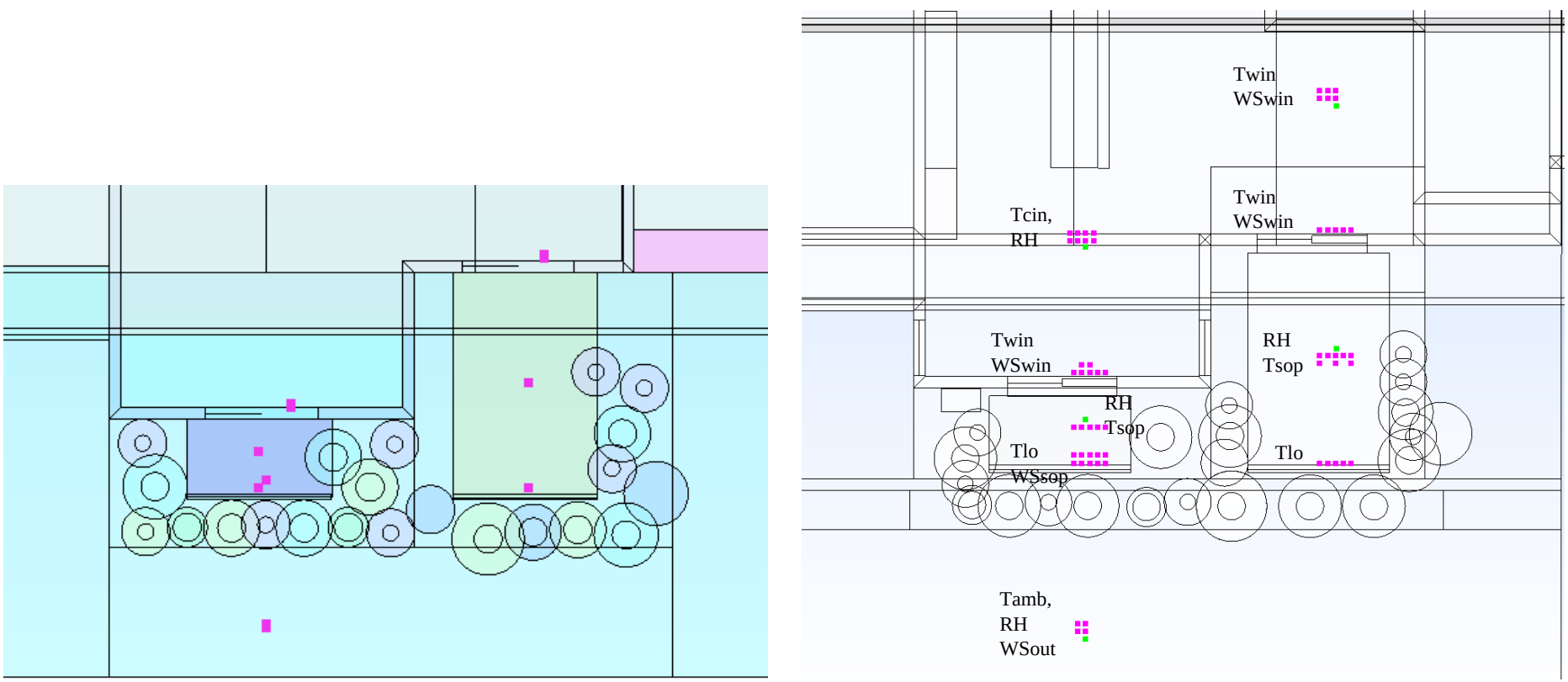

(a) VT -1

(b) Case S-0

Figure 0.14. Example for comparison for (a) single and (b) multiple measurement points during validation trial and error cases.

Thermal boundary condition settings

Table 0.2. Thermal boundary condition settings.

Spaces Outdoor space	Part	Ts [°C]	CHTC
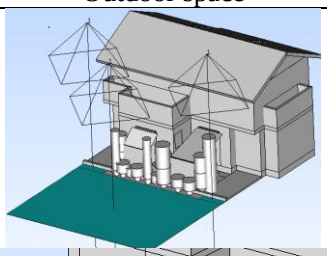	Outdoor ground	30.5	11.6
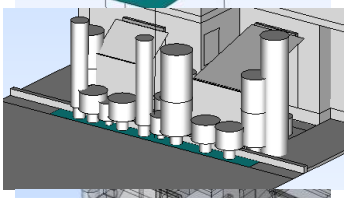	Ground below pots	25.5	11.6
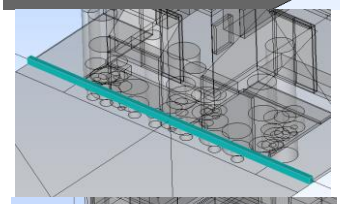	Blocks	29.0	11.6
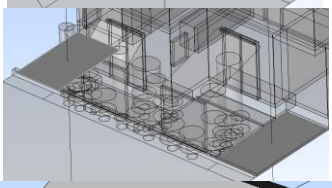	Ground sides	26.5	11.6
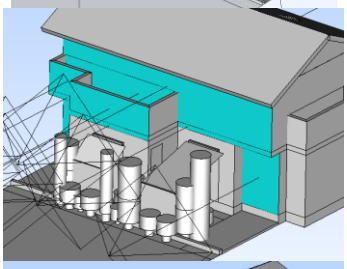	Southwest walls	30.0	11.6
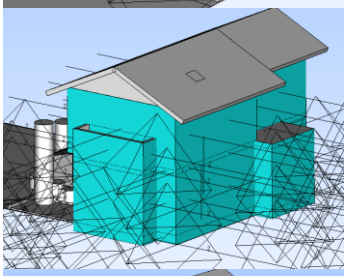	Northeast walls	30.5	11.6
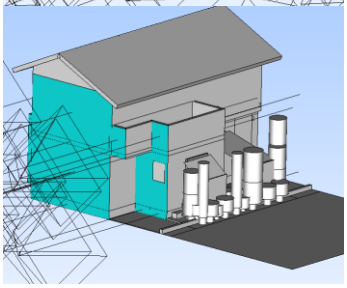	31.5	11.6	

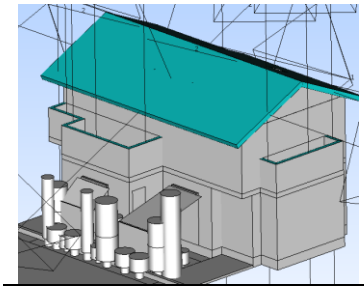	Roof	31.5	11.6
Semi-outdoor space			
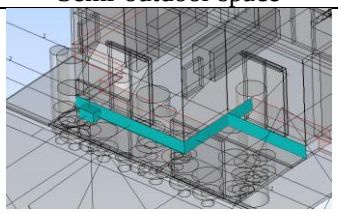	Base of wall (GL+0.0 to + 0.4 m)	27.5	11.6
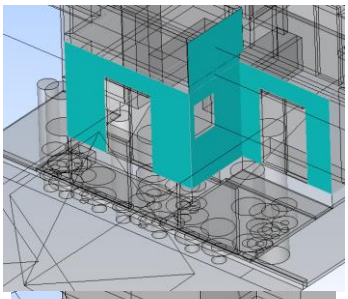	Walls inside semi-outdoor space	29.0	11.6
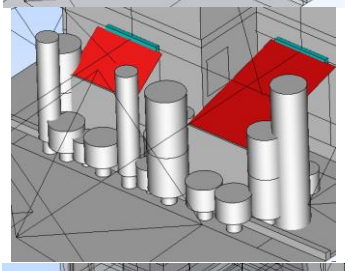	Sunscreen	30	11.6
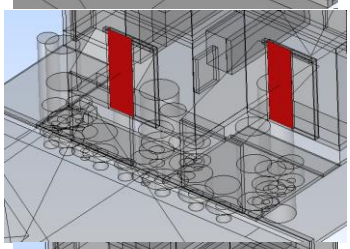	Window for Space A and Space B.	30.0 and 29.5	11.6
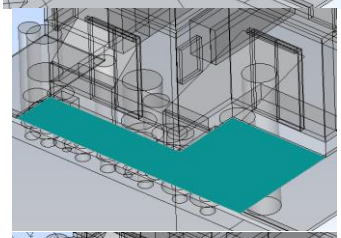	Wet shaded soil	21.0	11.6
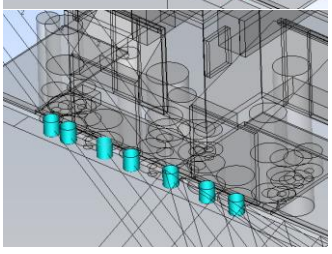	Unshaded pots	30.5	11.6

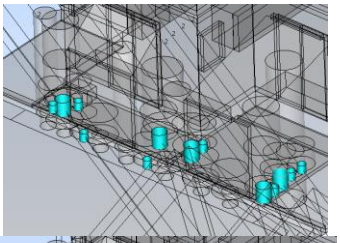	Shaded pots	28.5	11.6
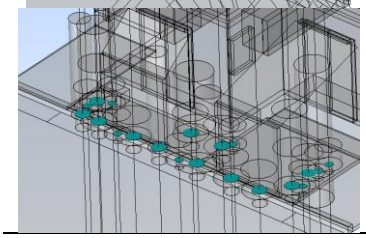	Soil in pots	24.0	11.6
Indoor space			
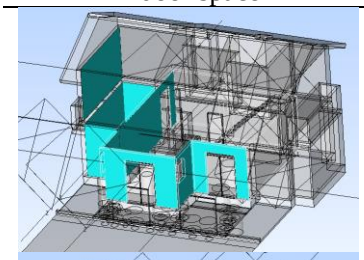	Indoor walls first floor (1) southwest	31.5	9.5
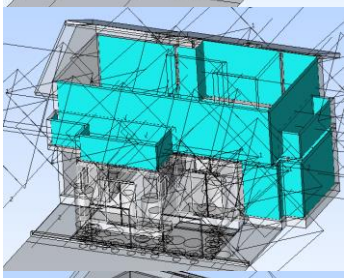	Indoor walls (3) - northeast	30.5	9.5
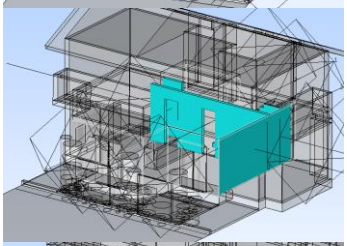	Indoor walls (2)	29.5	9.5
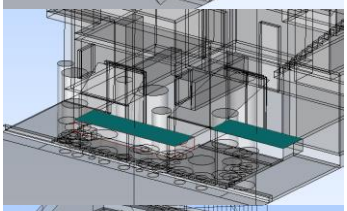	Floor inside window for Space A and Space B	31 and 30	
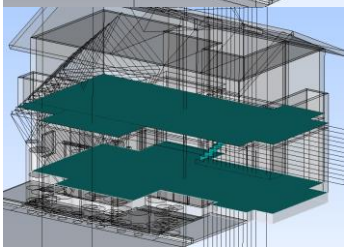	Floor	29.5	9.5

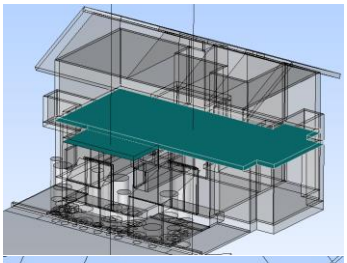	Ceiling first floor	30	9.5
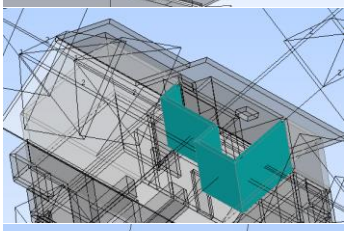	Walls second floor	29.5	9.5
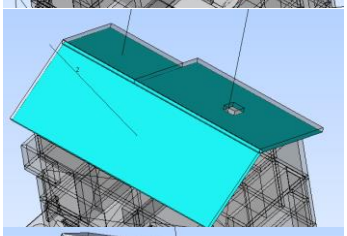	Roof ceiling	31.0	9.5
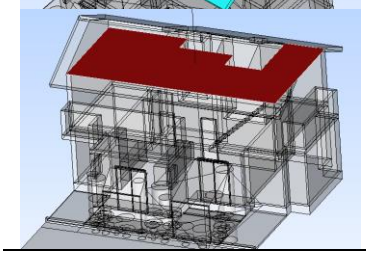	Second floor ceiling	30.0	9.5

Louver settings - Calculations for the porous media

Ratio (surface area / volume)

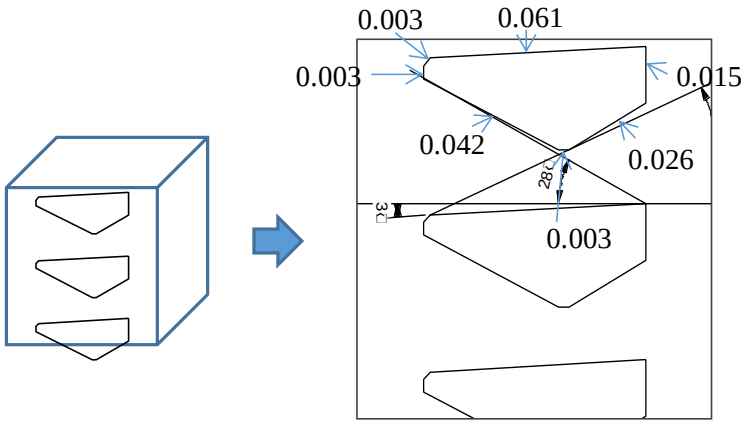

Surface area (circumference of a slat and number of louvers) = 0.153*0.1*2.56

Volume of mesh = 0.1*0.1*0.1

Ratio (surface area / volume) = 39.2 m^2/m^3

Porosity

Porosity = 1 – (volume ratio of primary material in porous media)

Therefore, first the volume ratio (one mesh) is calculated according to the louver's dimensions:

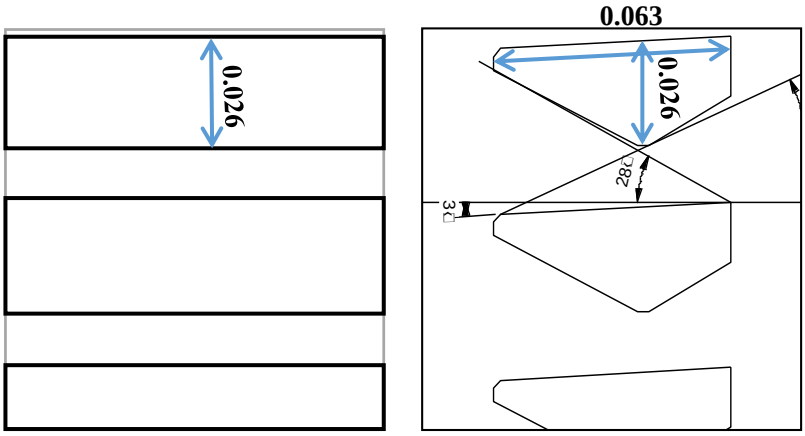

Y axis X axis

Volume ratio (0.063*0.026*0.5*0.1*2.56) / (0.1*0.1*0.1) = 0.21

Volume of a triangle = 0.063*0.026*0.5

Length of one mesh = 0.1

Louver slats in one mesh = 2.56

Volume of one mesh = 0.1*0.1*0.1

Porosity = 1 – 0.21 = 0.79

Cross section area ratio

X axis = (0.063*0.026*0.5*2.56) / (0.1*0.1) = 0.21

Y axis = (0.1*0.026*2.56) / (0.1*0.1) = 0.66

A.3 Optimization study: Trial and error cases

Trial and error cases for the optimization

Table 0.3. Trial and error cases for optimization of outdoor and indoor microclimates.

Case	Semi-outdoor space design										Indoor space design										
	L-W distance for Space B [m]			Surrounding vegetation				GL – FL difference [m]			Outdoor (out) to indoor (in) ventilation					In -In	In - Out	Indoor furniture and partitions		Opt.* cases	Va-ria-bles
	Exp.*	New		Exp.	New			Exp.	New		Space B	Space A and Space B			Space A						
Trial No.	2.8	1.8	1		1	2	3	0.4	0.2	0	Wingwall	Window casement double	Window sliding double	Window open 100% no glass		Door	Door	Fur-niture	Par-titions		
1	0				1			0													1
2	0					1		0								1					2
3		1		0				0													1
4		1		0				0								1					2
5		1		0						1											2
6		1		0					1							1		1			4
7		1		0						1						1		1	1		5
8	0			0				0			1					1	1			Case S-6	3
9		1		0				0			1					1	1			Case S-7	4
10		1		0					1		1					1	1			Case S-8	5
11		1		0					1		1					1	1	1			6
12			1	0					1		1					1	1	1			6
13		1		0					1		1				1	1	1				6
14			1	0					1		1		1			1	1	1			7
15		1		0					1		1			1		1	1				6

16		1		0			1	1		1		1	1			6
17		1			1		1	1		1		1	1			7
18		1			1		1	1	1			1	1			7
19		1		0			1	1	1			1	1		Case S-9	6
20			1	0			1	1	1			1	1		Case S-10	6

*Exp. = existent experiment settings. *Opt. = optimization.